

Electronic Supplementary Information
for:

**Deuteration of Pd-activated C(*sp*²)-H bonds in the Solid
State**

Alen Bjelopetrović,^{a,‡} Dajana Barišić,^{a,b,‡} Marina Juribašić Kulcsár,^{a,*} Ivan Halasz,^a
Manda Ćurić,^a and Stipe Lukin^{a,*}

^aRuđer Bošković Institute, Division of Physical Chemistry, Bijenička 54, HR-10000 Zagreb, Croatia

^bSelvita Ltd, Prilaz Baruna Filipovića 29, HR-10000 Zagreb, Croatia

Table of contents:

1. Experimental details	2
2. ¹ H NMR spectroscopy.....	13
3. ¹³ C NMR spectroscopy.....	50
4. Raman spectroscopy	59
5. IR spectroscopy.....	63
6. TG experiments	70
7. HRMS spectra	71
8. Computational study	86
9. References	103

1. Experimental details

1.1 General Methods

All chemicals and solvents used were of reagent grade and were used without additional purifications. **NMR spectra** were recorded in CDCl_3 and $\text{DMSO}-d_6$ on Bruker AV-300, AV-400 or AV-600 at 298 K. Chemical shifts refer to the tetramethylsilane (TMS) internal standard.

IR spectra were recorded using a Perkin-Elmer Spectrum Two spectrometer.

Thermogravimetric experiments were performed using Perkin Elmer Simultaneous Thermal Analyzer (STA) 6000.

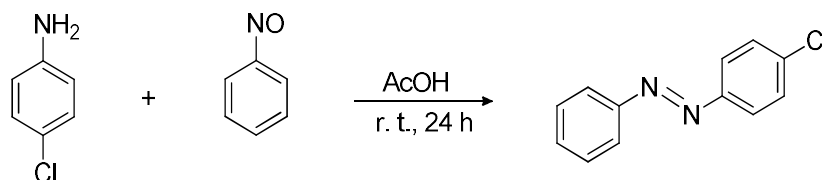
In-situ Raman monitoring was performed using a modular Raman system made of OceanOptics Maya2000Pro spectrometer, PD-LD (now Necsel) BlueBox Raman laser with the 785 nm excitation wavelength, and coupled with the B&W-Tek fibre optic Raman BAC102 probe that was approached to the bottom of the reaction PMMA jar. The setup and the analysis (baseline subtraction, and PMMA jar subtraction) were adopted from elsewhere.¹ Raman spectra were cropped in range around $900 - 1700 \text{ cm}^{-1}$ and normalized using L1 norm.

High-resolution mass spectra were acquired on an Agilent 6550 Series Accurate-Mass Quadrupole Time-of-Flight (Q-TOF). The electrospray ionization mass spectrometry (ESI-MS) analysis was performed in a positive-ion mode, ranging from m/z 100 to 1500. The capillary potential was 3500 V, the fragmentor voltage was 50 V, the drying gas flow was 11 L min^{-1} , and the temperature was $200 \text{ }^\circ\text{C}$. The sheath gas flow was 14 L min^{-1} , and the temperature was $250 \text{ }^\circ\text{C}$. Nitrogen was used as a drying and sheath gas. Solution of the sample in MeCN- H_2O (v/v 1:1) was introduced directly *via* an Agilent 1290 Infinity II UHPLC equipped with Zorbax Eclipse Plus C18, $3.0 \times 50 \text{ mm}$, $1.8 \mu\text{m}$ column, column temperature $40 \text{ }^\circ\text{C}$, elution using a gradient of two mobile phases: 0.1 % HCOOH in water (A) and 0.1 % HCOOH in MeCN (B), at flow rate 0.3 mL min^{-1} . Apart from these standard conditions, searching for the better conditions for the analysis, MeOH instead of MeCN in the mobile phase) was used for **8^p**.

1.2 Milling reactions

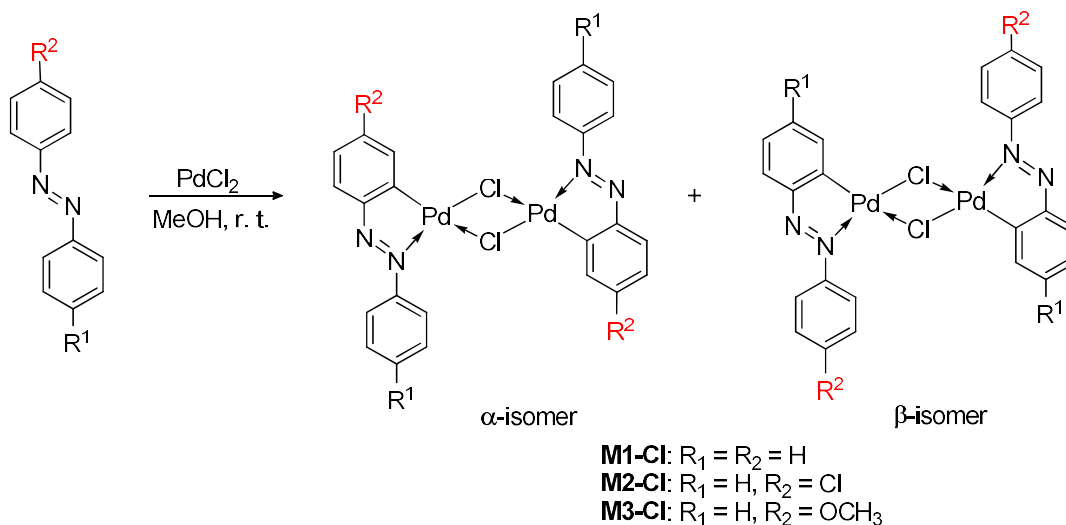
Experiments were performed using an IST500 mixer mill operating at 30 Hz with a built-in fan. To ensure data consistency, the reported experiments with each precursor were performed sequentially under analogous conditions and at an ambient temperature of $22 \pm 2 \text{ }^\circ\text{C}$. Reactions were performed in 14 mL poly(methylmethacrylate) (PMMA) transparent jars that allowed for *in situ* Raman monitoring. One zirconium(IV) oxide (ZrO_2 , 12 mm, 4.5 g) milling ball was used. Reactions were performed using approximately 225 mg of the reaction mixture. Reactions with L-alanine were performed using the same experimental setup as analogous reactions with L-cysteine.

1.3 Synthesis of 4-chlororazobenzene (2)

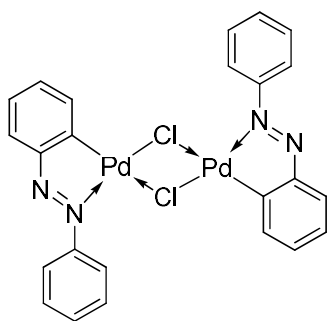


Compound **2** was prepared by Mill's coupling reaction of nitrosobenzene with *p*-substituted aniline.² 1.0 g (9.34 mmol) of nitrosobenzene was dissolved in 50 ml concentrated acetic acid. 1.2 g (9.34 mmol,) of *p*-chloroaniline was added to the solution and stirred for 24 h at room temperature. The solution was then neutralized with a saturated solution of NaHCO₃, resulting in precipitation of the product, which was then filtered under reduced pressure, washed with distilled water, and dried in air. The product was recrystallized from methanol, filtered and dried under reduced pressure. (1.4 g, 68 % isolated). Characterization data are consistent with previously published.³
¹H NMR (CDCl₃, 600 MHz, δ /ppm): 7.92 (dd, *J* = 8.1 Hz, 2H), 7.88 (d, *J* = 8.9 Hz, 2H), 7.51-7.46 (m, 5H).

1.4 Synthesis of the monocyclopalladated dimeric complexes **M1-Cl** - **M3-Cl**

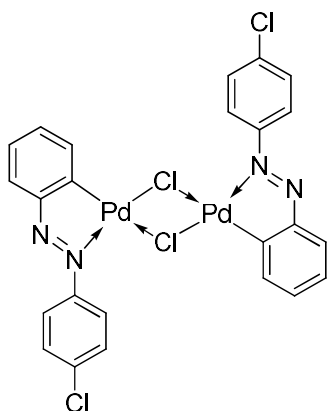


The monocyclopalladated dimeric complexes **M1-Cl** – **M3-Cl** were prepared in MeOH according to a known procedure.⁴ A mixture of 400.0 mg PdCl₂ (2.26 mmol) and the corresponding azobenzene was stirred for 24 h in 50 mL MeOH at room temperature. The resulting precipitate was filtered and dried under vacuum. The crude product was recrystallized from DMF, filtered, washed with Et₂O, and dried under vacuum.



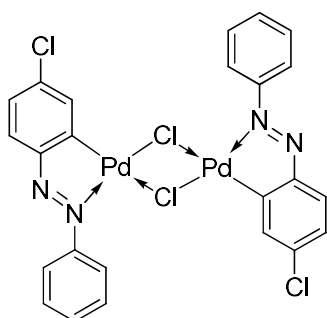
[(C₆H₅N=NC₆H₄)Pd(μ-Cl)]₂ (M1-Cl**). Following the general procedure, the title compound was obtained as an orange solid (394.3 mg, 54 % isolated). Characterization data are consistent with those previously published.⁴**

¹H NMR (DMSO-*d*₆, 300 MHz, δ /ppm): 7.94 (dd, *J* = 7.8 Hz, 1H), 7.72 (dd, *J* = 7.7 Hz, 1H), 7.47-7.63 (m, 5H), 7.28 (d, *J* = 7.4 Hz, 1H), 7.21 (dt, *J* = 7.2 Hz, 1H).



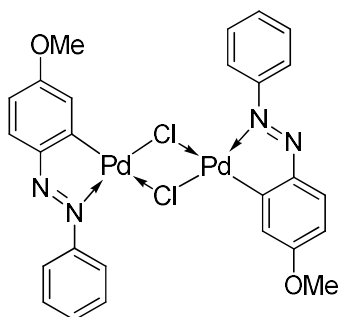
[4-Cl-C₆H₄N=NC₆H₄]Pd(μ-Cl)₂ (M2-Cl). Following the general procedure, the title compound was obtained as an orange solid of alfa and beta isomers (630.3 mg, 78 % isolated, $\alpha : \beta = 3 : 1$).

α -isomer: ¹H NMR (DMSO-*d*₆, 600 MHz, δ /ppm): 7.97 (dd, *J* = 7.8 Hz, 1H), 7.84 (d, *J* = 8.9 Hz, 2H), 7.75 (d, *J* = 7.8 Hz, 1H), 7.62 (d, *J* = 8.8 Hz, 2H), 7.29 (t, *J* = 7.44 Hz, 1H), 7.24 (t, *J* = 7.48 Hz, 1H).



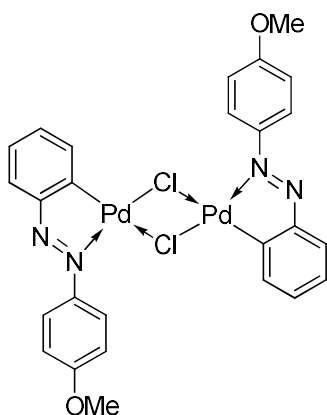
[4-Cl-C₆H₃N=NC₆H₅]Pd(μ-Cl)₂ (M2-Cl).

β -isomer: ¹H NMR (DMSO-*d*₆, 600 MHz, δ /ppm): 7.98 (ovp.), 7.90 (t, *J* = 8.3 Hz, 1H), 7.79 (d, *J* = 7.1, 1H), 7.67 (d, *J* = 7.5 Hz, 1H), 7.59-7.53 (m), 7.37 (dd, *J* = 7.9 Hz, 1H).



[(4-OMe-C₆H₃N=NC₆H₅)Pd(μ-Cl)₂ (M3-Cl). Following the general procedure, the title compound was obtained as an orange solid of alfa and beta isomers (622.4 mg, 78 % isolated, $\alpha : \beta = 1 : 1.2$).

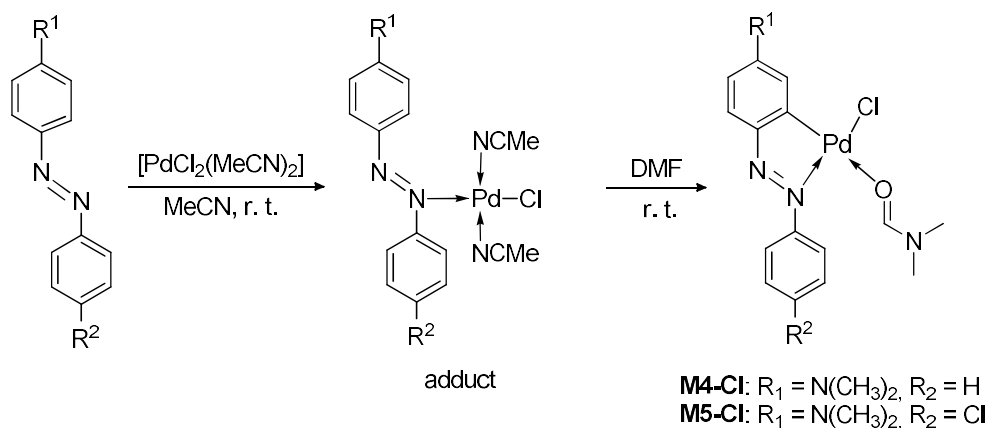
α -isomer: ¹H NMR (DMSO-*d*₆, 600 MHz, δ /ppm): 7.84 (d, *J* = 9.2 Hz, 2H), 7.52-7.49 (ovp.), 7.26 (t, *J* = 7.8 Hz, 1H), 7.17 (t, *J* = 7.9 Hz, 1H), 7.07 (d, *J* = 9.1 Hz, 2H), 3.86 (s, 3H).



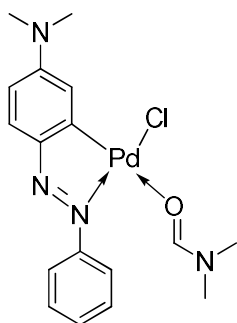
[(4-OMe-C₆H₄N=NC₆H₄)Pd(μ-Cl)₂ (M3-Cl).

β -isomer: ¹H NMR (DMSO-*d*₆, 600 MHz, δ /ppm): 7.84 (d, *J* = 8.2 Hz, 1H), 7.72-7.70 (m, 3H), 7.51-7.49 (ovp.), 7.23 -6.85 (ovp.), 6.85 (d, *J* = 8.1 Hz, 1H), 3.85 (s, 3H).

1.4 Synthesis of the monocyclopalladated monomeric complexes **M4-Cl** and **M5-Cl**

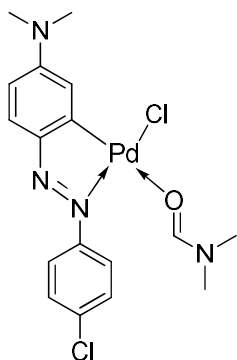


Monocyclopalladated monomeric complexes **M4-Cl** and **M5-Cl** were prepared by a recently developed method.⁵ 235.0 mg (0.90 mmol) $[PdCl_2(MeCN)_2]$ was dissolved in 30 mL acetonitrile at room temperature. One equivalent of the substituted azobenzene was added and stirred for 24 h at room temperature. The resulting precipitate was filtered and dried in air. It was then dissolved in 10 mL of DMF. After 7-8 days, the crystalline product was filtered and dried under vacuum.



$[PdCl(C_6H_5N=NC_6H_3NMe_2)(DMF)]$ (M4-Cl**).** Following the general procedure, the titled compound was obtained as a red crystalline solid (201.6 mg, 51 % isolated). Characterization data are consistent with those previously published.⁶

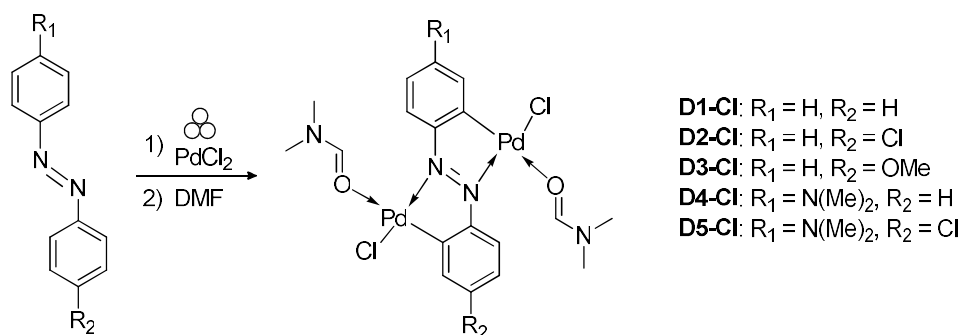
¹H NMR (DMSO-*d*₆, 400 MHz, δ /ppm): 7.95 (s, 1H), 7.61 (d, $J = 7.6$ Hz, 2H), 7.42 (t, $J = 7.4$ Hz, 2H), 7.35 (t, $J = 7.1$ Hz, 1H), 7.01 (s, br, 1H), 6.57 (d, $J = 8.7$ Hz, 1H), 3.12 (s, 6H), 2.89 (s, 3H), 2.73 (s, 3H).



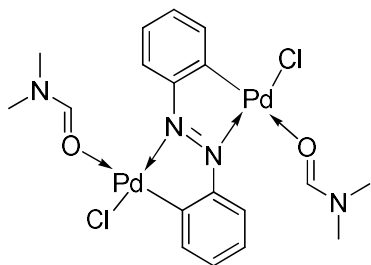
$[PdCl(ClC_6H_4N=NC_6H_3NMe_2)(DMF)]$ (M5-Cl**).** Following the general procedure, the titled compound was obtained as a red crystalline solid (243.0 mg, 57 % isolated). Characterization data are consistent with those previously published.⁵

¹H NMR (DMSO-*d*₆, 600 MHz, δ /ppm): 7.95 (s, 1H), 7.66 (d, $J = 8.6$ Hz, 2H), 7.64 (d, $J = 8.4$ Hz, 2H), 7.47 (d, $J = 8.1$ Hz, 1H), 7.02 (s, br, 1H), 6.59 (d, $J = 8.2$ Hz, 1H), 3.14 (s, 6H), 2.89 (s, 3H), 2.73 (s, 3H).

1.5 Synthesis of the dicyclopalladated monomeric complexes D1-Cl - D5-Cl

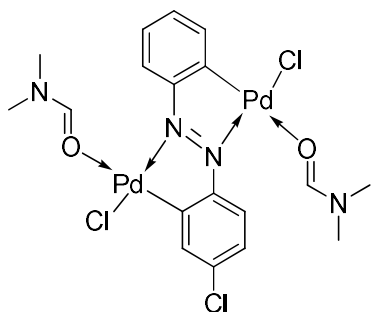


Dicyclopalladated monomeric complexes **D1-Cl** - **D5-Cl** were prepared according to a procedure developed by our group.⁵ The mixture of 0.80 mmol PdCl₂, 0.20 mmol of the corresponding azobenzene, 0.40 mmol NaOAc, and 15 μL H₂O was milled at 30 Hz. The milling time for **D1-Cl**, **D2-Cl**, and **D3-Cl** was 72 h, 5h for **D4-Cl**, and 3h for **D5-Cl**. The crude product was washed with water, dried in the air, and recrystallized from DMF.



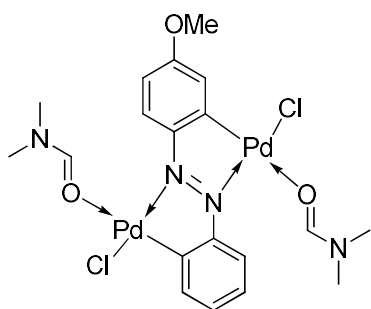
[{PdCl(DMF)}₂(μ -C₆H₄N=NC₆H₄)] (D1-Cl). Following the general procedure, the titled compound was obtained as a brown crystalline solid (65.9 mg, 54 % isolated). Characterization data are consistent with those previously published.⁷

¹H NMR (DMSO-*d*₆, 300 MHz, δ /ppm): 8.75 (d, $J = 6.2$ Hz, 2H), 7.95 (s, 1H), 7.97 (dd, $J = 7.6$ Hz, 2H), 7.20-7.25 (m, 4H), 2.89 (s, 3H), 2.73 (m, 3H).



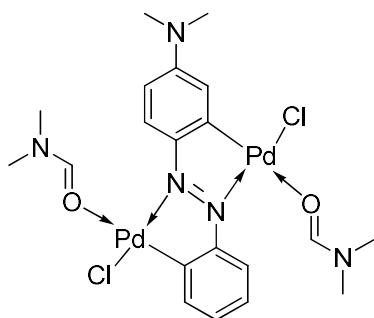
[{PdCl(DMF)}₂(μ -C₆H₃ClN=NC₆H₄)] (D2-Cl). Following the general procedure, the titled compound was obtained as a brown crystalline solid (69.9 mg, 47 % isolated). Characterization data are consistent with those previously published.⁸

¹H NMR (DMSO-*d*₆, 600 MHz, δ /ppm): 8.78 (d, $J = 8.9$ Hz, 1H), 8.74 (d, $J = 5.0$ Hz, 1H), 7.95 (s, 1H), 7.85-7.88 (m, 1H), 7.82 (s, 1H), 7.73 (dd, $J = 8.6$ Hz, 1H), 7.22-7.25 (m, 2H), 2.89 (s, 3H), 2.73 (s, 3H).



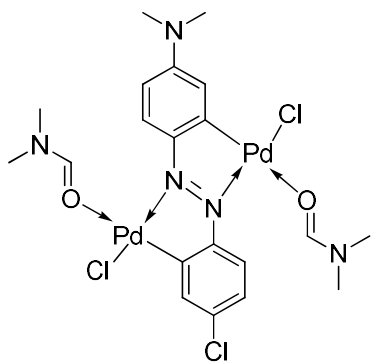
[{PdCl(DMF)}₂(μ -C₆H₃OCH₃N=NC₆H₄)] (D3-Cl). Following the general procedure, the titled compound was obtained as a brown crystalline solid (97.3 mg, 76 % isolated). Characterization data are consistent with those previously published.⁸

¹H NMR (DMSO-*d*₆, 600 MHz, δ /ppm): 9.14 (d, $J = 9.1$ Hz, 1H), 8.59 (d, $J = 7.6$ Hz, 1H), 7.95 (s, 1H), 7.80 (d, $J = 7.4$ Hz, 1H), 7.38 (s, 1H), 7.18 (t, $J = 7.4$ Hz, 1H), 7.10 (t, $J = 7.6$ Hz, 1H), 6.85 (dd, $J = 9.1$ Hz, 1H), 3.87 (s, 3H), 2.89 (s, 3H), 2.73 (s, 3H).



[{PdCl(DMF)}₂(μ-C₆H₄N=NC₆H₃NMe₂)] (D4-Cl). Following the general procedure, the titled compound was obtained as a black crystalline solid (108.4 mg, 83 % isolated). Characterization data are consistent those with previously published.^{6,8}

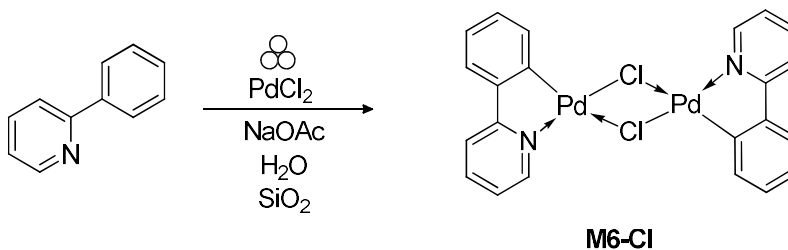
¹H NMR (DMSO-*d*₆, 600 MHz, δ/ppm): 8.50 (d, *J* = 9.0 Hz, 1H), 8.20 (d, *J* = 7.8 Hz, 1H), 7.95 (s, 1H), 7.67 (dd, *J* = 7.9 Hz, 1H), 7.21 (s, 1H), 7.04 (t, *J* = 3.23 Hz, 1H), 6.86 (t, *J* = 3.2 Hz, 1H), 6.62 (dd, *J* = 9.3 Hz, 1H), 3.18 (s, 6H), 2.89 (s, 3H), 2.73 (s, 3H).



[{PdCl(DMF)}₂(μ-C₆H₃NCl=NC₆H₃NMe₂)] (D5-Cl). Following the general procedure, the title compound was obtained as a black crystalline solid (115.5 mg, 84 % isolated). Characterization data are consistent with those previously published.⁵

¹H NMR (DMSO-*d*₆, 300 MHz, δ/ppm): 8.48 (d, *J* = 8.5 Hz, 1H), 8.26 (d, *J* = 8.4 Hz, 1H), 7.95 (s, 1H), 7.62 (s, 1H), 7.21 (s, 1H), 7.13 (dd, *J* = 8.5 Hz, 1H), 6.65 (dd, *J* = 9.3 Hz, 1H), 3.19 (s, 6H), 2.89 (s, 3H), 2.73 (s, 3H).

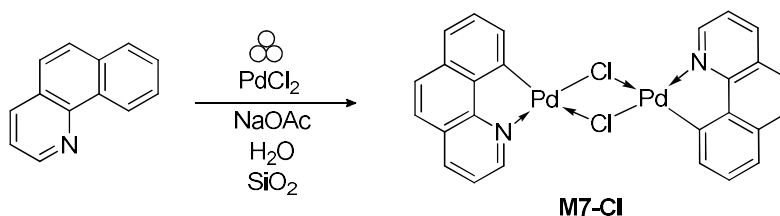
1.6 Synthesis of [(PPY)Pd(μ-Cl)]₂ (M6-Cl)



The reaction mixture of 71.5 μL (0.5 mmol) 4-phenylpyridine (PPY), 186.2 mg PdCl₂ (1.05 mmol), 41.0 mg NaOAc (0.5 mmol), 15 μL H₂O, and 150.0 mg SiO₂ was milled for 1.5 h. at 30 Hz. The reaction mixture was suspended in 15 mL of acetonitrile and filtered. The residue on the filter paper was rinsed with acetonitrile. Organic extracts were then combined and the solvent was evaporated under reduced pressure. The crude product was suspended in water, filtered, and rinsed with water, chloroform, and diethyl ether. The product was dried in the air and obtained as a yellow powder. (106.4 mg, 71 % isolated). Characterization data are consistent with those previously published.⁹

¹H NMR (DMSO-*d*₆, 600 MHz, δ/ppm): 9.26 (br.), 8.47 (br), 8.06 (br, 2H), 7.67 (t, *J* = 18.4 Hz, 2H), 7.45 (br, 1H), 7.07 (t, *J* = 25.3 Hz, 2H).

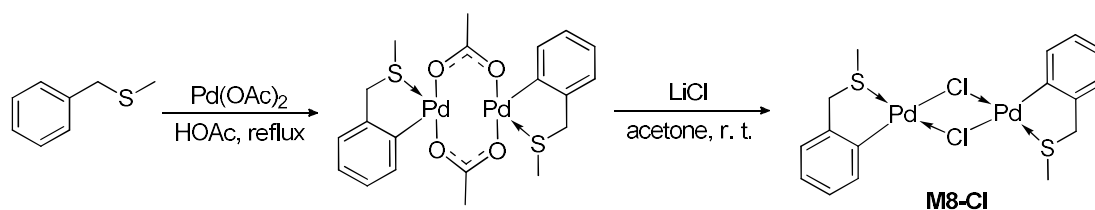
1.7 Synthesis of $[(\text{bhq})\text{Pd}(\mu\text{-Cl})_2]$ (**M7-Cl**)



The reaction mixture of 89.6 mg (0.5 mmol) of benzo[*h*]quinoline (bhq), 186.2 mg PdCl₂ (1.05 mmol), 41.0 mg (0.5 mmol) NaOAc, 15 μL H₂O, and 150.0 mg SiO₂ was milled for 1 h at 30 Hz. The reaction mixture was suspended in 15 mL of acetonitrile and filtered. The residue on the filter paper was rinsed with acetonitrile. Organic extracts were then combined and the solvent was evaporated under reduced pressure. The crude product was suspended in water, filtered, and rinsed with water, chloroform, and diethyl ether. The product was dried in the air and obtained as a yellow powder. (112.3 mg, 70 % isolated). Characterization data are consistent with those previously published.¹⁰

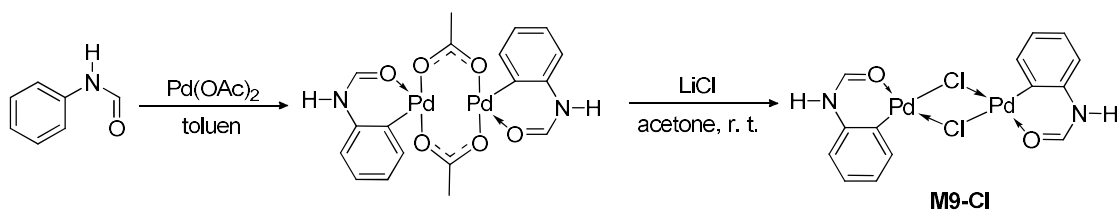
¹H NMR (DMSO-*d*₆, 600 MHz, δ/ppm): 9.47 (d, *J* = 4.6 Hz, 1H), 8.72 (d, *J* = 7.7, 1H), 8.24 (d, *J* = 7.2, 1H), 7.95 (d, *J* = 9.0, 1H), 7.91-7.78 (m, 3H), 7.78-7.70 (br), 7.69-7.60 (br), 7.55 (t, *J* = 7.5, 1H), 7.44-7.30 (br).

1.8 Synthesis of $[(\text{BMS})\text{Pd}(\mu\text{-Cl})_2]$ (**M8-Cl**)



Cyclopalladated dimeric complex **M8-Cl** was prepared according to a known procedure.¹¹ 200.0 mg (0.82 mmol) Pd(OAc)₂ was dissolved in 20 mL of concentrated HOAc. To this solution, 111.2 μL (0.82 mmol) benzyl methyl sulfide (BMS) was added, and the reaction mixture was refluxed for 8 h. Upon cooling, the reaction mixture was neutralized with a saturated aq. solution of NaHCO₃. The resulting yellowish precipitate was filtered, washed with water, and dried under reduced pressure. The dry product was stirred with 344.3 mg (8.12 mmol) of LiCl for 24 h in 10 mL of acetone. The resulting mixture was rinsed with water to remove LiCl and LiOAc, washed with acetone, and dried under reduced pressure. The product was isolated as yellowish powder insoluble in conventional solvents (155.2 mg, 68 % isolated).

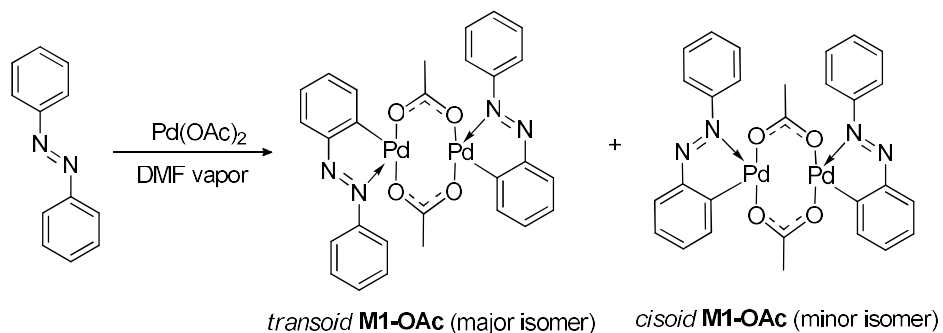
1.9 Synthesis of $[(AA)Pd(\mu-Cl)]_2$ (**M9-Cl**)



Cyclopalladated dimeric complex **M9-Cl** was prepared according to a known procedure.¹² 200.0 mg (0.82 mmol) $Pd(OAc)_2$ was dissolved in 20 mL of toluene. 110.6 mg (0.82 mmol) of acetanilide (AA) was added, and the reaction mixture was refluxed for 8 h and cooled to the ambient temperature afterwards. The resulting yellow-greenish precipitate was filtered, washed with water, and dried under reduced pressure. The dry product was then stirred for 24 h with 344.3 mg (8.12 mmol) of LiCl in 10 mL of acetone. The resulting mixture was rinsed with water to remove LiCl and LiOAc, washed with acetone and dried under reduced pressure. The product was obtained as a pale yellow powder (137.2 mg, 64 % isolated).

1H NMR (DMSO- d_6 , 300 MHz, δ /ppm): 11.44 (s, 1H), 7.65 (d, $J = 7.8$ Hz, 1H), 7.03 (br, 1H), 6.90 (br, 2H), 7.27 (s, 3H).

1.10 Synthesis of $[(C_6H_5N=NC_6H_4)Pd(\mu-OAc)]_2$ (**M1-OAc**)

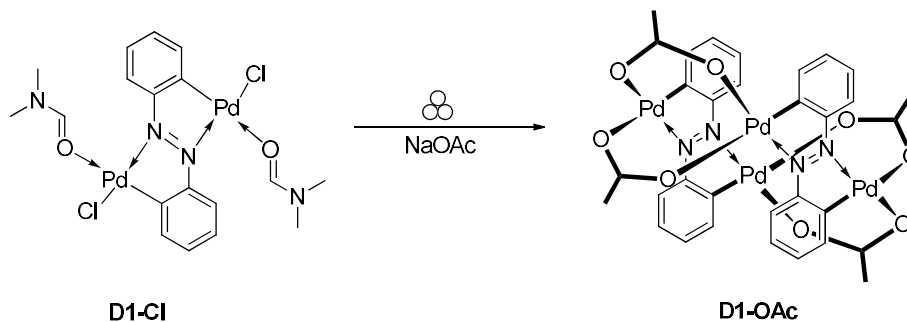


Monocyclopalladated dimeric complex **M1-OAc** was prepared using the accelerated aging method developed by our group.¹³ The mixture of 50.0 mg (0.27 mmol) of azobenzene and 61.6 mg (0.27 mmol) $Pd(OAc)_2$ was homogenized by gentle grinding in an agate mortar. It was put in a closed vial saturated with DMF vapors at ambient temperature for five days. The product was dried on air (97% isolated).

Transoid isomer: 1H NMR ($CDCl_3$, 600 MHz, δ /ppm): 7.70 (dd, $J = 7.7$ Hz, 1H), 7.37 (t, $J = 7.9$ Hz, 1H), 7.34 (d, $J = 8.1$ Hz, 2H), 7.25 (t, $J = 7.9$ Hz, 2H), 7.14 (dt, $J = 7.5$ Hz, 1H), 6.80 (dt, $J = 7.6$ Hz, 1H), 6.49 (dd, $J = 7.8$ Hz, 1H), 2.08 (s, 3H).

Cisoid isomer: 1H NMR ($CDCl_3$, 600 MHz, δ /ppm): 7.55 (dd, $J = 7.7$ Hz, 1H), 7.51 (d, $J = 8.1$ Hz, 2H), 7.37 (ovp., 1H), 7.19 (t, $J = 7.9$ Hz, 2H), 7.14 (ovp., 1H), 6.97 (dt, $J = 7.5$ Hz, 1H), 6.72 (dt, $J = 7.9$ Hz, 1H), 2.34 (s, 3H), 1.79 (3H, s).

1.11 Synthesis of $[\text{Pd}(\mu\text{-OAc})_2(\mu\text{-C}_6\text{H}_5\text{N}=\text{NC}_6\text{H}_4)\text{Pd}]_2$ (**D1-OAc**)



Dicyclopalladated dimeric complex **D1-OAc** was prepared using the solid-state anion exchange method developed by our group.¹⁴ The mixture of 40.0 mg (0.07 mmol) **D1-Cl** and 216.6 mg (2.64 mmol) NaOAc was milled for 3 h. The resulting mixture was washed with water, dried under reduced pressure, and recrystallized from CHCl_3 . The product was obtained as a black powder (28.3 mg, 84 % isolated). The procedure was repeated three times to obtain the product for the deuteration reaction. ^1H NMR (CDCl_3 , 600 MHz, δ/ppm): 8.03 (d, $J = 8.2$ Hz, 2H), 6.68-6.88 (m, 6H), 2.20 (s, 3H), 2.19 (s, 3H).

1.12 Deuteration of L-Cysteine

3.0 g of **L-Cys** was dissolved in 16 mL of D_2O . The solution was refluxed for 1 h, evaporated under reduced pressure, and cooled to ambient temperature. This procedure was repeated twice using a new portion of D_2O . The deuteration of cysteine was confirmed by IR and Raman spectroscopies (Figs. S83, S91 and S92).

1.13. Deuteration of 1-adamantanethiol and 4-chlorothiophenol

1.0 g of 1-adamantanethiol or 4-chlorothiophenol was dissolved in 15 mL EtOD. The solution was refluxed for 1 h, evaporated under reduced pressure, and cooled to ambient temperature. The procedure was repeated twice using a new portion of EtOD. The deuteration was confirmed by IR and ^1H NMR spectroscopies (Figs. S17, S18, S93 and S94).

1.14 Deuteration reactions – general procedures

The mixture of 0.14 mmol dimeric monocyclopalladated (**M1-Cl** - **M3-Cl**, **M6-Cl** - **M9-Cl**, **M1-OAc**) or monomeric dicyclopalladated complexes (**D1-Cl** - **D5-Cl**, **D1-OAc**) and 1.12 mmol of **Cys**^{4D} (4 equiv. *per* Pd) was milled at ambient temperature. In the reactions of monomeric monocyclopalladated complexes (**M4-Cl** and **M5-Cl**) with **Cys**^{4D}, 0.28 mmol of starting complex was used. The completeness of the reactions was confirmed by *in situ* Raman monitoring, where possible, and by recording ^1H NMR spectra of samples taken from the reaction mixtures. Reaction times, yields, and deuteration ratios are given in the manuscript. Reaction mixtures remained a powder throughout the milling process. The resulting organic products were suspended in 15 mL of *n*-hexane and filtered. The residue on the filter paper was washed with 2x5 mL of *n*-hexane. The extracts were then combined, and the solvent was evaporated under reduced pressure. The products obtained were dissolved in a small amount of

chloroform and further purified by column chromatography using SiO₂ as the solid phase and chloroform as the eluent.

In selected cases, after extraction with *n*-hexane, the solid residue was dried in air, washed with water to remove excess **Cys**^{4D}, and dried in air. The remaining insoluble brown residue of [Pd(**Cys**^{3D})₂] was obtained in good yield (80-87 %).

To confirm the formation of a cyclopalladated intermediate with cysteine coordinated to the palladium ion in the cyclopalladated complex, an additional experiment was performed. The reaction mixture of 90.3 mg (0.14 mmol) **M1-Cl**, 33.9 mg (0.28 mmol) native **Cys**, 26.5 mg (0.28 mmol) NaOAc, and 150.0 mg NaCl as milling auxiliary was milled for 75 min. The ¹H NMR spectrum of the resulting mixture confirmed the formation of the cyclopalladated intermediate **M1-1** (Figs. S63 and S64).

1.15 Optimization of the reactions conditions

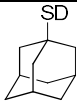

To optimize reaction conditions, **M1-Cl** (0.14 mmol) or **D1-Cl** (0.28 mmol) and 1.12 mmol **Cys**^{4D} (4 equiv. *per* palladium atom) were milled at ambient temperature for 8, 10, 15 and 24 h.

To screen for different D-sources, **D1-Cl** (0.28 mmol) was milled with 1.12 mmol of **D₂O**, **EtOD**, **ND₄Cl**, 1-adamantanethiol-*d*, 4-chlorothiophenol-*d* or **Cys**^{4D} for 15 h. After milling, reaction mixtures of **D1-Cl** and (1-adamantanethiol)-*d* or (4-chlorothiophenol)-*d* were a sticky paste due to the low melting point of the reactants. Conversion and deuteration degree were estimated by ¹H NMR.

In the case of **D1-Cl** additional reactions with NaOAc or DMAP (2.28 mmol) as solid additives as well as with D₂O (1.14 mmol) as a liquid additive were performed. The reaction mixtures were milled at ambient temperature for 15 h.

In the case of **M1-Cl** additional reaction with DMF (0.28 mmol) as a liquid additive was performed. The reaction mixture was milled at ambient temperature for 15 h.

Table S1. Optimization of reaction conditions.^a

Entry	Precursor	D-source	D-source equiv. <i>per</i> Pd	Solid additive	Liquid additive	<i>t</i> (h)	Deuteration (%) ^b	Yield ^c (%)
1	D1-Cl	D ₂ O	4	none	none	15	-	0
2	D1-Cl	EtOD	4	none	none	15	-	0
3	D1-Cl	ND ₄ Cl	4	none	none	15	-	0
4	D1-Cl		4	none	none	15	54	31
5	D1-Cl		4	none	none	15	-	trace
6	D1-Cl	Gly	4	none	none	15	-	0
7	D1-Cl	L-Ala	4	none	none	15	-	0
8	D1-Cl	Cys	1	none	none	15	-	22 ^d
9	D1-Cl	Cys	2	none	none	15	-	60 ^d
10	D1-Cl	Cys	4	none	none	15	-	79 ^d
11	D1-Cl	Cys ^{4D}	4	none	none	8	83	66
12	D1-Cl	Cys ^{4D}	4	none	none	10	84	72
12	D1-Cl	Cys ^{4D}	4	none	none	15	84	83
13	D1-Cl	Cys ^{4D}	4	none	none	24	84	82

14	D1-Cl	Cys ^{4D e}	10	none	none	15	85	80
16	D1-Cl	Cys ^{4D}	4	none	D ₂ O ^f	15	84	82
17	D1-Cl	Cys ^{4D}	4	NaOAc ^g	none	15	55	7
18	D1-Cl	Cys ^{4D}	4	DMAP ^g	none	15	-	trace
19	M1-Cl	Cys	1	none	none	15	-	10 ^d
20	M1-Cl	Cys	2	none	none	15	-	46 ^d
21	M1-Cl	Cys	4	none	none	15	-	88 ^d
22	M1-Cl	Cys ^{4D}	4	none	none	8	61	62
23	M1-Cl	Cys ^{4D}	4	none	none	10	61	70
24	M1-Cl	Cys ^{4D}	4	none	none	15	61	77
25	M1-Cl	Cys ^{4D}	4	none	none	24	61	78
26	M1-Cl	Cys ^{4D e}	10	none	none	15	62	79
27	M1-Cl	Cys ^{4D}	4	none	DMF ^h	24	60	40
28	1	Cys ^{4D i}	8	none	none	15	-	97 ^d
29	1	Cys ^{4D j}	8	none	none	15	-	97 ^d

^aReaction conditions: mixer mill, 30 Hz, 14 mL poly(methyl methacrylate) (PMMA) jar, one ZrO₂ milling ball (diameter 10 mm, 4.5 g), precursor (0.14 mmol), D-source (4 equiv. *per* Pd if not stated otherwise). ^bPercentage of deuteration (average for all magnetically equivalent nuclei) at the site of the D incorporation. ^cIsolated yield. ^dNative **1** was isolated. ^e20 equiv. *per* precursor (10 equiv. *per* Pd). ^f16 equiv. *per* precursor (8 equiv. *per* Pd). ^g2 equiv. *per* precursor (1 equiv. *per* Pd). ^hTwo equiv. *per* precursor (1 equiv. *per* Pd). ⁱ8 equiv. *per* precursor of Cys^{4D} and 5 mol% equiv. PdCl₂. ^j8 equiv. *per* precursor of Cys^{4D} and 1 equiv. of PdCl₂.

1.16 Mechanochemical synthesis of [Pd(Cys^{3D})₂]

The mixture of 200.0 mg (1.7 mmol) of native Cys and 146.0 mg (0.83 mmol) PdCl₂ were milled for 4 h at ambient temperature. The formation of [Pd(Cys^{3D})₂] complex was supported by the IR spectra (Fig. S104).

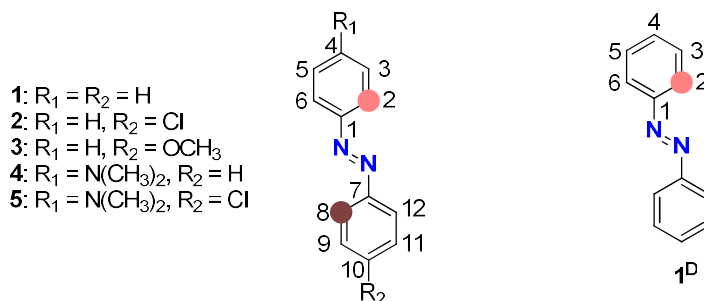
1.17 Computational details. Calculations were carried out using B3LYP hybrid functional combined with an empirical Grimme's D3 dispersion correction¹⁵ (B3LYP-D3) implemented in Gaussian16.¹⁶ Pd atoms were modeled by the Stuttgart–Dresden (SDD) pseudopotential and the accompanying SDD basis set.¹⁷ Standard 6-311+G** basis set was used for C, H/D, N, O, S and Cl atoms.

For the deuteration of the monocyclopalladated azobenzene additional methods apart from the B3LYP-D3/6-311+G**/SDD(Pd)/gas phase were tested: 1) a small basis set: B3LYP-D3/6-31G*/SDD(Pd)/gas phase; 2) no empirical dispersion correction: B3LYP/6-311+G**/SDD(Pd)/gas phase; 3) more modern basis set: B3LYP-D3/def2tzvp/gas phase; 4) more modern functional: ωB97x-D/6-311+G**/SDD(Pd)/gas phase; 5) solvation effects modeled with the polarizable continuum model (PCM)¹⁹ for DMF as implemented in Gaussian16: B3LYP-D3/6-311+G**/SDD(Pd)/PCM(DMF); 6) solvation effects modeled with the polarizable continuum model (PCM)¹⁹ for propanoic acid: B3LYP-D3/6-311+G**/SDD(Pd)/PCM(propanoic acid). Results are presented in Table S2.

Full geometry optimizations were accompanied by vibrational frequency calculations that identified calculated stationary points as minima (reactants and products) or first-order saddle points (transition states). Nature of the transition states was confirmed by intrinsic reaction coordinate (IRC) searches¹⁸ followed by full geometry optimizations. Reported energies are free energies given at 298.15 K and 1 atm. No additional corrections were applied.

2. ^1H NMR spectroscopy

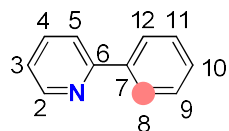
^1H NMR data for the deuterated products 1^{D} - 9^{D} and $1^{2\text{D}}$ - $5^{2\text{D}}$ (298 K, δ / ppm, J_{HH} / Hz). Signals are marked as s – singlet, d – doublet, t – triplet, m – multiplet. Atom numbering is given in the schemes below. Integrals of the signals assigned to hydrogens that are partly exchanged with deuterium are in red.



	1^{D} (CDCl_3)	$1^{2\text{D}}$ (CDCl_3)
H-2,6	7.92 dd, 3.39H $J = 8.1, 1.4$	7.92 dd, 1.16H $J = 8.3, 1.4$
H-3,4,5	7.55-7.46 m, 6H	7.55-7.47 m, 3H

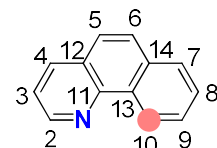
	2^{D} (CDCl_3)	$2^{2\text{D}}$ (CDCl_3)	3^{D} (CDCl_3)	$3^{2\text{D}}$ (CDCl_3)
H-2,6	7.87 d, 1.87H $J = 8.8$ Hz	7.88 d, 1.36H $J = 8.8$	7.93 d, 1.61H $J = 8.9$	7.93 d, 1.22H $J = 9.6$
H-3,5	7.50 t, 2H $J = 7.0$	7.51 t, 2H $J = 7.5$	7.51 t, 2H $J = 6.7$	7.49 t, 2H $J = 6.8$
H-4	7.56-7.46 m, 1H	7.56-7.46 m, 1H	7.44 t, 1H $J = 6.9$	7.43 t, 1H $J = 6.9$
H-8,12	7.91 dd, 1.50H $J = 8.3, 1.9$	7.91 dd, 1.12H $J = 8.4, 1.6$	7.88 dd, 1.65H $J = 8.2, 1.5$	7.88 d, 1.14H $J = 7.8$
H-9,11	7.56-7.46 m, 2H	7.56-7.46 m, 2H	7.02 d, 2H $J = 8.9$	7.02 d, 2H $J = 8.8$
CH_3	-	-	3.90 s, 3H	3.90 s, 3H

	4^{D} (CDCl_3)	$4^{2\text{D}}$ (CDCl_3)	5^{D} (CDCl_3)	$5^{2\text{D}}$ (CDCl_3)
H-2,6	7.89 d, 1.44H $J = 9.3$	7.88 d, 1.29H $J = 9.3$	7.86 d, 1.48H $J = 9.2$	7.87 d, 1.22H $J = 9.2$
H-3,5	6.76 d, 2H $J = 9.3$	6.80-6.74 m, 2H	6.75 d, 2H $J = 9.2$	6.77-6.74 m, 2H
H-8,12	7.85 dd, 2H $J = 8.5, 1.1$	7.84 dd, 1.21H $J = 8.5, 1.1$	7.79 d, 2H $J = 8.7$	7.78 d, 1.30H $J = 8.7$
H-9,11	7.48 t, 2H $J = 7.5$	7.51-7.45 m, 2H	7.43 d, 2H $J = 7.3$	7.45-7.42 m, 2H
H-10	7.38 t, 1H $J = 7.3$	7.41 t, 1H $J = 7.3$	-	-
CH_3	3.08 s, 6H	3.08 s, 6H	3.09 s, 6H	3.09 s, 6H



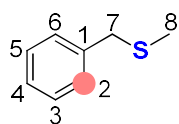
2-phenylpyridine (6)

	6^p (CDCl₃)
H-2	8.71-8.68 m, 1H
H-3	7.24-7.21 m, 1H
H-4	7.77-7.72 m, 2H
H-5	7.77-7.72 m, 2H
H-8,12	8.00 d, 1.31H <i>J</i> = 8.0
H-9,11	7.48 t, 2H <i>J</i> = 7.3
H-10	7.43-7.40 m, 1H

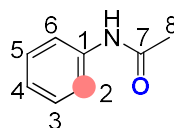


benzo[*h*]quinoline (7)

	7^p (CDCl₃)
H-2	9.01 dd, 1H <i>J</i> = 4.6, 1.7
H-3	7.54 dd, 1H <i>J</i> = 8.3, 4.3
H-4	8.19 dd, 1H <i>J</i> = 8.1, 1.8
H-5	7.70 d, 1H <i>J</i> = 8.8
H-6	7.82 d, 1H <i>J</i> = 8.8
H-7	7.92 dd, 1H <i>J</i> = 7.6, 1.6
H-8	7.79-7.72 m, 2H
H-9	7.79-7.72 m, 2H
H-10	9.30 d, 0.31H <i>J</i> = 8.5



benzyl methyl sulphide (8)



acetanilide (9)

	8^p (DMSO-<i>d</i>₆)	9^p (DMSO-<i>d</i>₆)
H-2,6	7.35-7.27 m, 1.29H	7.57 dd, 1.39H <i>J</i> = 8.8, 0.9
H-3,5	7.35-7.27 m, 2H	7.28 t, 2H <i>J</i> = 7.9
H-4	7.27-7.21 m, 1H	7.01 t, 1H <i>J</i> = 7.4
H-7	3.68 s, 2H	-
H-8	1.94 s, 3H	2.03 s, 3H
NH	-	9.90 s, 1H

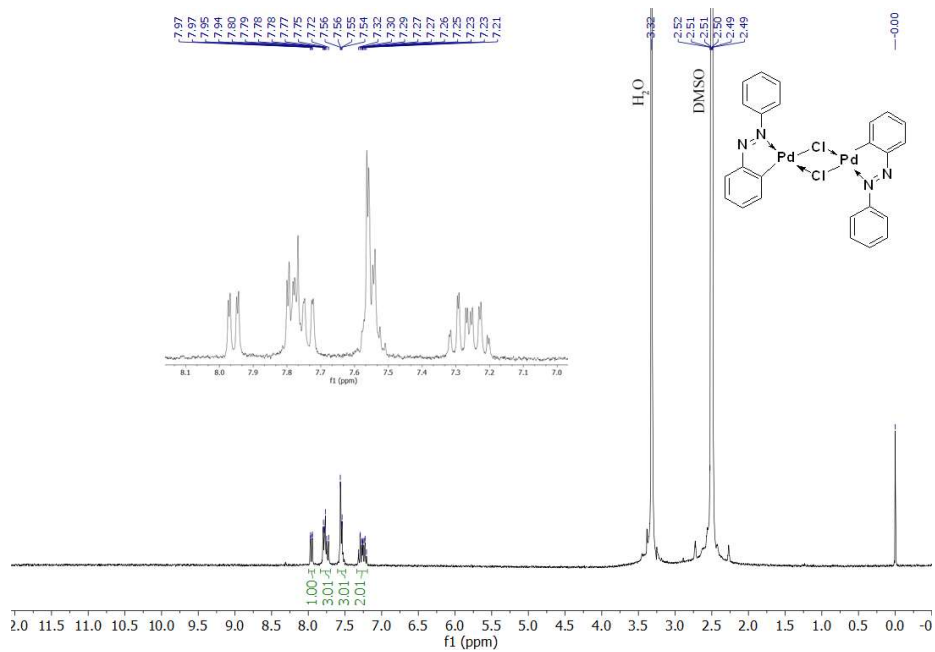


Fig. S1. ^1H NMR spectrum of **M1-Cl** in $\text{DMSO-}d_6$ at 298 K (300 MHz).

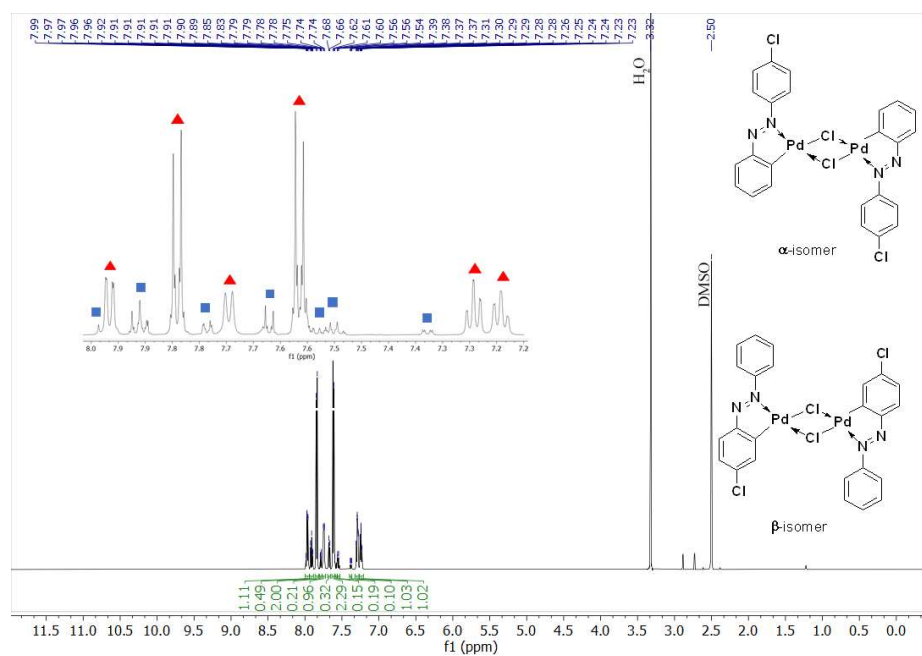


Fig. S2. ^1H NMR spectrum of **M2-Cl** in $\text{DMSO-}d_6$ at 298 K (600 MHz). α -isomer signals marked with red rectangles and β -isomer signals with blue squares.

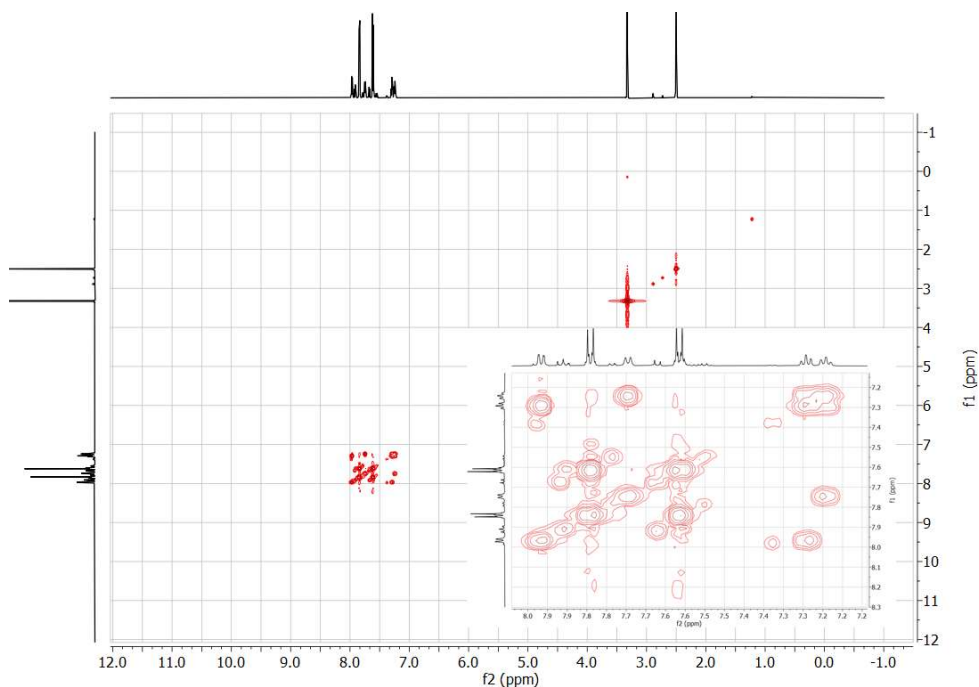


Fig. S3. 2D ^1H - ^1H COSY NMR spectrum of **M2-Cl** in $\text{DMSO-}d_6$ at 298 K (600 MHz).

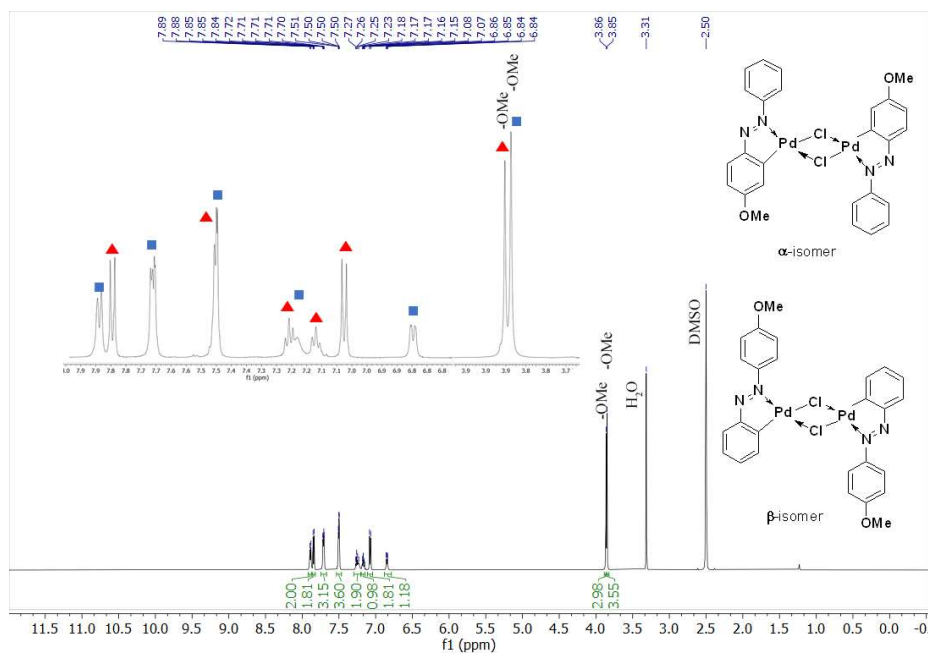


Fig. S4. ^1H NMR spectrum of **M3-Cl** in $\text{DMSO-}d_6$ at 298 K (600 MHz). α -isomer signals marked with red rectangles and β -isomer signals with blue squares.

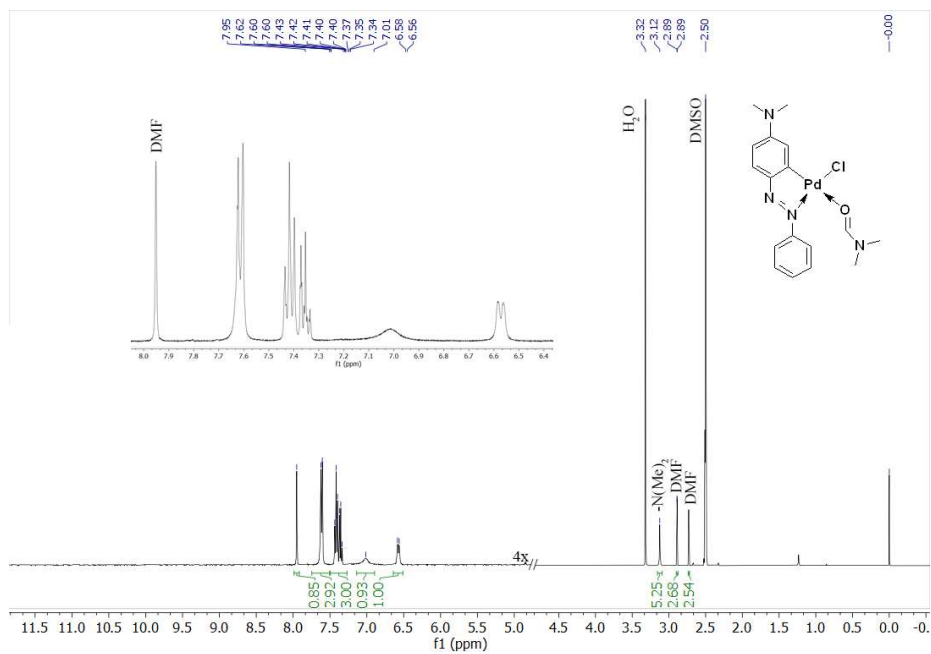


Fig. S5. ^1H NMR spectrum of **M4-Cl** in $\text{DMSO-}d_6$ at 298 K (600 MHz).

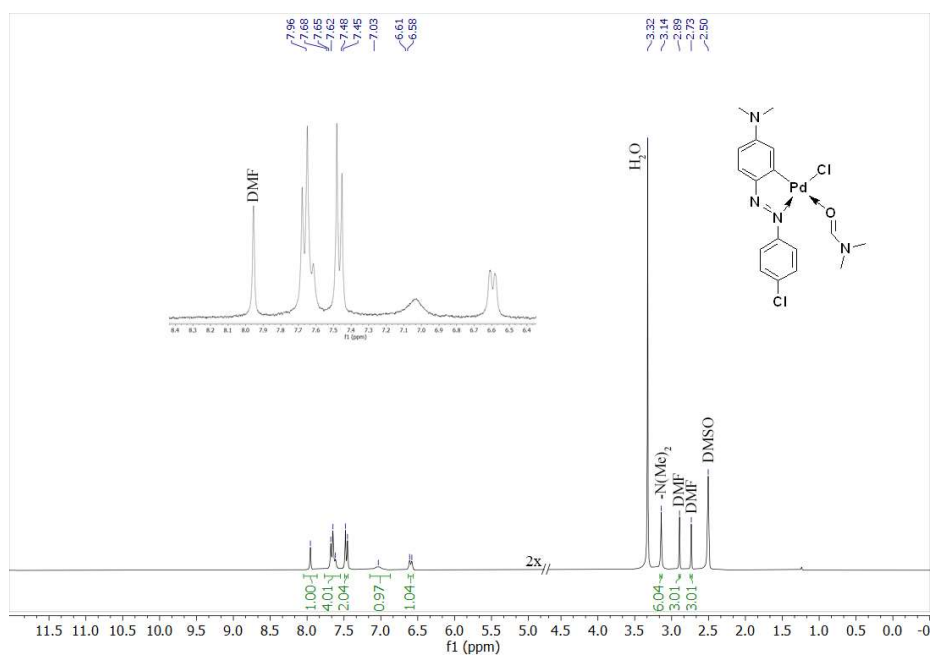


Fig. S6. ^1H NMR spectrum of **M5-Cl** in $\text{DMSO-}d_6$, at 298 K (600 MHz).

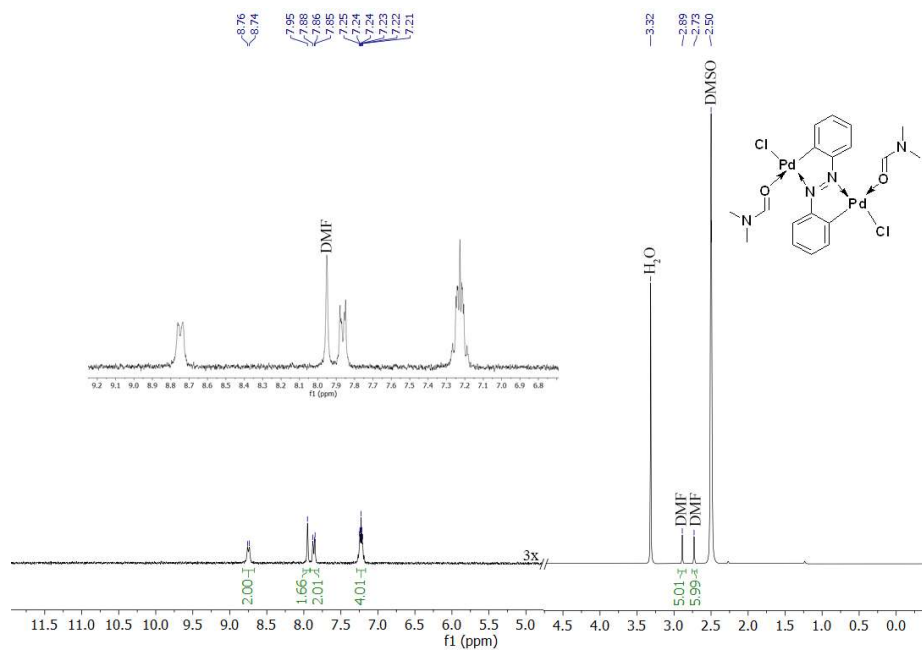


Fig. S7. ^1H NMR spectrum of **D1-Cl** in $\text{DMSO-}d_6$ at 298 K (300 MHz).

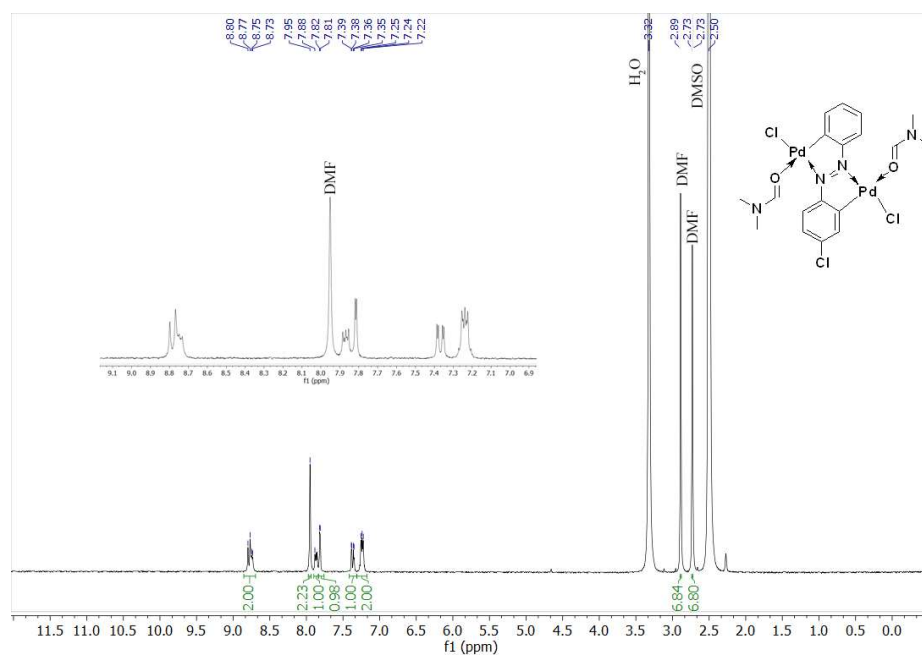


Fig. S8. ^1H NMR spectrum of **D2-Cl** in $\text{DMSO-}d_6$ at 298 K (300 MHz).

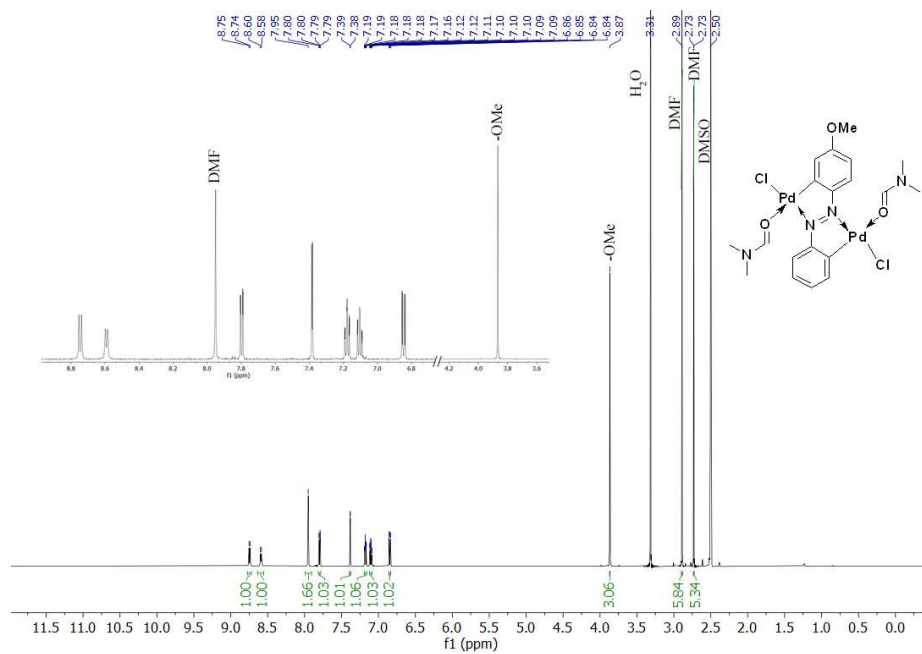


Fig. S9. ^1H NMR spectrum of D3-Cl in DMSO- d_6 at 298 K (600 MHz).

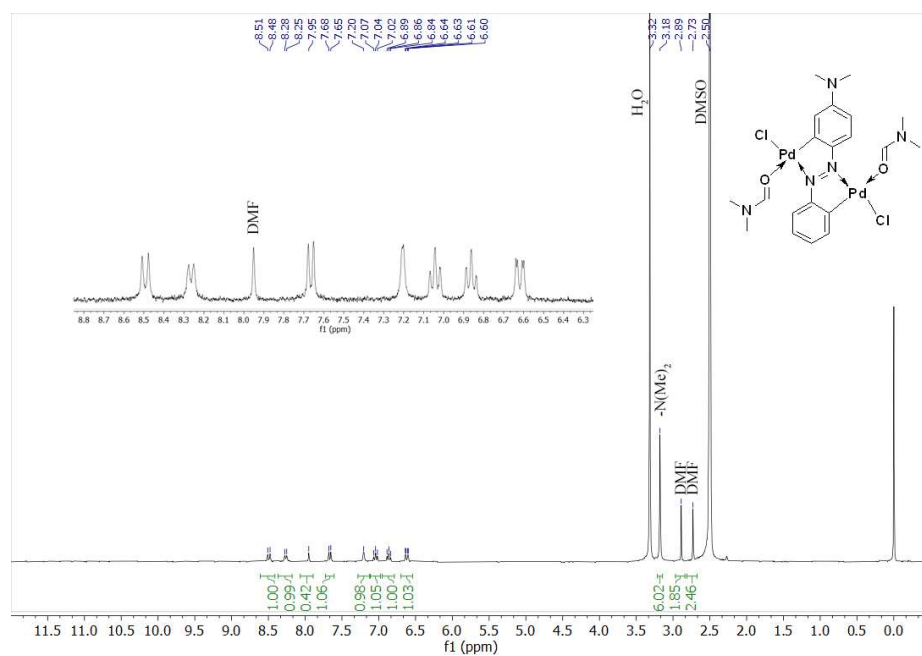


Fig. S10. ^1H NMR spectrum of D4-Cl in DMSO- d_6 at 298 K (300 MHz).

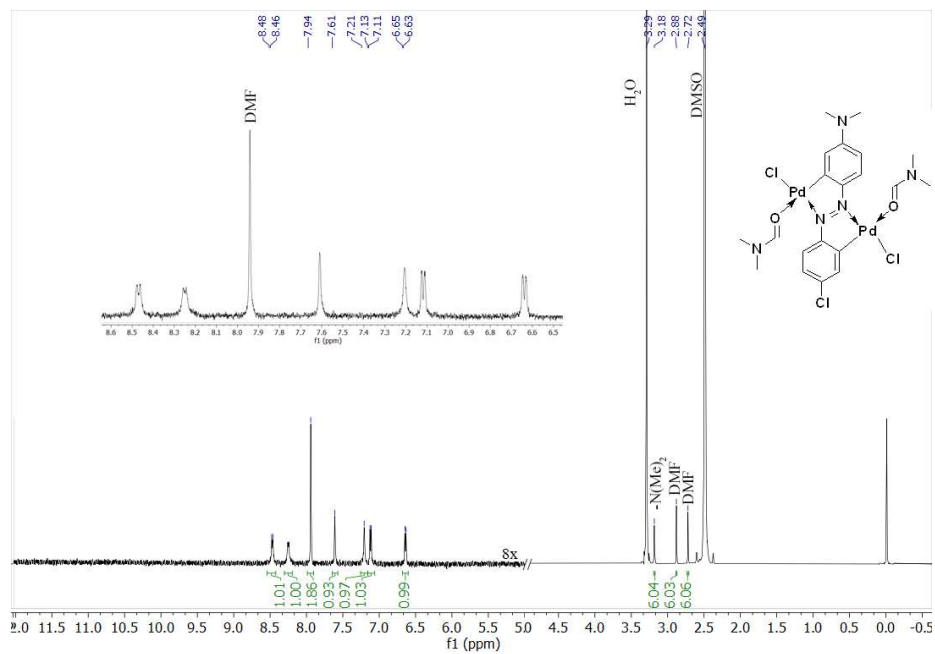


Fig. S11. ^1H NMR spectrum of **D5-Cl** in $\text{DMSO-}d_6$ at 298 K (300 MHz).

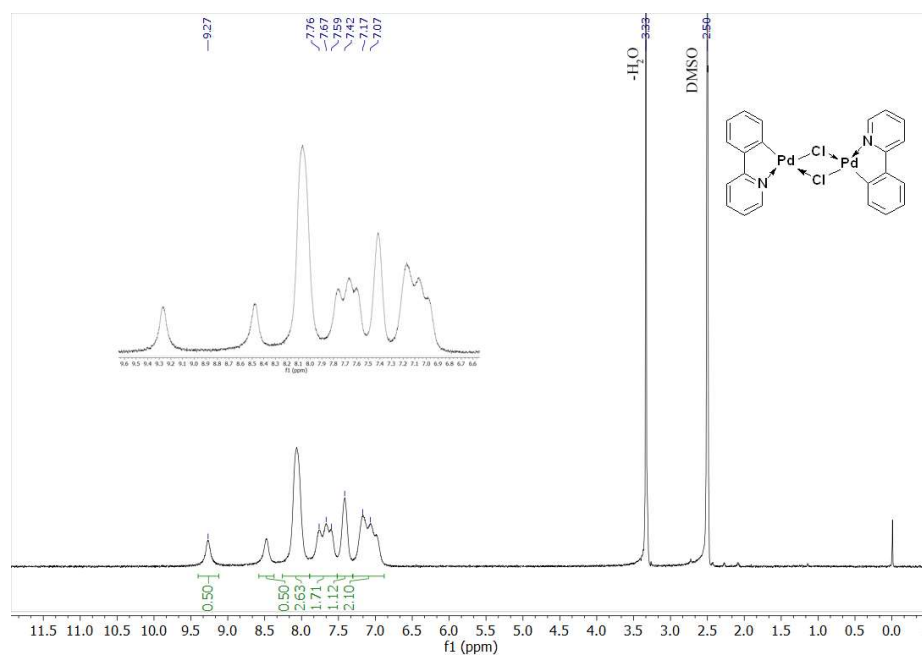


Fig. S12. ^1H NMR spectrum of **M6-Cl** in $\text{DMSO-}d_6$ at 298 K (300 MHz).

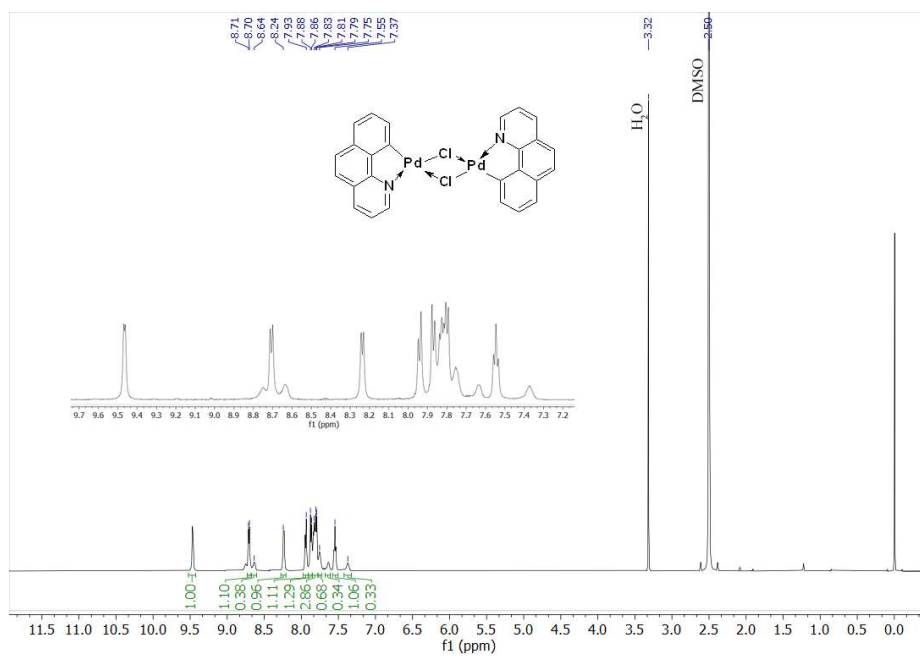


Fig. S13. ^1H NMR spectrum of **M7-Cl** in $\text{DMSO-}d_6$ at 298 K (600 MHz).

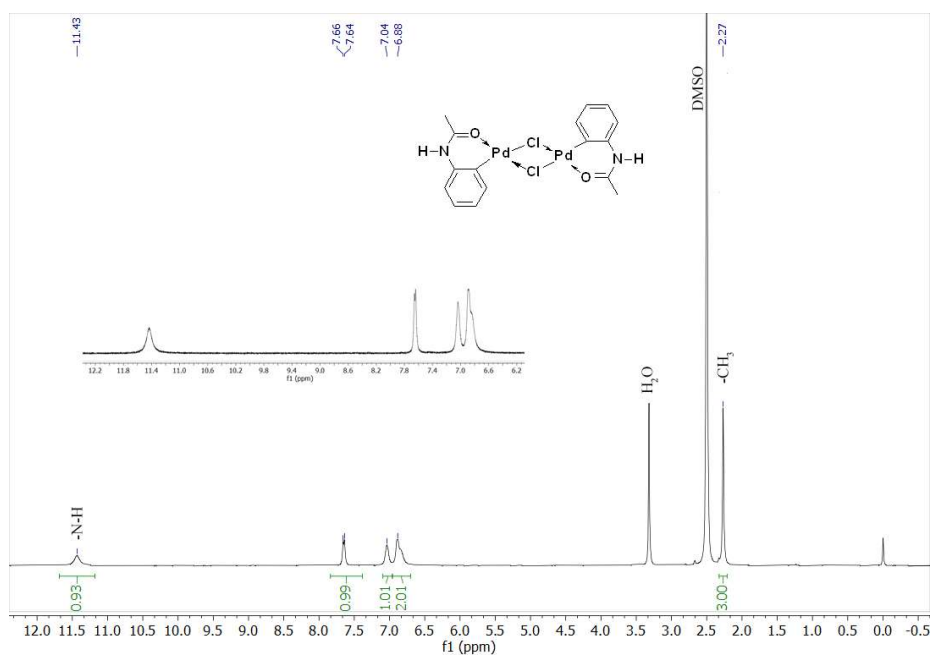


Fig. S14. ^1H NMR spectrum of **M9-Cl** in $\text{DMSO-}d_6$ at 298 K (300 MHz).

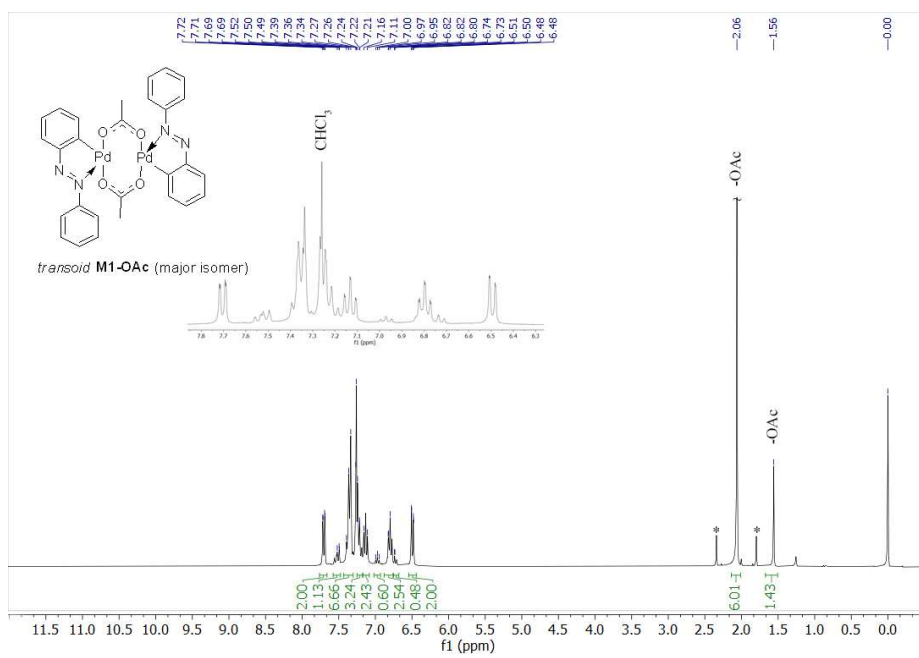


Fig. S15. ¹H NMR spectrum of **M1-OAc** in CDCl₃ at 298 K (600 MHz).

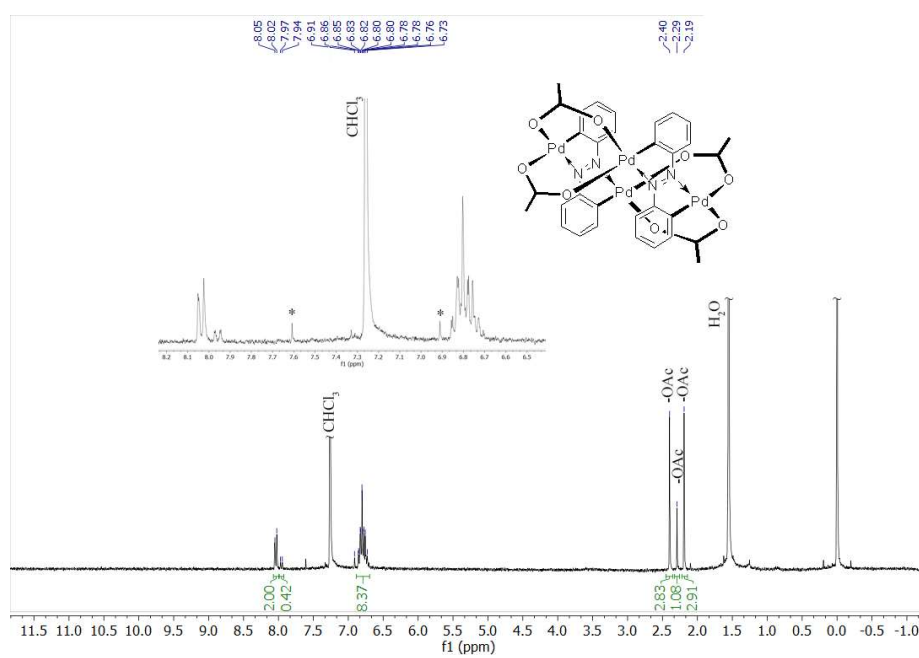


Fig. S16. ¹H NMR spectrum of **D1-OAc** in DMSO-*d*₆ at 298 K (600 MHz).

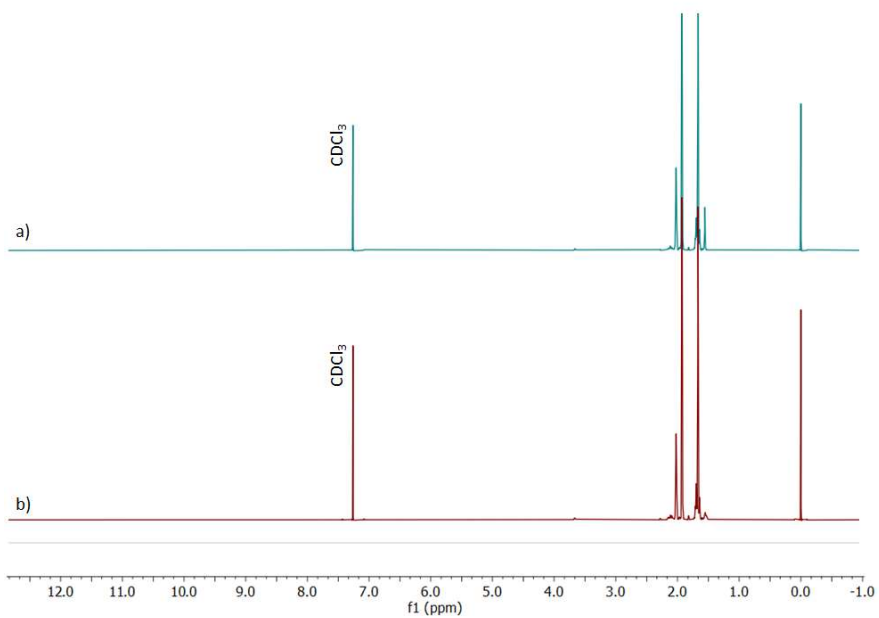


Fig. S17. ¹H NMR spectra of a) native and b) deuterated 1-adamantanethiol in CDCl₃ at 298 K (600 MHz).

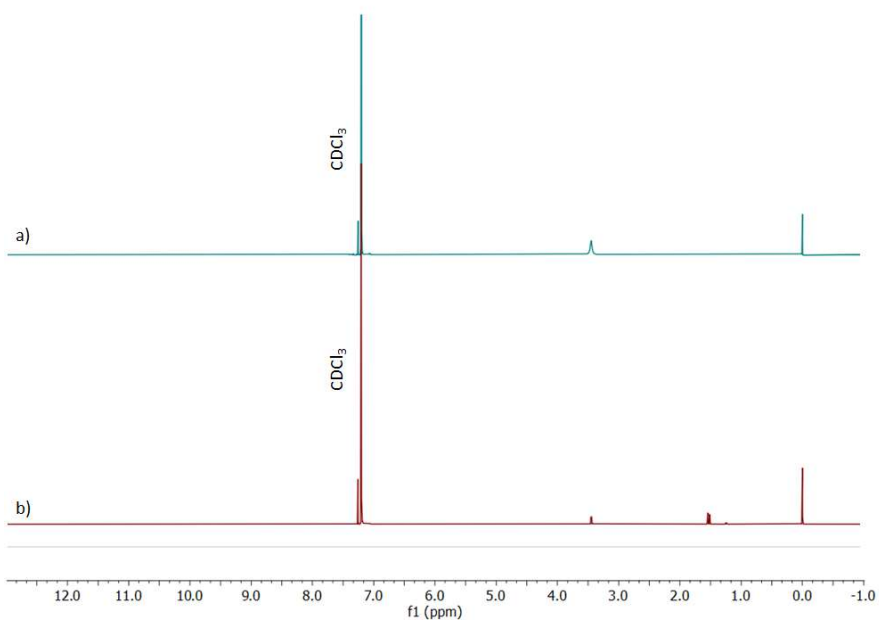


Fig. S18. ¹H NMR spectra of a) native and b) deuterated *p*-chlorothiophenol in CDCl₃ at 298 K (600 MHz).

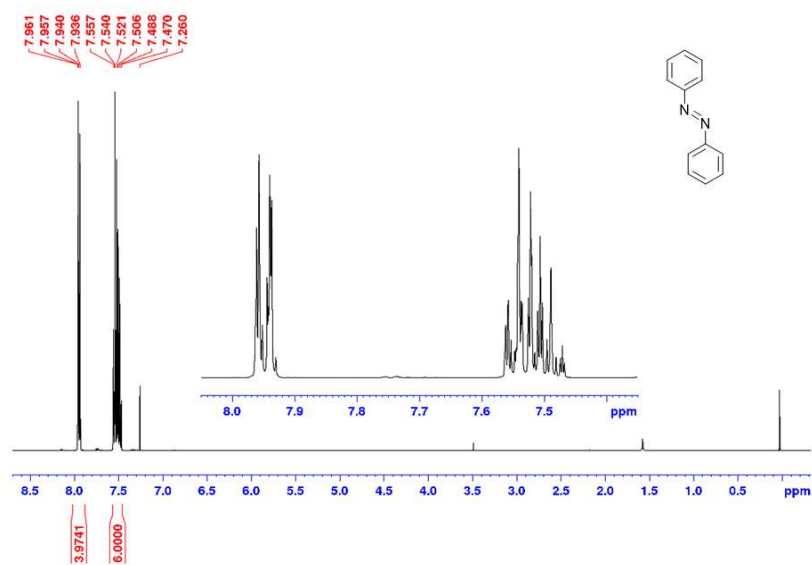


Fig. S19. ¹H NMR spectrum of native **1** in CDCl₃ at 298 K (400 MHz).

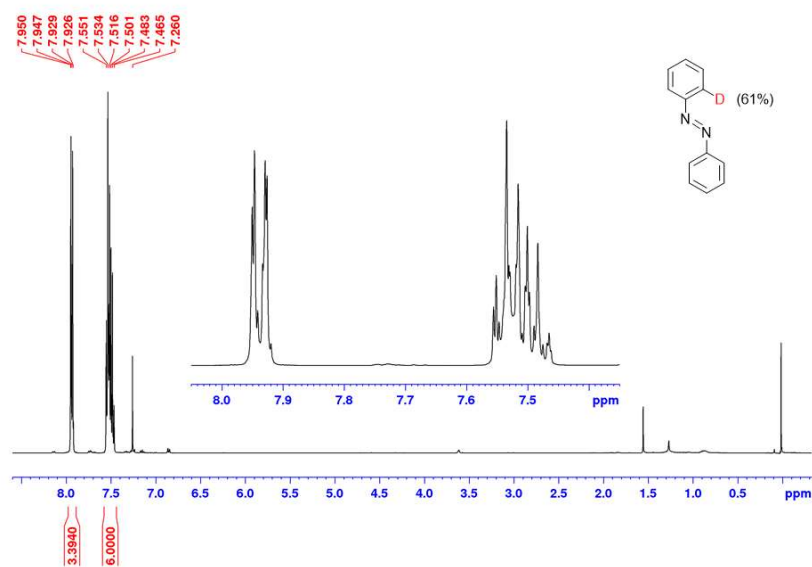


Fig. S20. ¹H NMR spectrum in CDCl₃ at 298 K (400 MHz) of **1^D** synthesized by the reaction of **M1-Cl** (0.14 mmol) and **Cys^{4D}** (1.12 mmol) under ball-milling conditions.

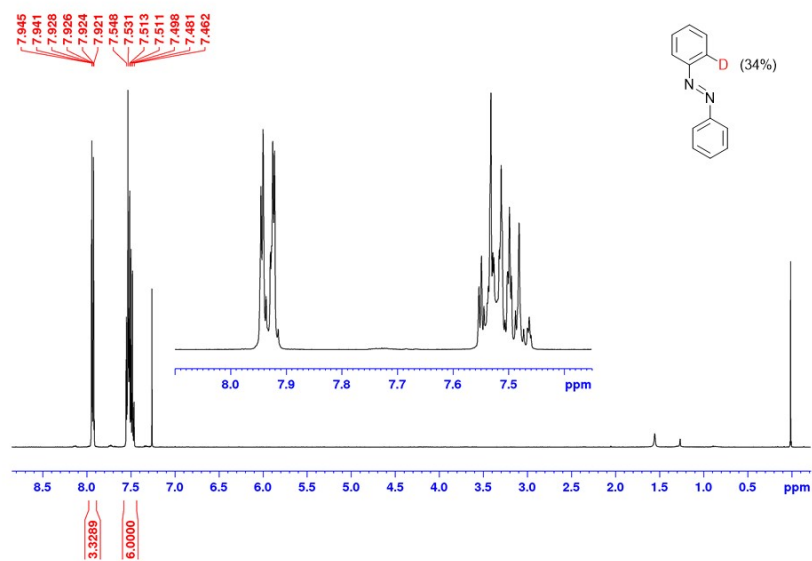


Fig. S21. ¹H NMR spectrum in CDCl₃ at 298 K (400 MHz) of **1^P** synthesized by the reaction of **M1-OAc** (0.14 mmol) and **Cys^{4D}** (1.12 mmol) under ball-milling conditions.

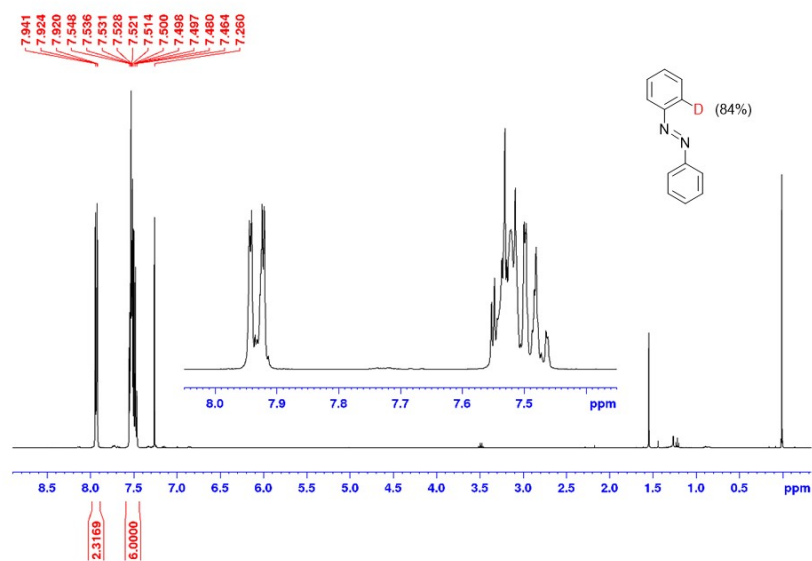


Fig. S22. ¹H NMR spectrum in CDCl₃ at 298 K (400 MHz) of **1^{2D}** synthesized by the reaction of **D1-Cl** (0.14 mmol) and **Cys^{4D}** (1.12 mmol) under ball-milling conditions.

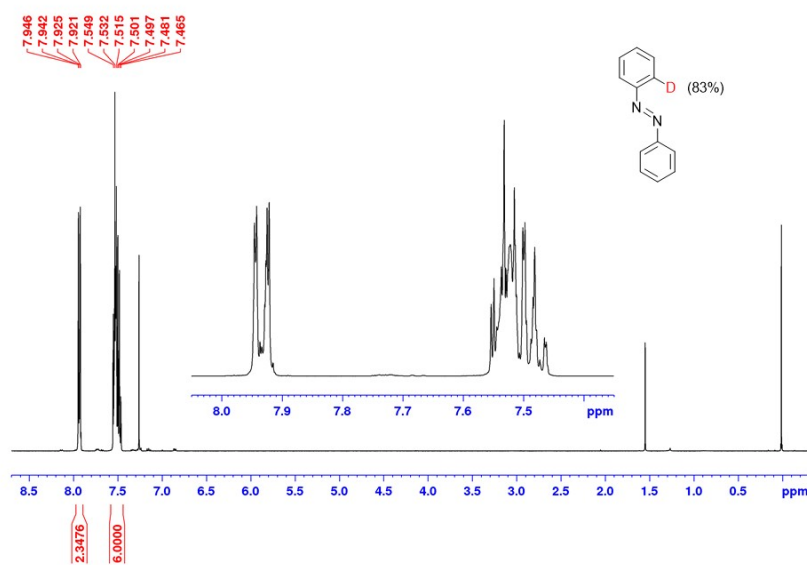


Fig. S23. ¹H NMR spectrum in CDCl₃ at 298 K (400 MHz) of **12D** synthesized by the reaction of **D1-OAc** (0.14 mmol) and **Cys^{4D}** (1.12 mmol) under ball-milling conditions.

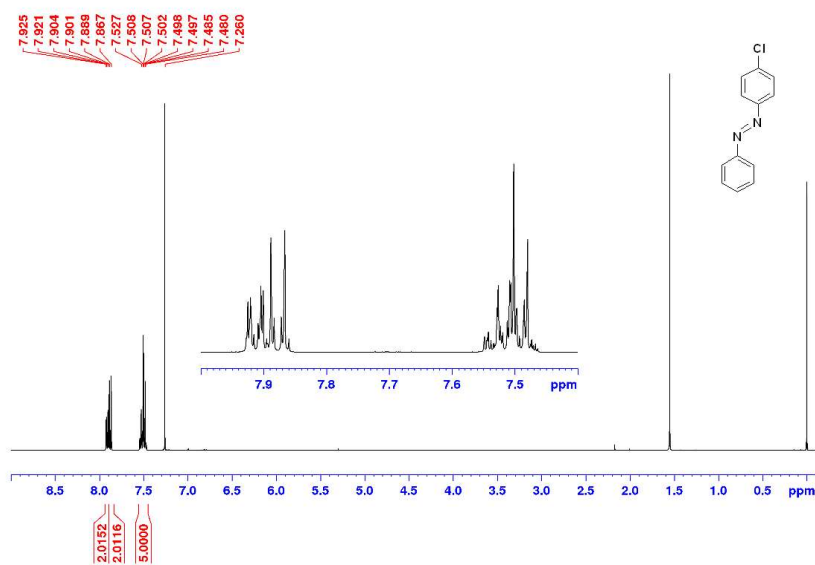


Fig. S24. ¹H NMR spectrum of native **2** in CDCl₃ at 298 K (400 MHz).

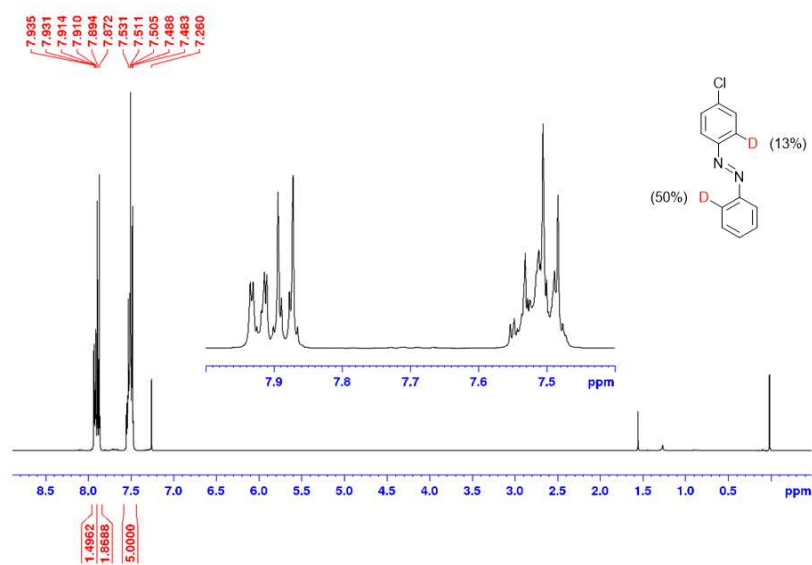


Fig. S25. ¹H NMR spectrum in CDCl₃ at 298 K (400 MHz) of **2^D** synthesized by the reaction of **M2-Cl** (0.14 mmol) and **Cys^{4D}** (1.12 mmol) under ball-milling conditions.

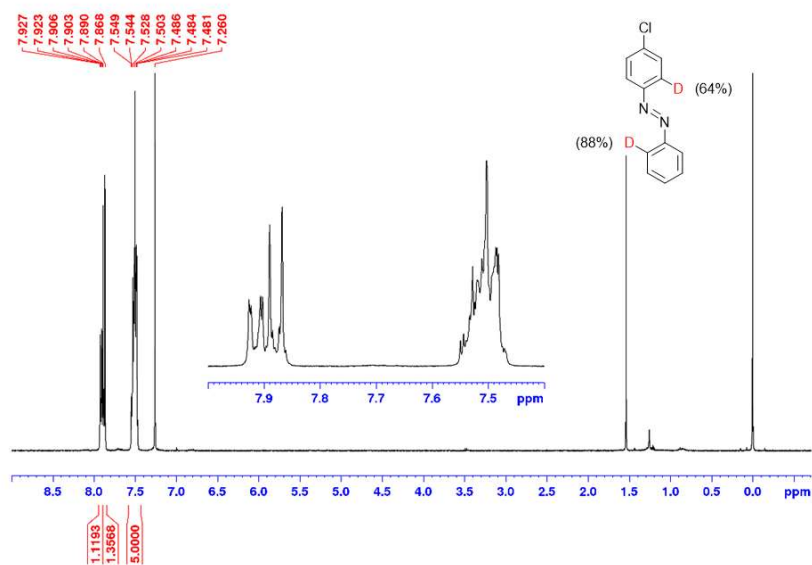


Fig. S26. ¹H NMR spectrum in CDCl₃ at 298 K (400 MHz) of **2^{2D}** synthesized by the reaction of **D2-Cl** (0.14 mmol) and **Cys^{4D}** (1.12 mmol) under ball-milling conditions.

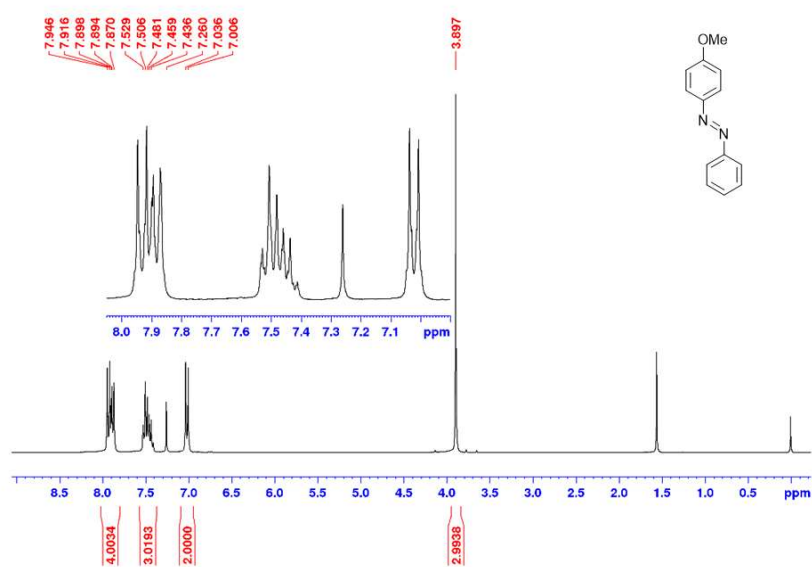


Fig. S27. ^1H NMR spectrum of native **3** in CDCl_3 at 298 K (400 MHz).

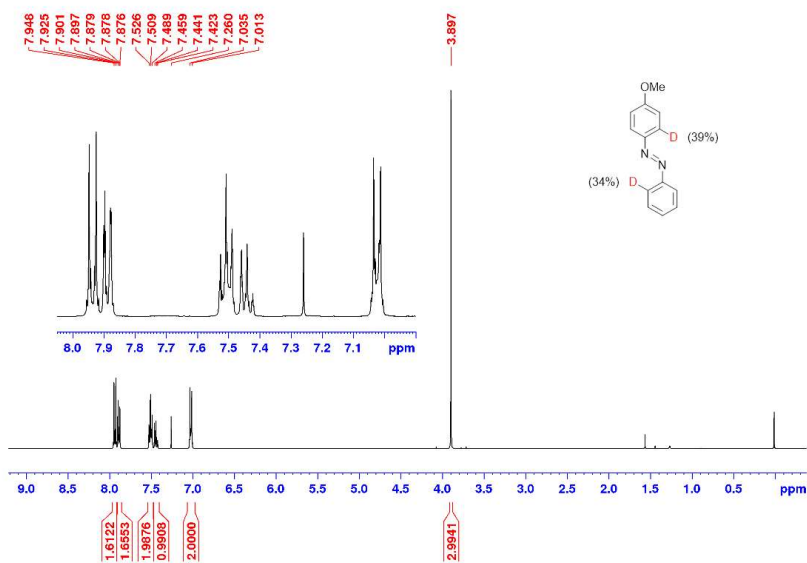


Fig. S28. ^1H NMR spectrum in CDCl_3 at 298 K (400 MHz) of **3^D** synthesized by the reaction of **M3-Cl** (0.14 mmol) and **Cys^{4D}** (1.12 mmol) under ball-milling conditions.

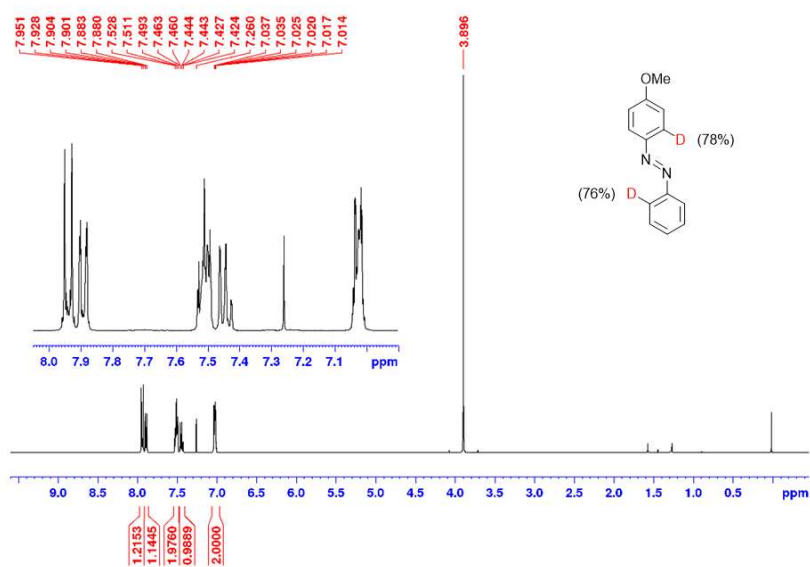


Fig. S29. ¹H NMR spectrum in CDCl₃ at 298 K (400 MHz) of **3^{2D}** synthesized by the reaction of **D3-Cl** (0.14 mmol) and **Cys^{4D}** (1.12 mmol) under ball-milling conditions.

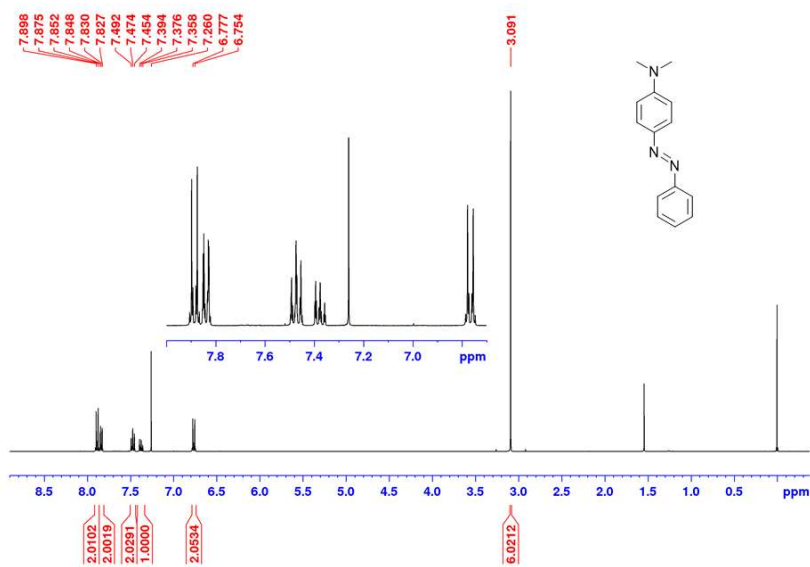


Fig. S30. ¹H NMR spectrum of native **4** in CDCl₃ at 298 K (400 MHz).

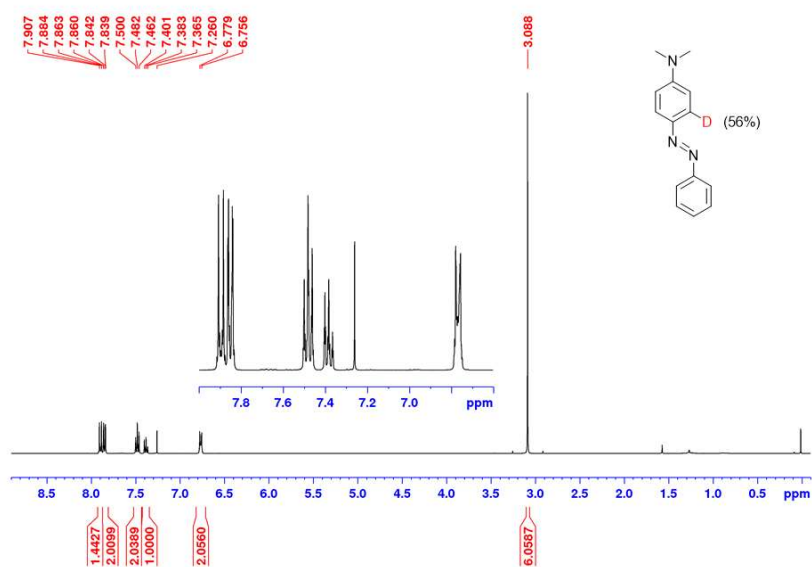


Fig. S31. ¹H NMR spectrum in CDCl₃ at 298 K (400 MHz) of **4^D** synthesized by the reaction of **M4-Cl** (0.28 mmol) and **Cys^{4D}** (1.12 mmol) under ball-milling conditions.

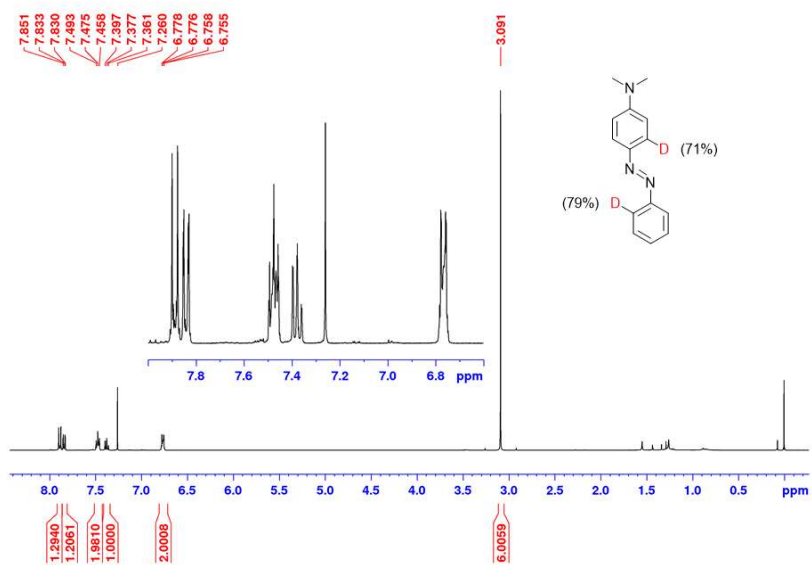


Fig. S32. ¹H NMR spectrum in CDCl₃ at 298 K (400 MHz) of **4^{2D}** synthesized by the reaction of **D4-Cl** (0.14 mmol) and **Cys^{4D}** (1.12 mmol) under ball-milling conditions.

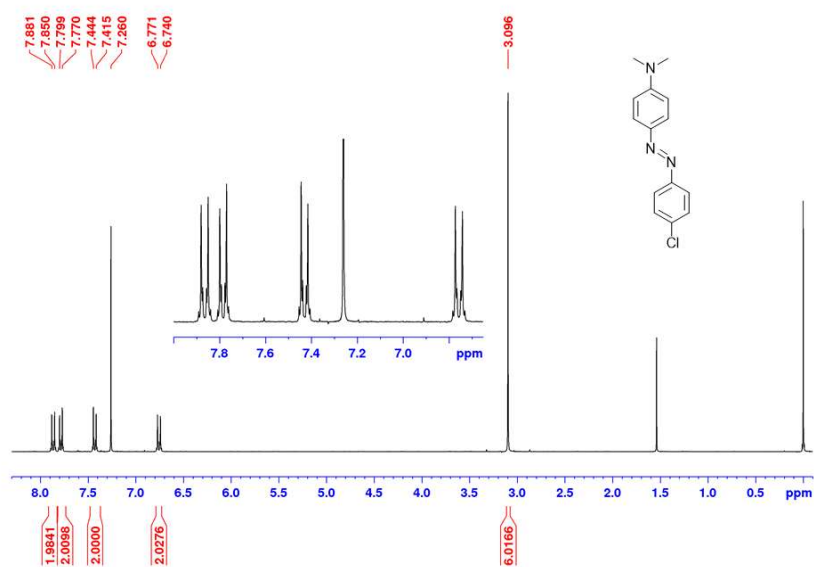


Fig. S33. ^1H NMR spectrum of native **5** in CDCl_3 at 298 K (400 MHz).

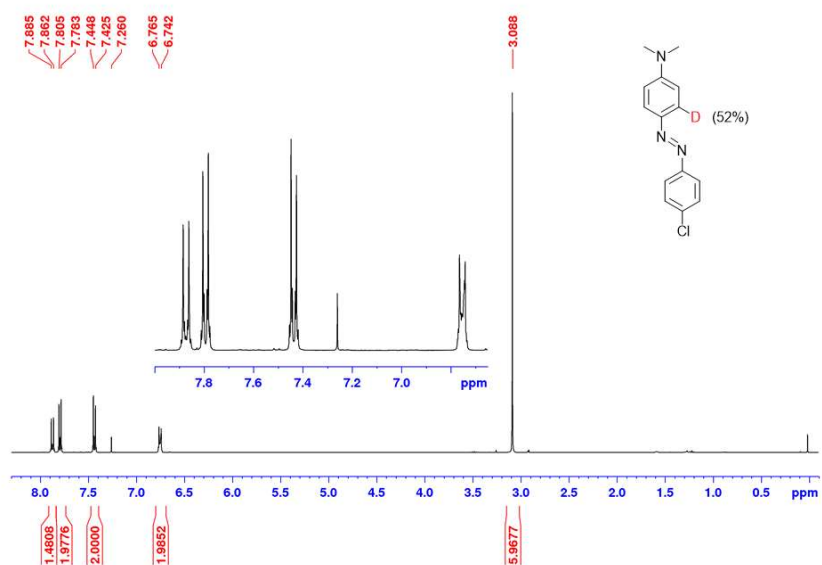


Fig. S34. ^1H NMR spectrum in CDCl_3 at 298 K (400 MHz) of **5^D** synthesized by the reaction of **M5-Cl** (0.28 mmol) and **Cys^{4D}** (1.12 mmol) under ball-milling conditions.

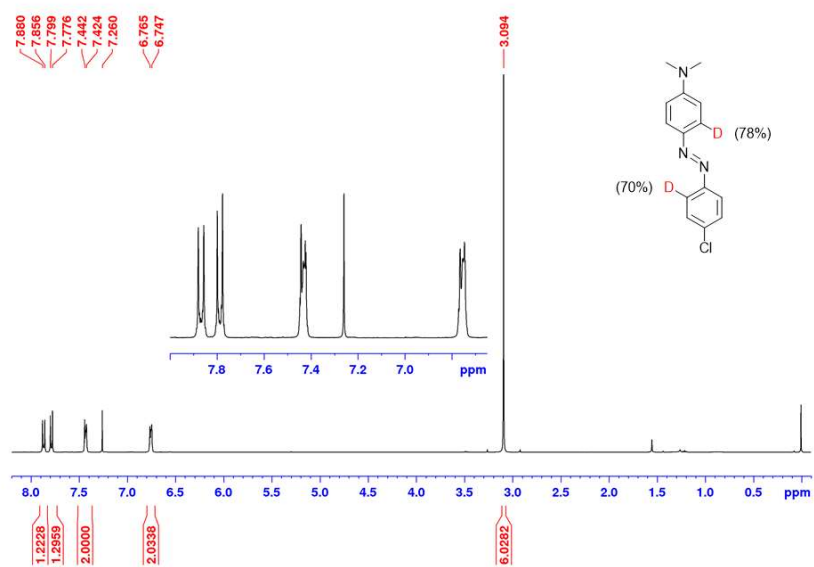


Fig. S35. ^1H NMR spectrum in CDCl_3 at 298 K (400 MHz) of 5^{2D} synthesized by the reaction of D5-Cl (0.14 mmol) and Cys^{4D} (1.12 mmol) under ball-milling conditions.

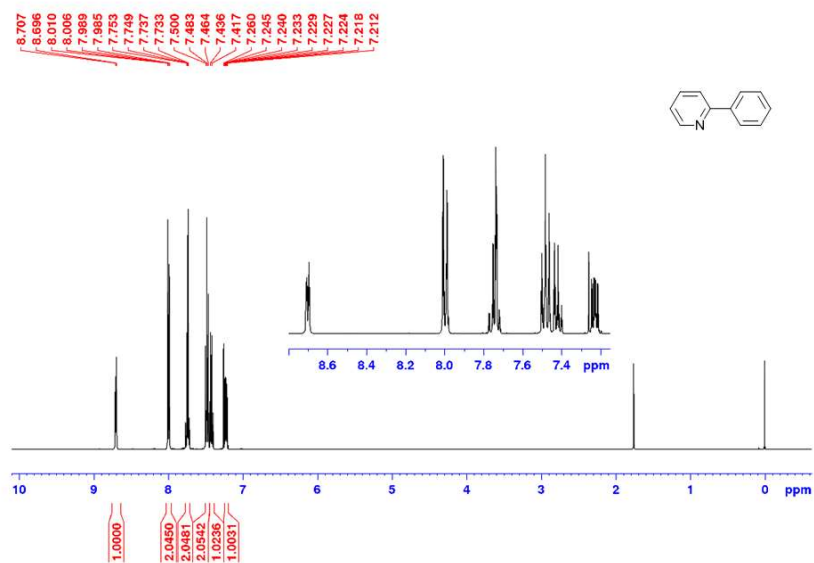


Fig. S36. ^1H NMR spectrum of native **6** in CDCl_3 at 298 K (400 MHz).

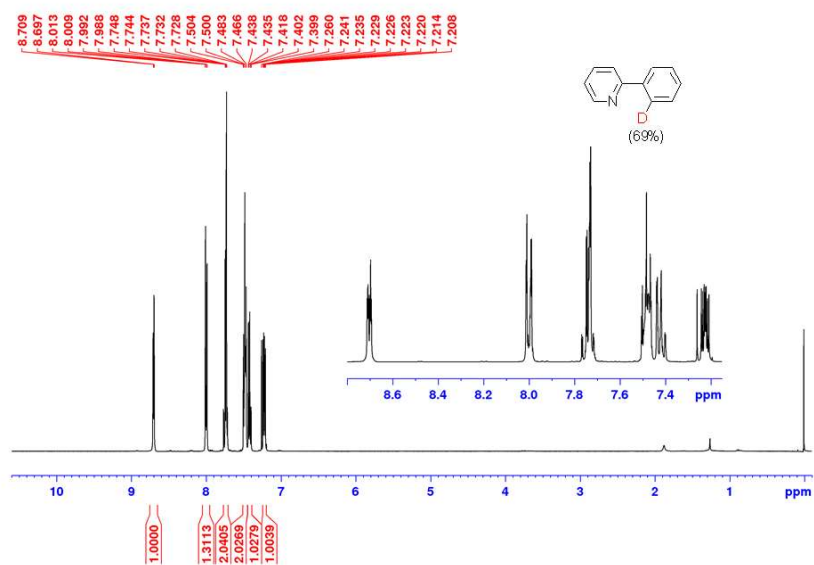


Fig. S37. ¹H NMR spectrum in CDCl₃ at 298 K (400 MHz) of **6P** synthesized by the reaction of **M6-Cl** (0.14 mmol) and **Cys**^{4D} (1.12 mmol) under ball-milling conditions.

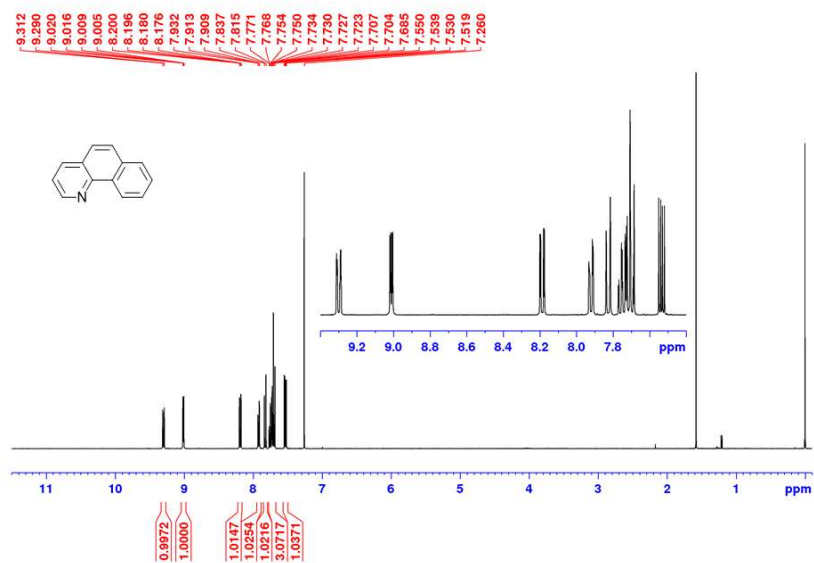


Fig. S38. ¹H NMR spectrum of native **7** in CDCl₃ at 298 K (400 MHz).

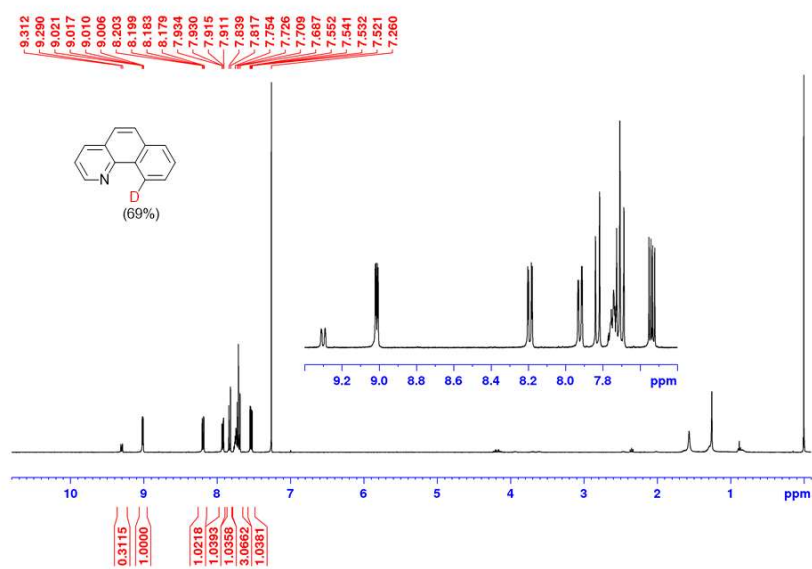


Fig. S39. ¹H NMR spectrum in CDCl₃ at 298 K (400 MHz) of **7D** synthesized by the reaction of **M7-Cl** (0.14 mmol) and **Cys^{4D}** (1.12 mmol) under ball-milling conditions.

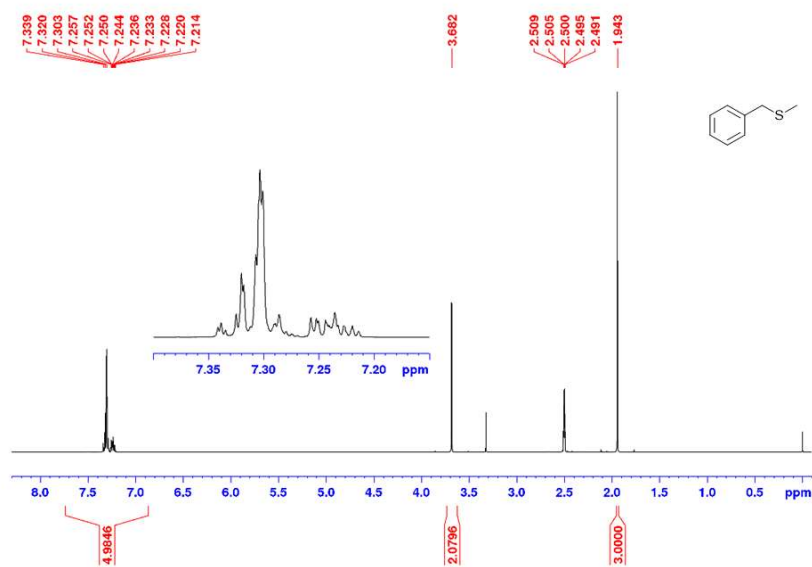


Fig. S40. ¹H NMR spectrum of native **8** in DMSO-*d*₆ at 298 K (400 MHz).

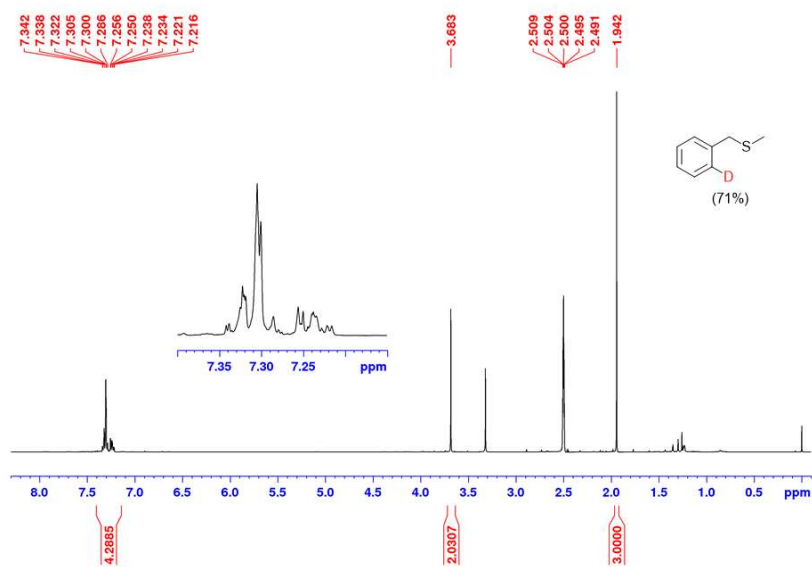


Fig. S41. ^1H NMR spectrum in $\text{DMSO-}d_6$ at 298 K (400 MHz) of **8P** synthesized by the reaction of **M8-Cl** (0.14 mmol) and **Cys^{4D}** (1.12 mmol) under ball-milling conditions.

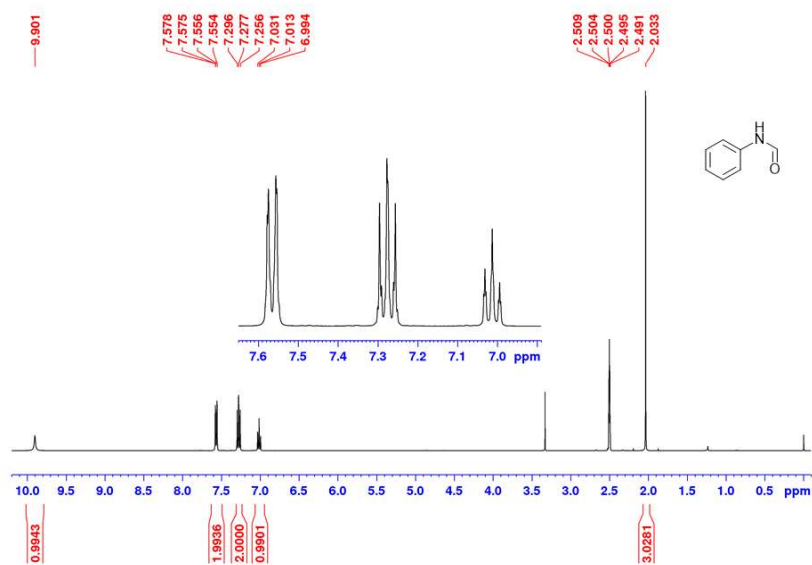


Fig. S42. ^1H NMR spectrum of native **9** in $\text{DMSO-}d_6$ at 298 K (400 MHz).

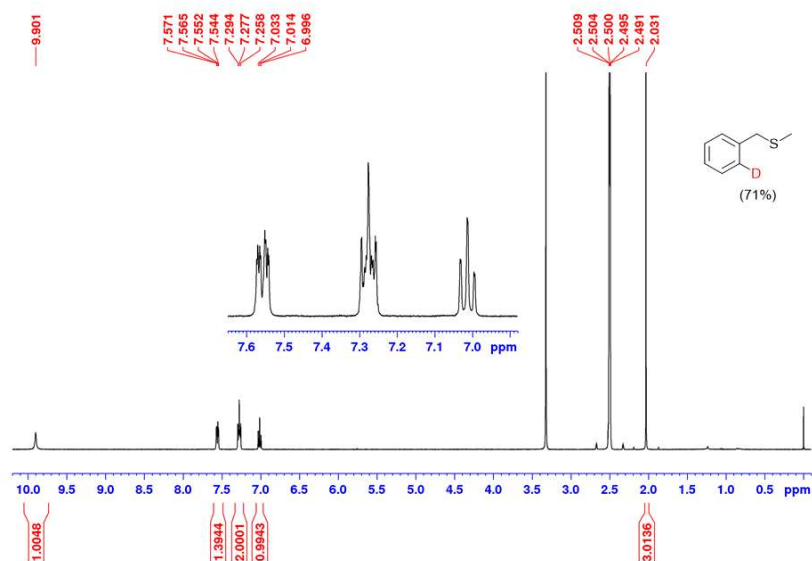


Fig. S43. ^1H NMR spectrum in $\text{DMSO-}d_6$ at 298 K (400 MHz) of **9P** synthesized by the reaction of **M9-Cl** (0.14 mmol) and **Cys^{4D}** (1.12 mmol) under ball-milling conditions.

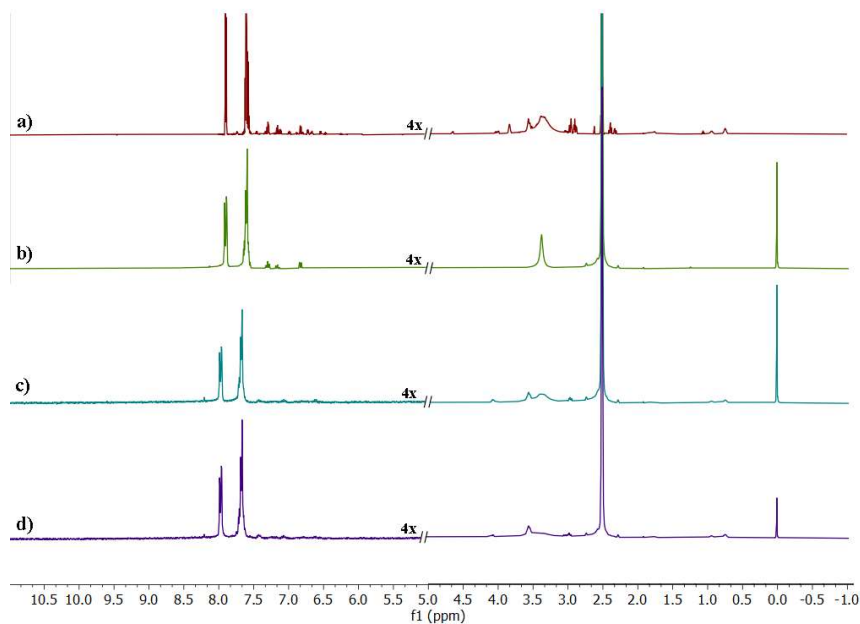


Fig. S44. ^1H NMR spectra in $\text{DMSO-}d_6$ at 298 K (300 MHz) of crude reaction mixtures of **M1-Cl** (0.14 mmol) and **Cys^{4D}** (1.12 mmol) milled for a) 8 h, b) 10 h, c) 15 h and d) 24 h. Relative intensities of the signals of **1P**, intermediates and **M1-Cl** are not representative due to low solubility of **M1-Cl** and intermediates in DMSO.

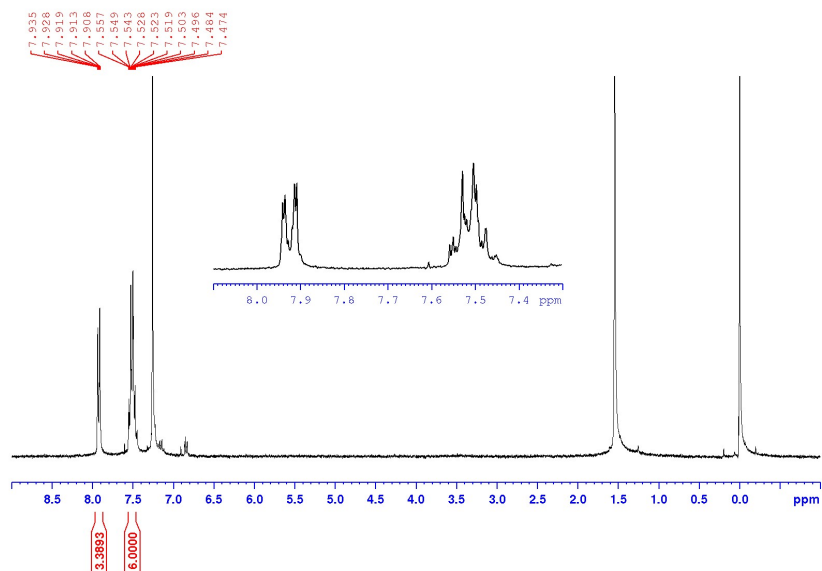


Fig. S45. ^1H NMR spectrum in CDCl_3 at 298 K (300 MHz) of 1^{P} synthesized by the reaction of **M1-Cl** (0.14 mmol) and **Cys^{4D}** (1.12 mmol) under ball-milling conditions. Reaction time was 8 h.

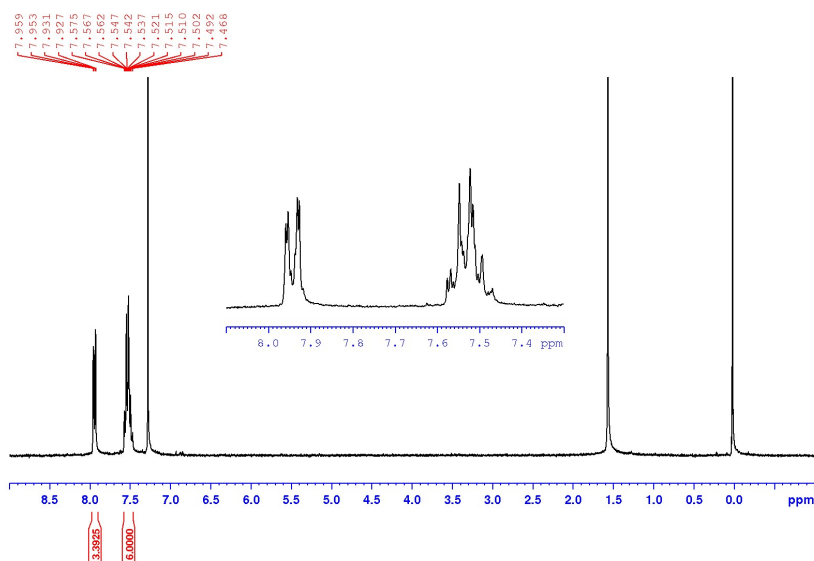


Fig. S46. ^1H NMR spectrum in CDCl_3 at 298 K (300 MHz) of 1^{P} synthesized by the reaction of **M1-Cl** (0.14 mmol) and **Cys^{4D}** (1.12 mmol) under ball-milling conditions. Reaction time was 10 h.

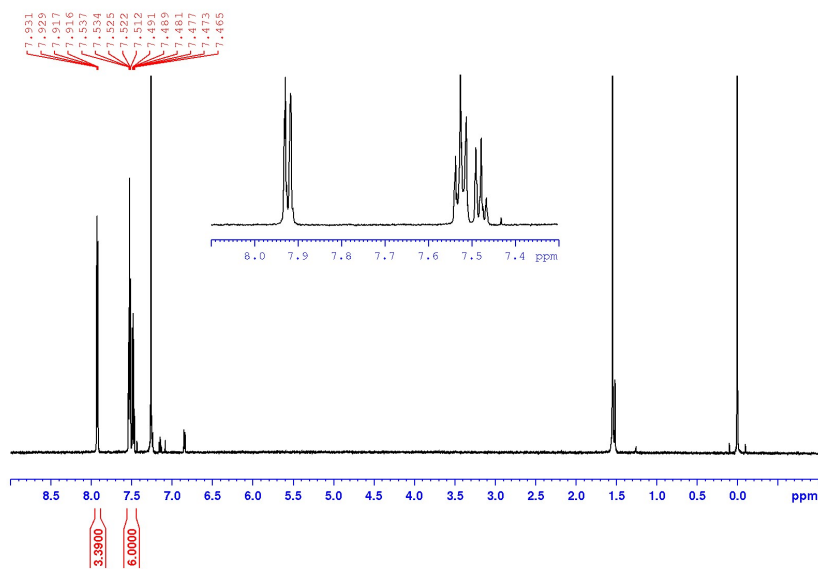


Fig. S47. ^1H NMR spectrum in CDCl_3 at 298 K (600 MHz) of $\mathbf{1}^{\text{P}}$ synthesized by the reaction of $\mathbf{M1-Cl}$ (0.14 mmol) and \mathbf{Cys}^{4D} (1.12 mmol) under ball-milling conditions. Reaction time was 24 h.

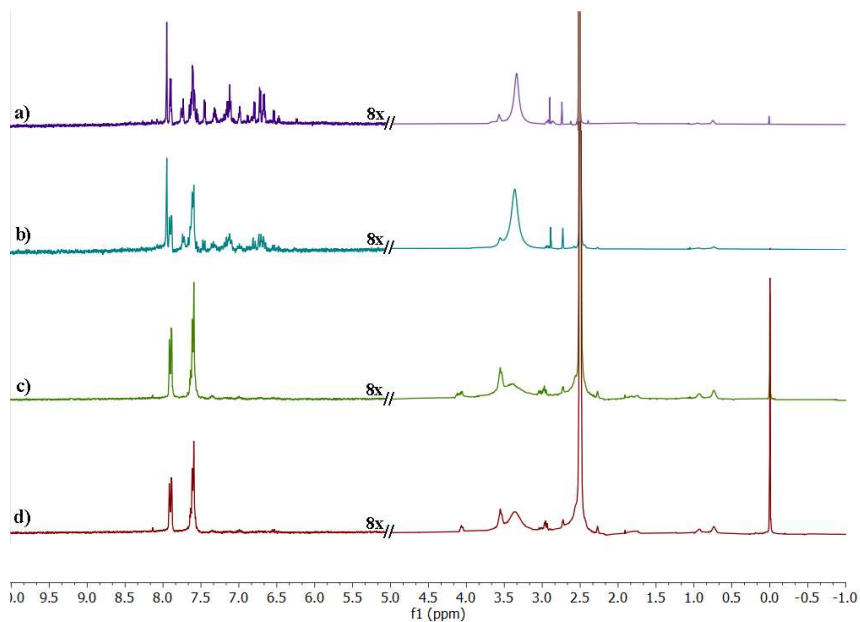


Fig. S48. ^1H NMR spectra in $\text{DMSO}-d_6$ at 298 K (300 MHz) of crude reaction mixtures of $\mathbf{D1-Cl}$ (0.28 mmol) and \mathbf{Cys}^{4D} (1.12 mmol) milled for a) 8 h, b) 10 h, c) 15 h and d) 24 h. Relative intensities of the signals of $\mathbf{1}^{\text{P}}$, intermediates and $\mathbf{D1-Cl}$ are not representative due to low solubility of $\mathbf{D1-Cl}$ and intermediates in DMSO.

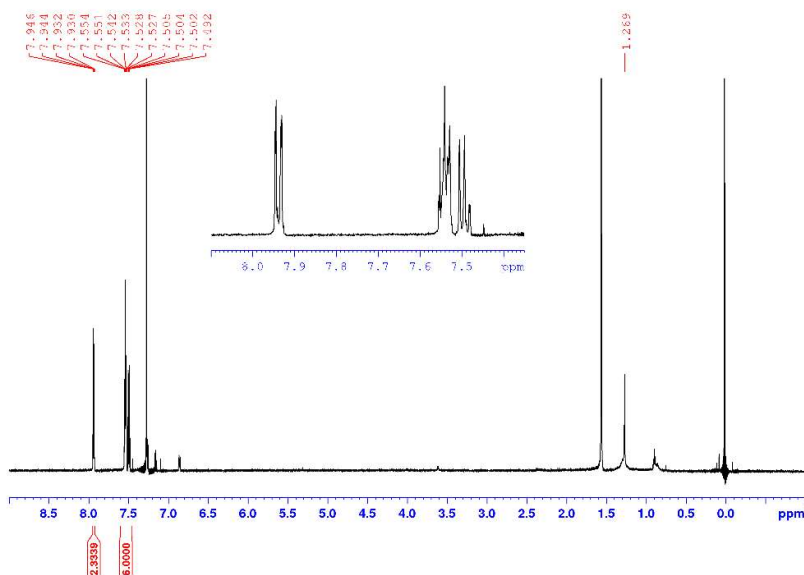


Fig. S49. ^1H NMR spectrum in CDCl_3 at 298 K (600 MHz) of $1^{2\text{D}}$ synthesized by the reaction of **D1-Cl** (0.28 mmol) and **Cys $^{4\text{D}}$** (1.12 mmol) under ball-milling conditions. Reaction time was 8 h.

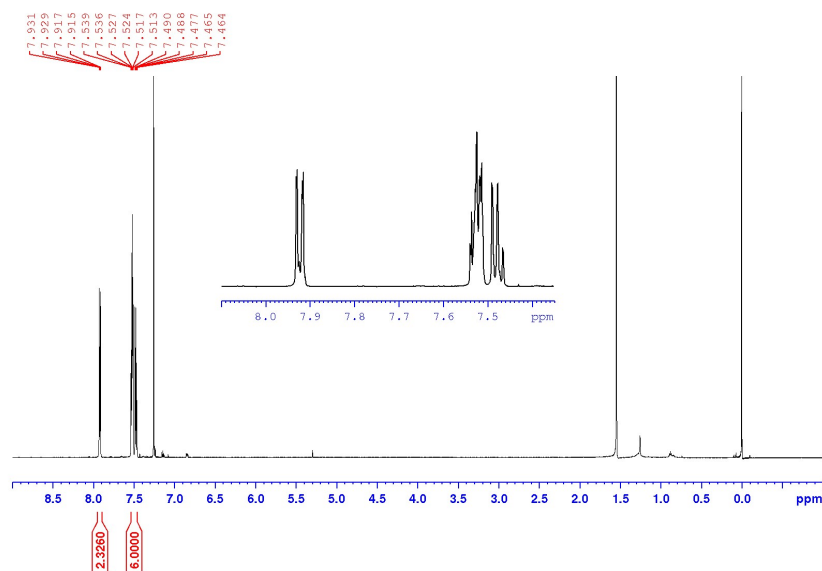


Fig. S50. ^1H NMR spectrum in CDCl_3 at 298 K (600 MHz) of $1^{2\text{D}}$ synthesized by the reaction of **D1-Cl** (0.28 mmol) and **Cys $^{4\text{D}}$** (1.12 mmol) under ball-milling conditions. Reaction time was 10 h.

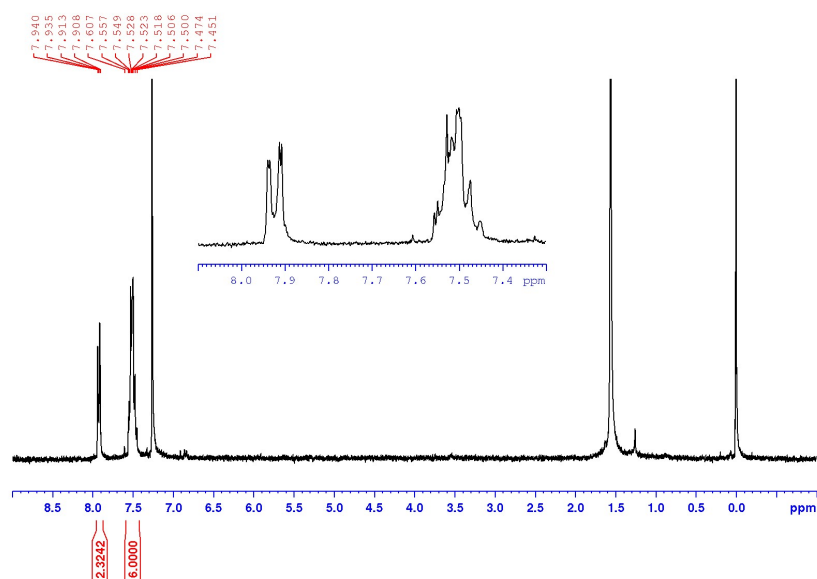


Fig. S51. ^1H NMR spectrum in CDCl_3 at 298 K (300 MHz) of 12^{D} synthesized by the reaction of **D1-Cl** (0.28 mmol) and **Cys^{4D}** (1.12 mmol) under ball-milling conditions. Reaction time was 24 h.

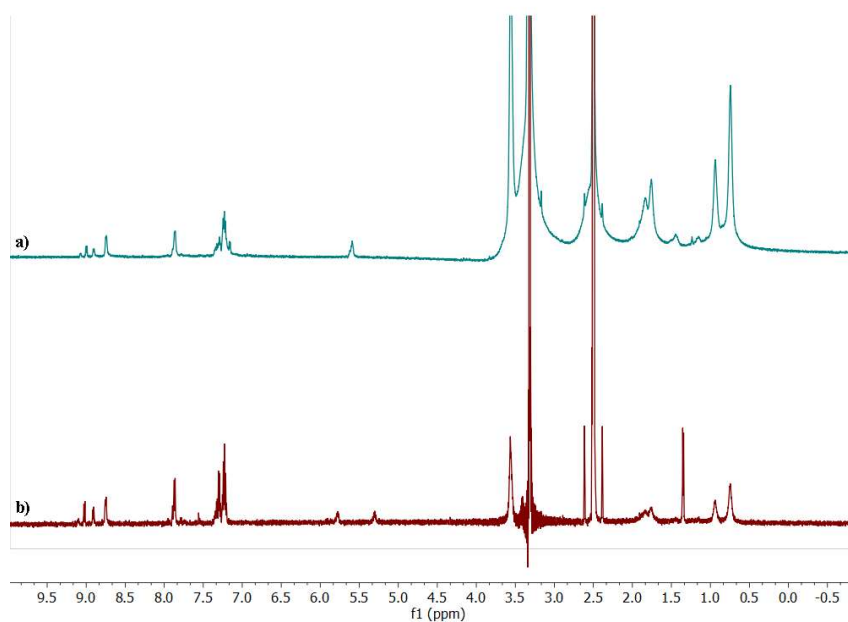


Fig. S52. ^1H NMR spectra in $\text{DMSO}-d_6$ at 298 K (300 MHz) of crude reaction mixtures consisted of **D1-Cl** (0.28 mmol) and a) **Gly** (1.12 mmol) or b) **L-Ala** (1.12 mmol). Reaction mixtures were milled for 15 h and washed with water.

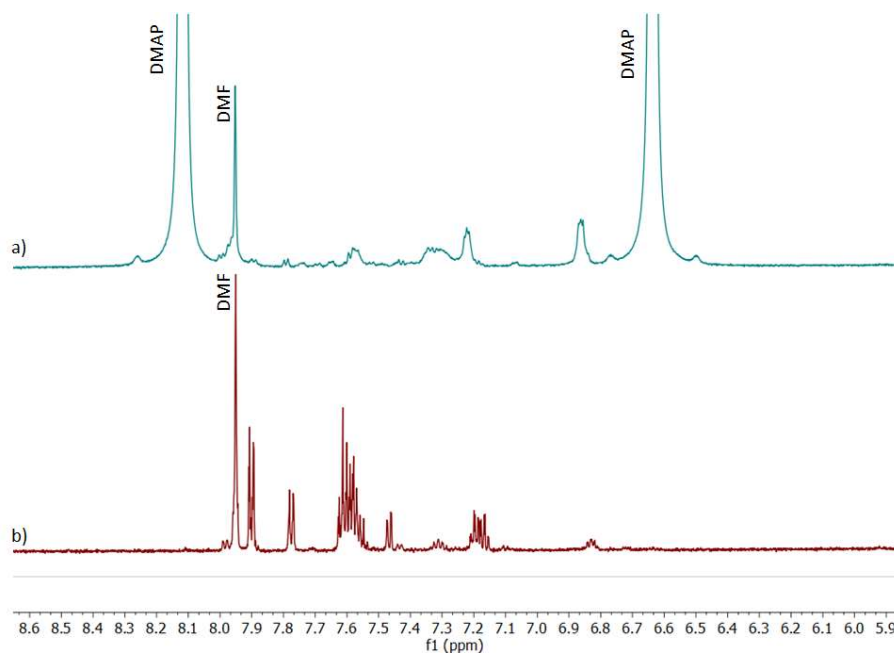


Fig. S53. Aromatic part of ^1H NMR spectra in $\text{DMSO-}d_6$ at 298 K (600 MHz) of crude reaction mixtures of **D1-Cl** (0.28 mmol) and **Cys^{4D}** (1.12 mmol) with addition of a) DMAP (2.24 mmol) and b) NaOAc (2.24 mmol) as solid additives. Reaction mixtures were milled for 15 h. Relative intensities of the signals of **1^D**, intermediates and **D1-Cl** are not representative due to low solubility of **D1-Cl** and intermediates in DMSO.

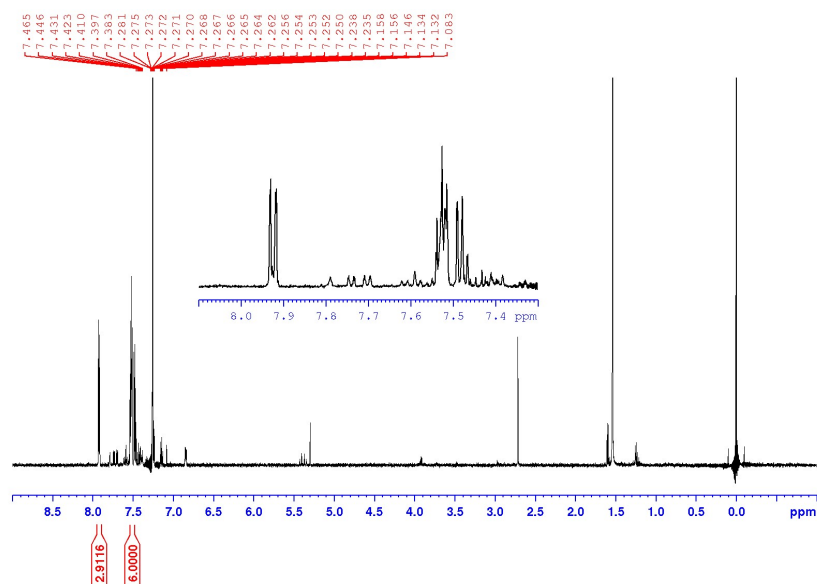


Fig. S54. ^1H NMR spectrum in CDCl_3 at 298 K (600 MHz) of **1^{2D}** synthesized by the reaction of **D1-Cl** (0.28 mmol) and **Cys^{4D}** (1.12 mmol) with addition of NaOAc (2.24 mmol) under ball-milling conditions. Reaction time was 15 h.

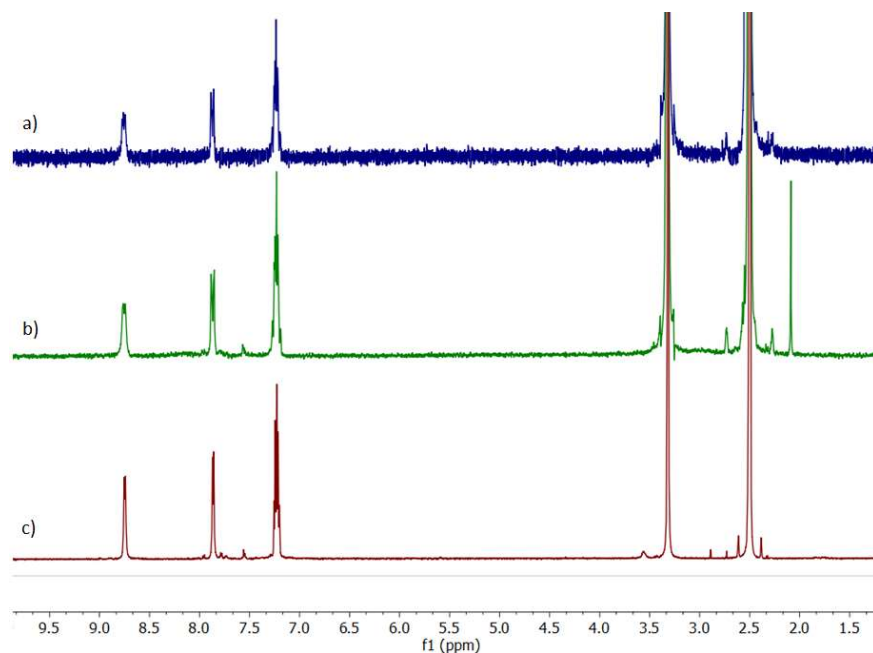


Fig. S55. ¹H NMR spectra in DMSO-*d*₆ at 298 K (600 MHz) of reaction mixtures of **D1-Cl** (0.28 mmol) and a) **D₂O** (1.12 mmol), b) **EtOD** (1.12 mmol) or c) **ND₄Cl** (1.12 mmol). Reaction mixtures were milled for 15 h. Samples of reaction mixtures a) and b) were dried in air and c) the reaction mixture was rinsed with water and dried in air prior to recording NMR spectra.

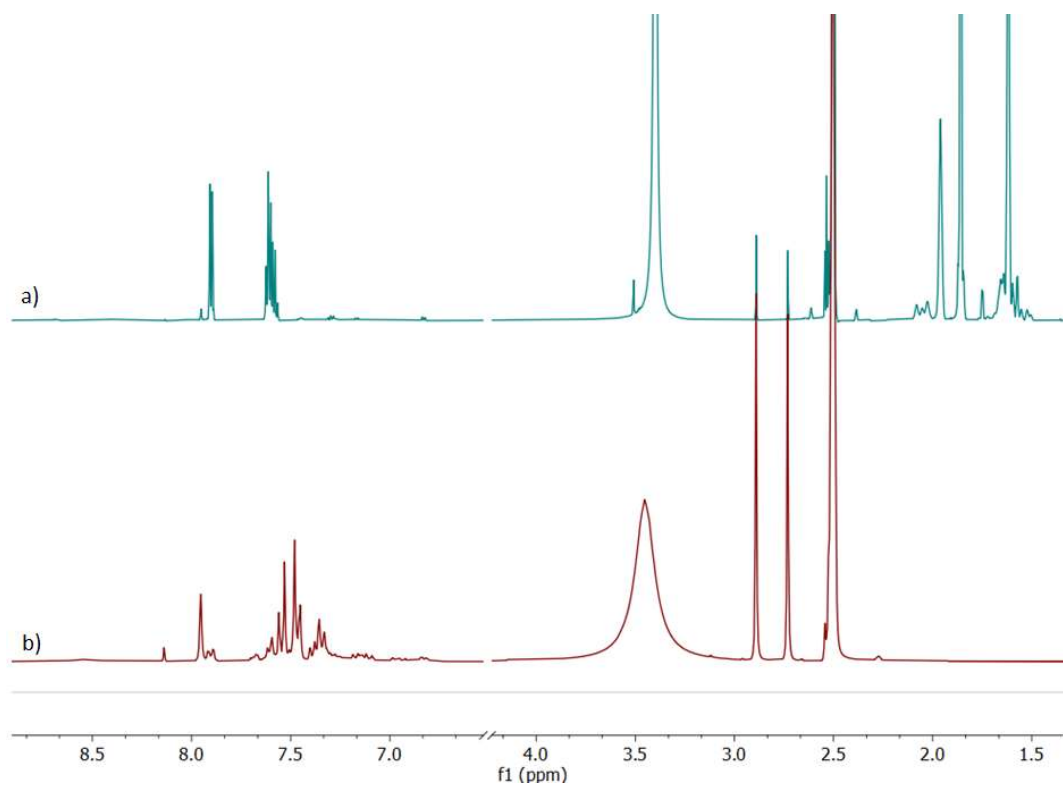


Fig. S56. ¹H NMR spectra in DMSO-*d*₆ at 298 K (600 MHz) of crude reaction mixtures of **D1-Cl** (0.28 mmol) and: a) **(1-adamantanethiol)-*d*** (1.12 mmol) or b) **(4-chlorothiophenol)-*d*** (1.12 mmol). Reaction mixtures were milled for 15 h.

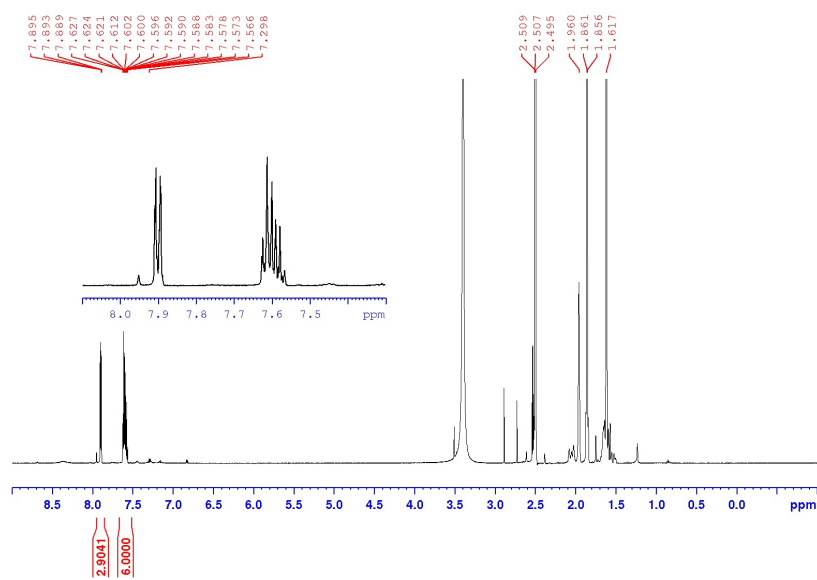


Fig. S57. ^1H NMR spectrum in $\text{DMSO-}d_6$ at 298 K (600 MHz) of $\mathbf{1}^{2\text{D}}$ synthesized by the reaction of $\mathbf{D1-Cl}$ (0.28 mmol) and ($\mathbf{1}$ -adamantanethiol)- \mathbf{d} (1.12 mmol) under ball-milling conditions. Reaction time was 15 h.

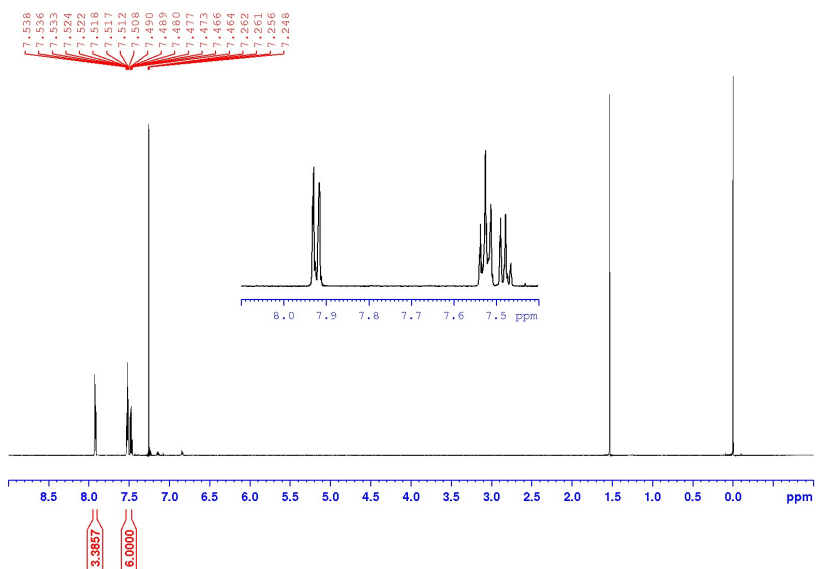


Fig. S58. ^1H NMR spectrum in CDCl_3 at 298 K (600 MHz) of $\mathbf{1}^{\text{P}}$ synthesized by the reaction of $\mathbf{M1-Cl}$ (0.14 mmol) and excess of $\text{Cys}^{4\text{D}}$ (2.80 mmol) under ball-milling conditions. Reaction time was 15 h.

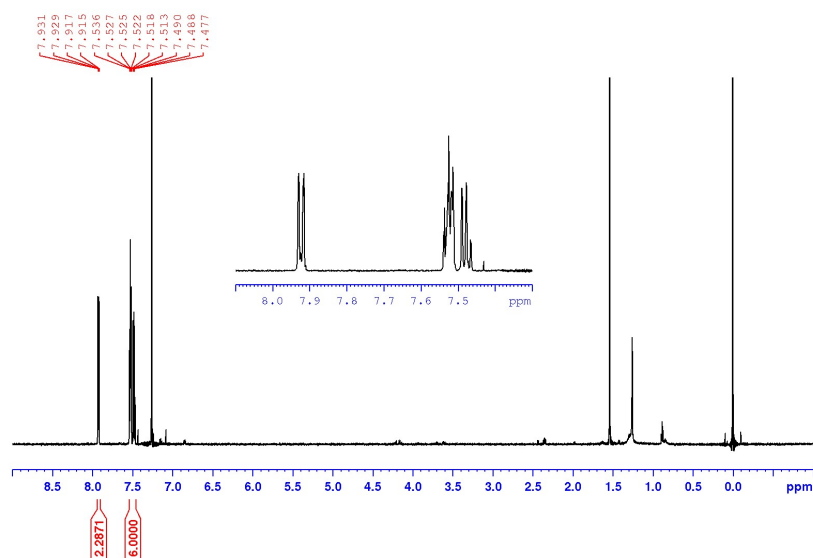


Fig. S59. ^1H NMR spectrum in CDCl_3 at 298 K (600 MHz) of $1^{2\text{D}}$ synthesized by the reaction of **D1-CI** (0.14 mmol) and excess of **Cys $^{4\text{D}}$** (2.80 mmol) under ball-milling conditions. Reaction time was 15 h.

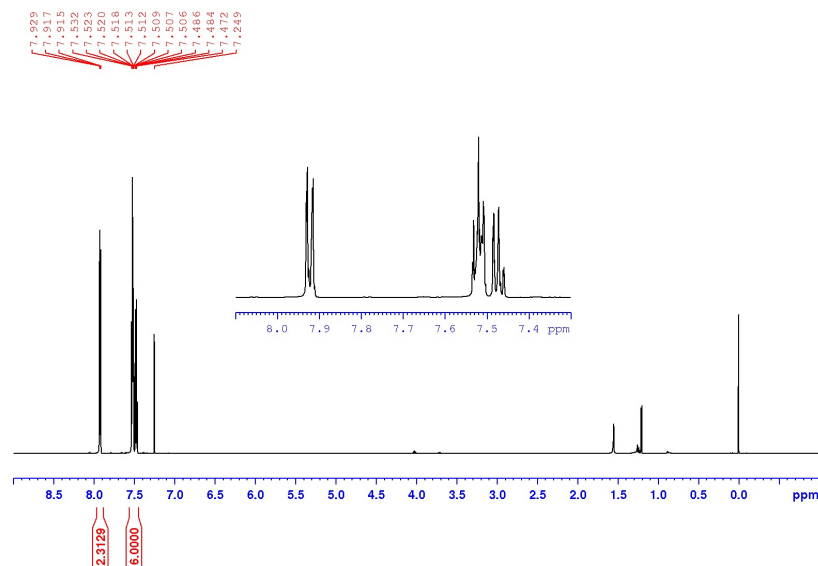


Fig. S60. ^1H NMR spectrum in CDCl_3 at 298 K (600 MHz) of $1^{2\text{D}}$ synthesized by the reaction of **D1-CI** (0.14 mmol) and **Cys $^{4\text{D}}$** (1.12 mmol) with addition of **D $_2$ O** (2.24 mmol) under ball-milling conditions. Reaction time was 15 h.

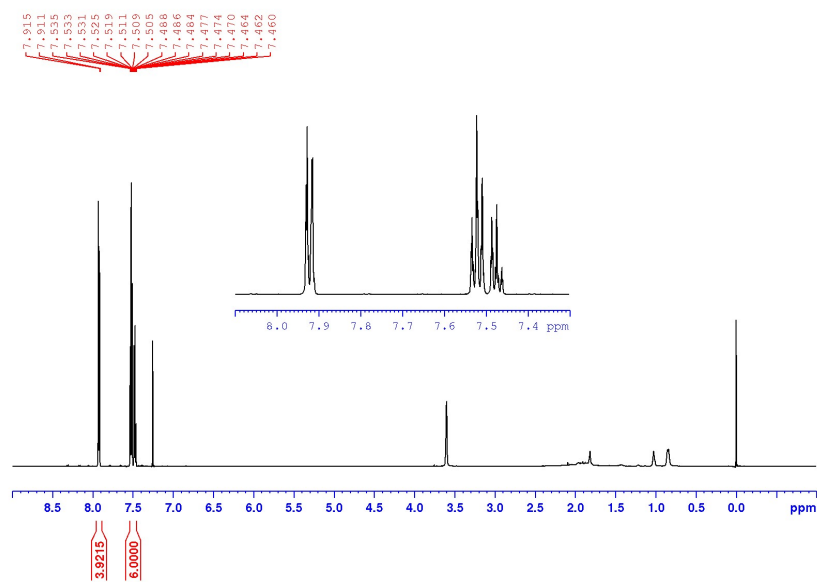


Fig. S61. ^1H NMR spectrum in CDCl_3 at 298 K (600 MHz) of **1** obtained by the reaction with **Cys**^{4D} (1.12 mmol, 1 equiv.) and **PdCl**₂ (0.007 mmol, 5 mol%) under ball-milling conditions. Reaction time was 15 h.

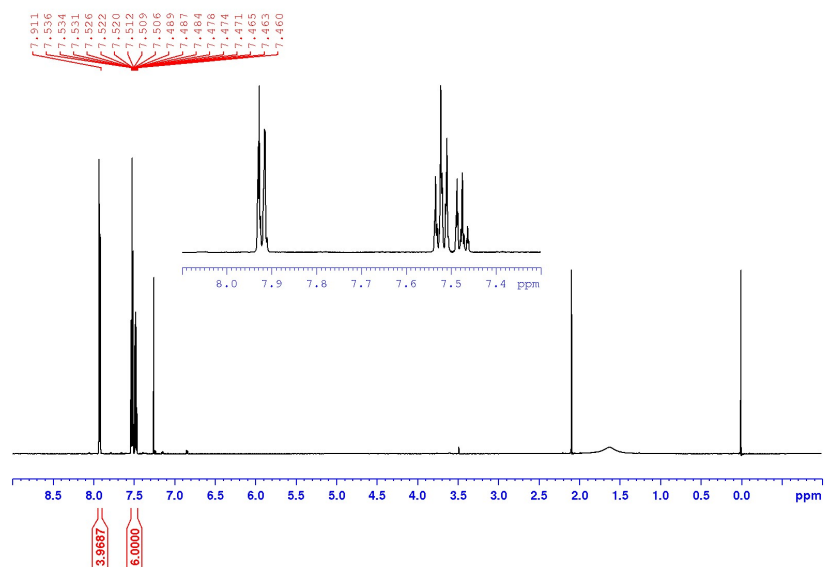


Fig. S62. ^1H NMR spectrum in CDCl_3 at 298 K (600 MHz) of **1** obtained by the reaction with **Cys**^{4D} (1.12 mmol, 8 equiv.) and **PdCl**₂ (0.14 mmol, 1 equiv.) under ball-milling conditions. Reaction time was 15 h.

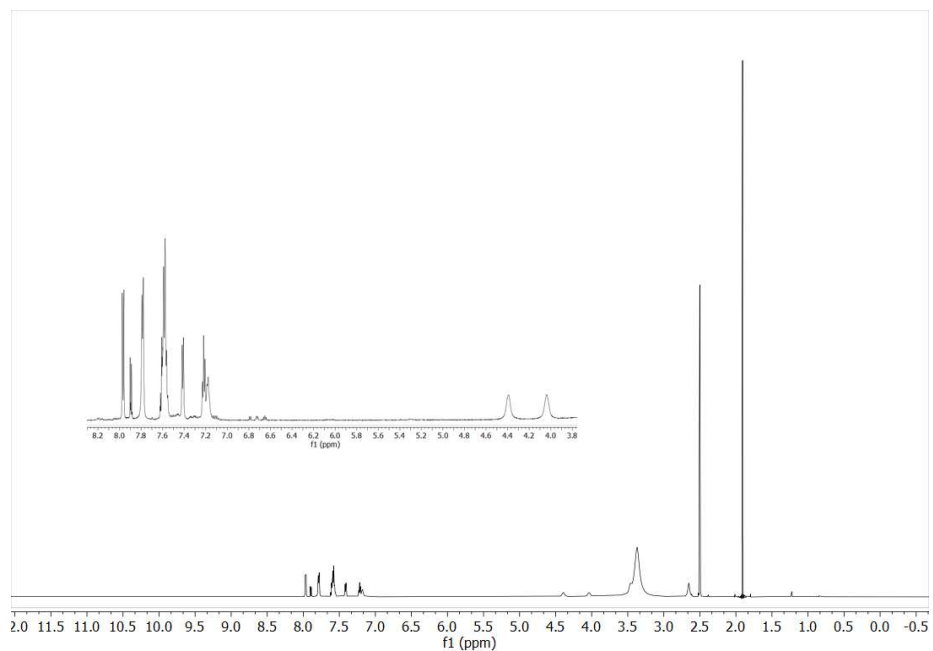


Fig. S63. ^1H NMR spectrum ($\text{DMSO-}d_6$, 298 K, 600 MHz) of the crude reaction mixture recorded after 75 min milling of the native **L-Cys** (0.14 mmol), **M1-Cl**, (0.28 mmol), NaOAc (0.28 mmol), and 150.0 mg NaCl as milling auxiliary. The spectrum is attributed to the monopalladated cysteine complex **M1-1**. ^1H NMR (δ/ppm): 7.96 (dd, $J = 7.95$ Hz, 2H), 7.89 (dd, $J = 8.1$ Hz, 2H), 7.79 (d, $J = 7.2$, 2H), 7.63-7.53 (m, 6H), 7.41 (d, $J = 7.8$ Hz, 2H), 7.22 (t, $J = 7.2$ 2H), 7.18 (t, $J = 6.8$, 1H), 4.39 (br m, 1H, NH), 4.04 (br m, 1H, NH), 3.46 (br m, 1H, CH), 2.65 (br m, 2H, CH_2).

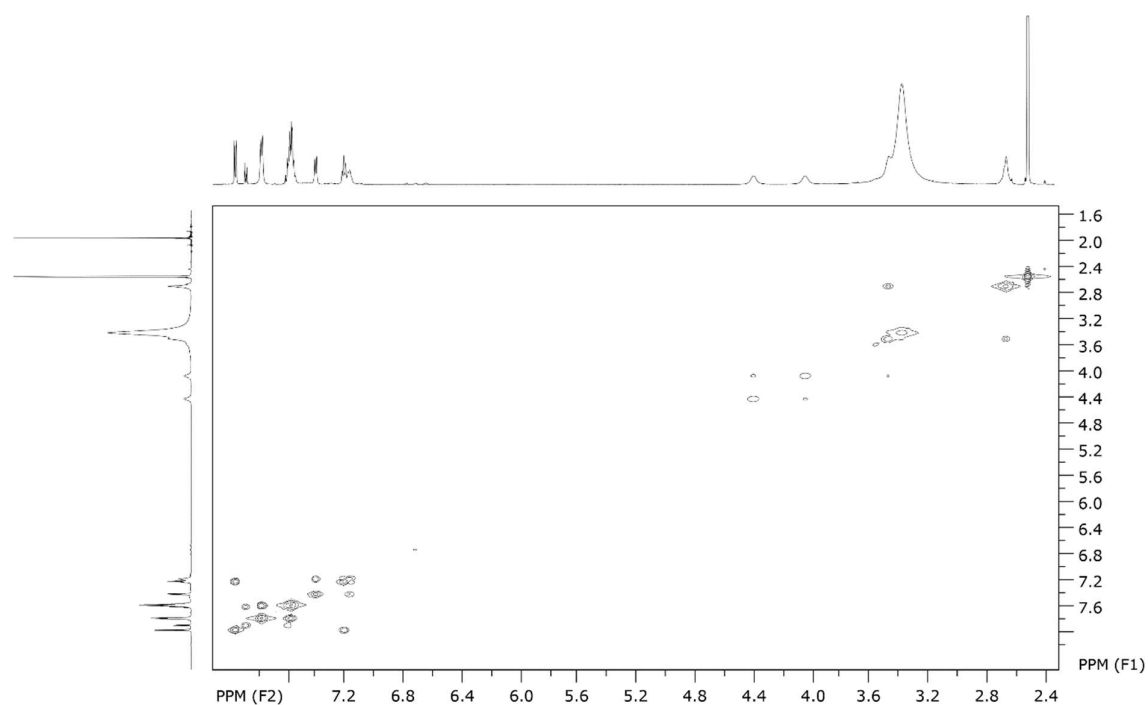


Fig. S64. ^1H - ^1H COSY spectrum (DMSO- d_6 , 298 K, 600 MHz) of the crude reaction mixture recorded after 75 min of milling **L-Cys** (0.14 mmol), **M1-Cl**, (0.28 mmol), NaOAc (0.28 mmol), and 150.0 mg NaCl as a milling auxiliary.

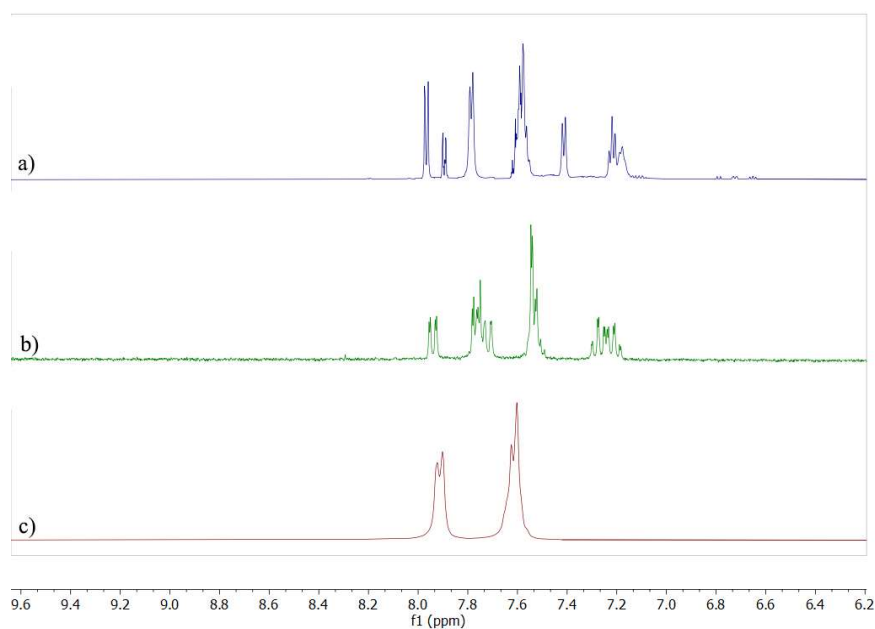


Fig. S65. Aromatic parts of ^1H NMR spectra in DMSO- d_6 at 298 K (600 MHz): of: a) crude reaction mixture recorded after 75 min milling of the native **L-Cys** (0.14 mmol), **M1-Cl**, (0.28 mmol), NaOAc (0.28 mmol), and 150.0 mg NaCl as a milling auxiliary, b) **M1-Cl**, and c) **1**.

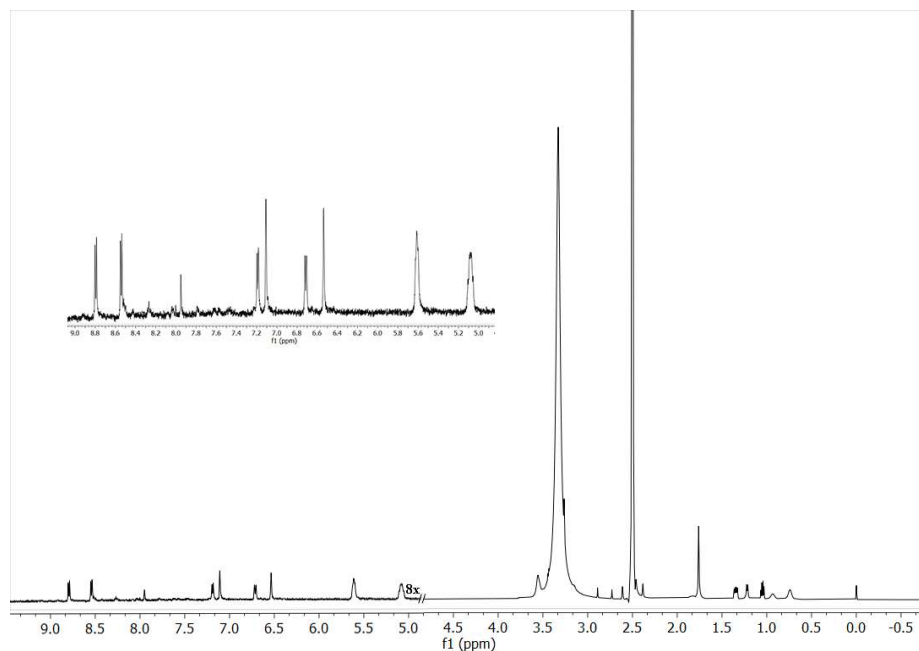


Fig. S66. ^1H NMR spectrum ($\text{DMSO-}d_6$, 298 K, 600 MHz) of the product of the reaction of the native **L-Ala** (2.8 mmol) and **D7-Cl**, (0.28 mmol). Reaction mixture was milled for 15 h, washed with water and dried in air. Selected data (δ/ppm): 8.79 (d, J 9.1 Hz, 1H), 8.54 (d, J = 8.9 Hz, 1H), 7.19 (d, J = 9.1 Hz, 1H), 7.11 (1, 1H), 6.71 (d, J = 9.6 Hz, 1H), 6.54 (s, 1H), 5.61 (br m, 2H, NH), 5.08 (br m, 2H, NH). Two observed signals for amino protons in **L-Ala** indicate formation of the chelate complex.

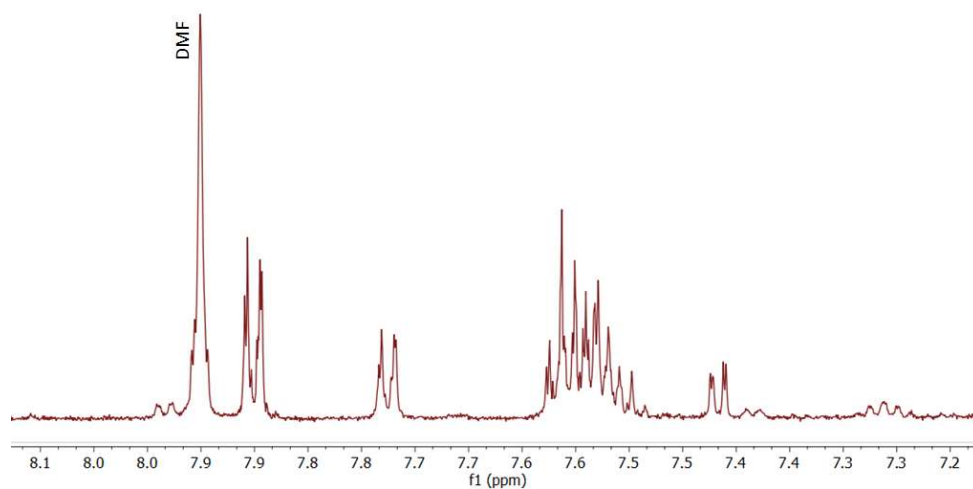


Fig. S67. Aromatic part of ^1H NMR spectrum in $\text{DMSO-}d_6$ at 298 K (600 MHz) of crude reaction mixture of **M1-Cl** (0.14 mmol) with **Cys^{4D}** (1.12 mmol) with **DMF** (0.28 mmol) as a liquid additive. Reaction time was 15 h.

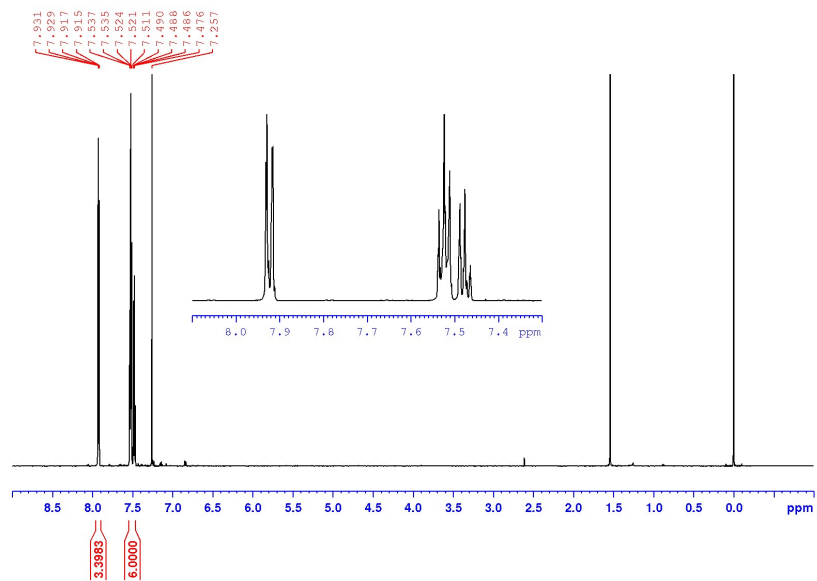
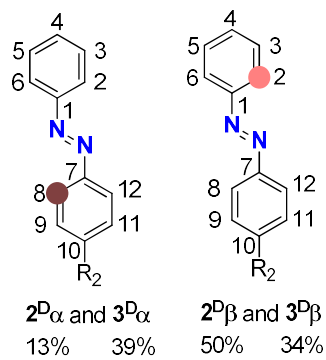
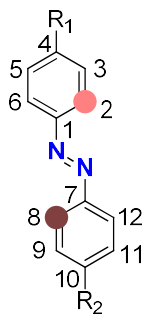


Fig. S68. ^1H NMR spectrum in CDCl_3 at 298 K (300 MHz) of $\mathbf{1}^{\text{D}}$ obtained by reaction of $\mathbf{M1-Cl}$ (0.14 mmol) with Cys^{4D} (1.12 mmol) with DMF (0.28 mmol) as a liquid additive. Reaction time was 15 h.

3. ^{13}C NMR spectroscopy

^{13}C NMR data for the deuterated products 1^{D} - 9^{D} and $1^{2\text{D}}$ - $5^{2\text{D}}$ (298 K, δ / ppm, $^1J_{\text{CD}}$ / Hz). Signals are singlets except those that are marked as t – triplet. The proposed assignment of the observed peaks is listed using the atom numbering given in the schemes below. Carbon that has a bound deuterium and its first neighbour carbons are in blue. Spectra are drawn in Figs. S69-S82.

- 1: $\text{R}_1 = \text{R}_2 = \text{H}$
- 2: $\text{R}_1 = \text{H}, \text{R}_2 = \text{Cl}$
- 3: $\text{R}_1 = \text{H}, \text{R}_2 = \text{OCH}_3$
- 4: $\text{R}_1 = \text{N}(\text{CH}_3)_2, \text{R}_2 = \text{H}$
- 5: $\text{R}_1 = \text{N}(\text{CH}_3)_2, \text{R}_2 = \text{Cl}$



	1 (CDCl_3)	$1^{2\text{D}}$ (CDCl_3)
C-1	152.78	152.80
C-2,6	122.98	122.68 t $J = 25.0$
C-3,5	129.20	129.12
C-4	131.08	131.13

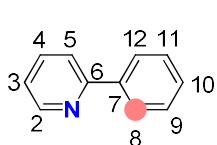
	1 (CDCl_3)	1^{D} (CDCl_3)
C-1	152.78	152.73
C-2	122.98	122.66 t $J = 24.9$
C-3	129.20	129.10
C-4	131.08	131.11
C-5	129.20	129.20
C-6	122.98	122.98
C-7	152.78	152.78
C-8,12	122.98	122.98
C-9,11	129.20	129.20
C-10	131.08	131.08

	2 (CDCl_3)	$2^{\text{D}\alpha^*}$ (CDCl_3)	$2^{\text{D}\beta}$ (CDCl_3)	$2^{2\text{D}}$ (CDCl_3)
C-1	152.59	152.59	152.52	152.56
C-2	123.08	123.07	122.76 t $J = 25.0$	122.76 t $J = 25.0$
C-3	129.27	129.27	129.16	129.17
C-4	131.41	131.41	131.41	131.42
C-5	129.24	129.27	129.27	129.28
C-6	123.08	123.07	123.07	123.09
C-7	151.11	151.05	151.10	151.08 151.13
C-8	124.26	*	124.26	123.96 t $J = 24.4$
C-9	129.47	129.37	129.47	129.38
C-10	137.03	137.02	137.02	137.05
C-11	129.47	129.47	129.47	129.48
C-12	124.26	124.26	124.26	124.29
CH_3	-	-	-	-

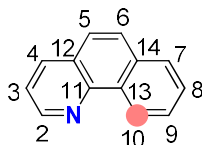
	3 (CDCl_3)	$3^{\text{D}\alpha}$ (CDCl_3)	$3^{\text{D}\beta}$ (CDCl_3)	3 ($\text{DMSO}-d_6$)	$3^{2\text{D}}$ ($\text{DMSO}-d_6$)
	152.88	152.88	152.84	152.04	151.99
	124.87	124.87	124.57 t $J = 24.5$	124.61	124.32 t $J = 24.5$
	129.14	129.14	129.03	129.40	129.30
	130.47	130.47	130.47	130.83	130.83
	129.14	129.14	129.14	129.40	129.40
	124.87	124.87	124.87	124.61	124.62
	147.13	147.07	147.13	146.19	146.13
	122.68	122.36 t $J = 24.6$	122.68	122.26	121.96 t $J = 24.6$
	114.32	114.24	114.32	114.63	114.54
	162.17	162.17	162.17	162.07	162.06
	114.32	114.32	114.32	114.63	114.64
	122.68	122.70	122.70	122.26	122.26
	55.64	55.67	55.67	55.61	55.68

* Amount of the compound $2^{\text{D}\alpha}$ in the sample 2^{D} is small (deuteration degree at C-8 is only 13%) so signals are not clearly observed.

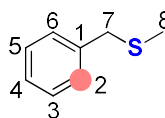
	4 (CDCl ₃)	4 ^D (CDCl ₃)	4 ^{2D} (CDCl ₃)	5 (CDCl ₃)	5 ^D (CDCl ₃)	5 ^{2D} (CDCl ₃)
C-1	143.78	143.78	143.82	143.62	143.56	143.61
C-2	125.09	124.72 t <i>J</i> = 24.9	124.77 t <i>J</i> = 24.9	123.57	123.27 t <i>J</i> = 24.6	123.27 t <i>J</i> = 24.6
C-3	111.62	111.52	111.56	111.65	111.56	111.52
C-4	153.35	153.35	153.31	152.73	152.73	152.72
C-5	111.62	111.62	111.66	111.65	111.66	111.62
C-6	125.09	125.09	125.10	123.57	123.57	123.57
C-7	152.54	152.54	152.58	151.73	151.73	151.76
C-8	122.32	122.32	122.08 t <i>J</i> = 24.6	125.28	125.27	125.08 t <i>J</i> = 24.5
C-9	129.05	129.05	128.97	129.26	129.26	129.14
C-10	129.48	129.48	129.51	135.07	135.07	135.05
C-11	129.05	129.05	129.07	129.26	129.26	129.24
C-12	122.32	122.32	122.34	125.28	125.27	125.27
CH ₃	40.42	40.42	40.46	40.44	40.45	40.42



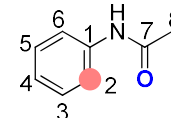
2-phenylpyridine (6)



benzo[h]quinoline (7)



benzyl methyl sulphide (8)



acetanilide (9)

	6 (CDCl ₃)	6 ^D (CDCl ₃)	7 (CDCl ₃)	7 ^D (CDCl ₃)	8 (DMSO- <i>d</i> ₆)	8 ^D (DMSO- <i>d</i> ₆)	9 (CDCl ₃)	9 ^D (CDCl ₃)
C-1	-	-	-	-	138.45	138.37	138.01	137.95
C-2	149.70	149.69	148.89	148.89	128.80	128.50 t <i>J</i> = 23.4	120.02	119.74 t <i>J</i> = 24.5
C-3	120.59	120.59	121.85	121.85	128.29	128.18	129.13	129.03
C-4	136.78	136.78	135.88	135.88	126.72	126.72	124.46	124.46
C-5	122.13	122.13	125.42	125.42	128.29	128.29	129.13	129.13
C-6	157.49	157.47	127.04	127.04	128.80	128.80	120.02	119.98
C-7	139.42	139.35	128.28	128.28	37.10	37.05	168.43	168.49
C-8	126.95	126.66 t <i>J</i> = 24.3	127.16	127.16	14.26	14.34	24.75	24.74
C-9	128.78	128.67	127.90	127.83	-	-	-	-
C-10	128.98	128.98	124.46	124.19 t <i>J</i> = 24.7	-	-	-	-
C-11	128.78	128.78	146.65	146.65	-	-	-	-
C-12	126.95	126.95	126.48	126.48	-	-	-	-
C-13	-	-	131.58	131.53	-	-	-	-
C-14	-	-	133.71	133.69	-	-	-	-

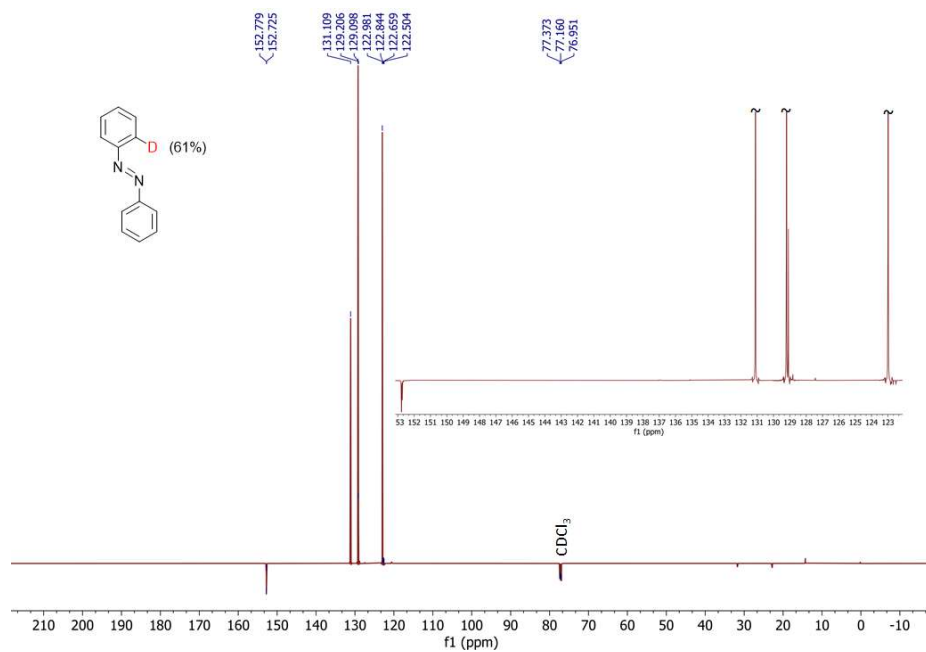


Fig. S69. ¹³C NMR spectrum of **1^D** in CDCl₃ at 298 K (151 MHz).

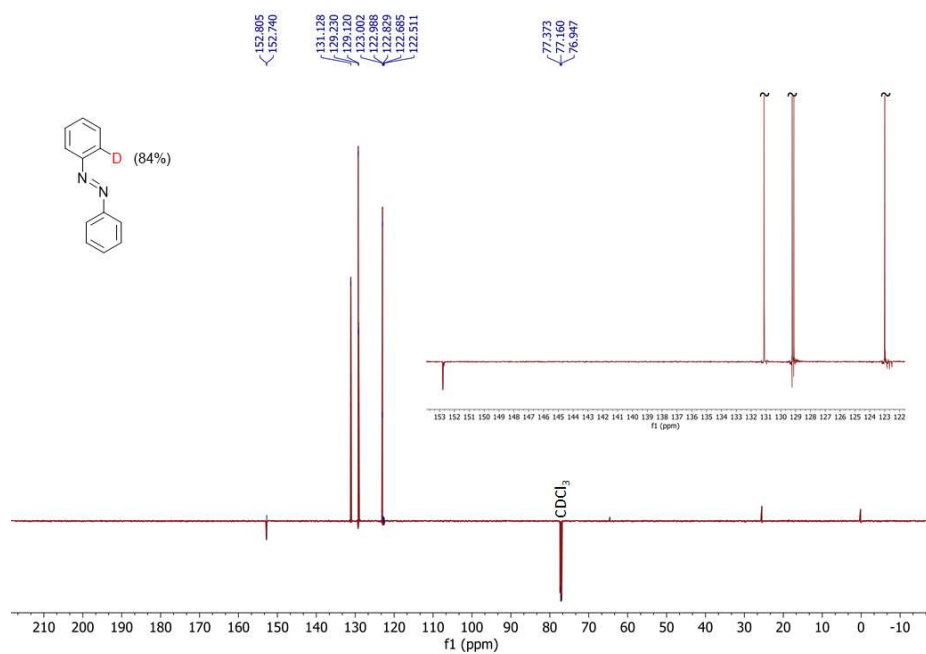


Fig. S70. ¹³C NMR spectrum of **1^{2D}** in CDCl₃ at 298 K (151 MHz).

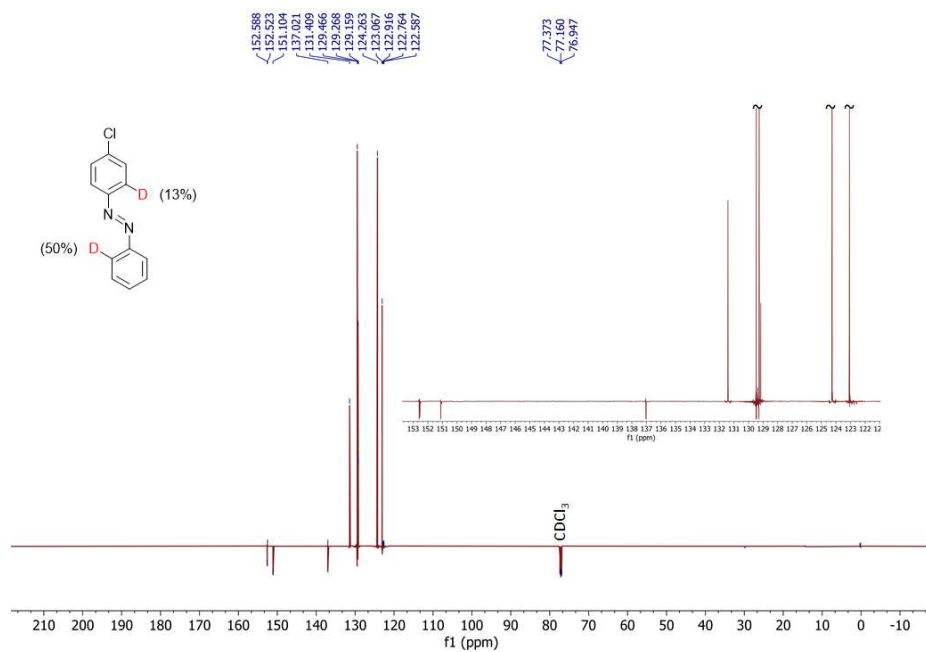


Fig. S71. ¹³C NMR spectrum of **2^D** in CDCl₃ at 298 K (151 MHz).

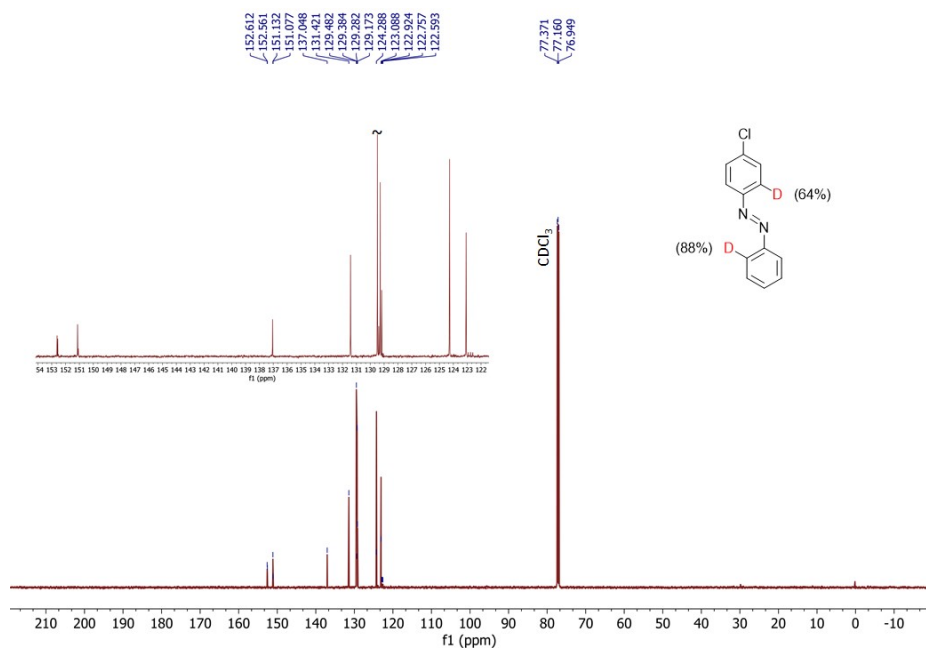


Fig. S72. ¹³C NMR spectrum of **2^{2D}** in CDCl₃ at 298 K (151 MHz).

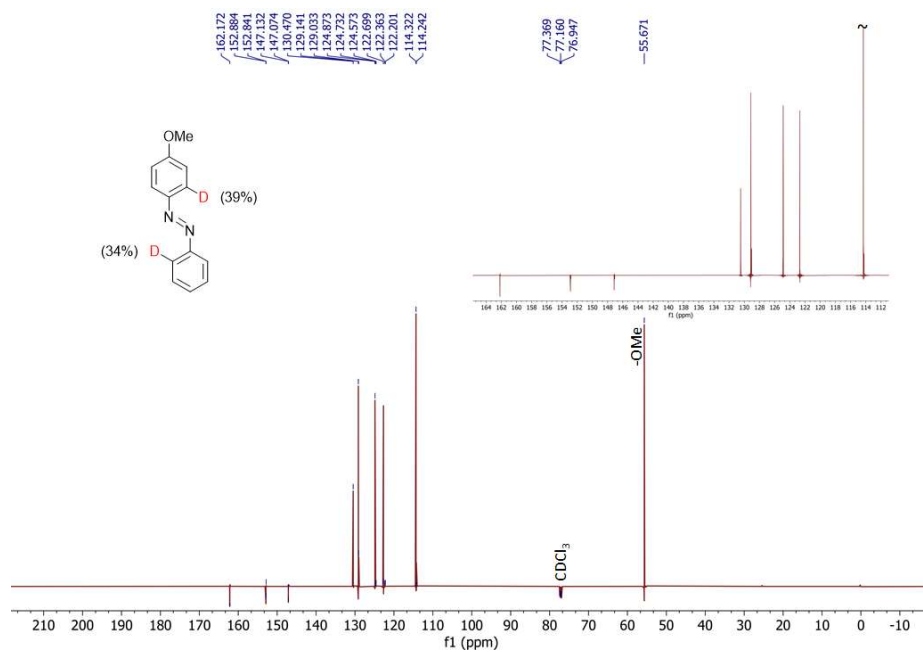


Fig. S73. ^{13}C NMR spectrum of **3^D** in CDCl_3 at 298 K (151 MHz).

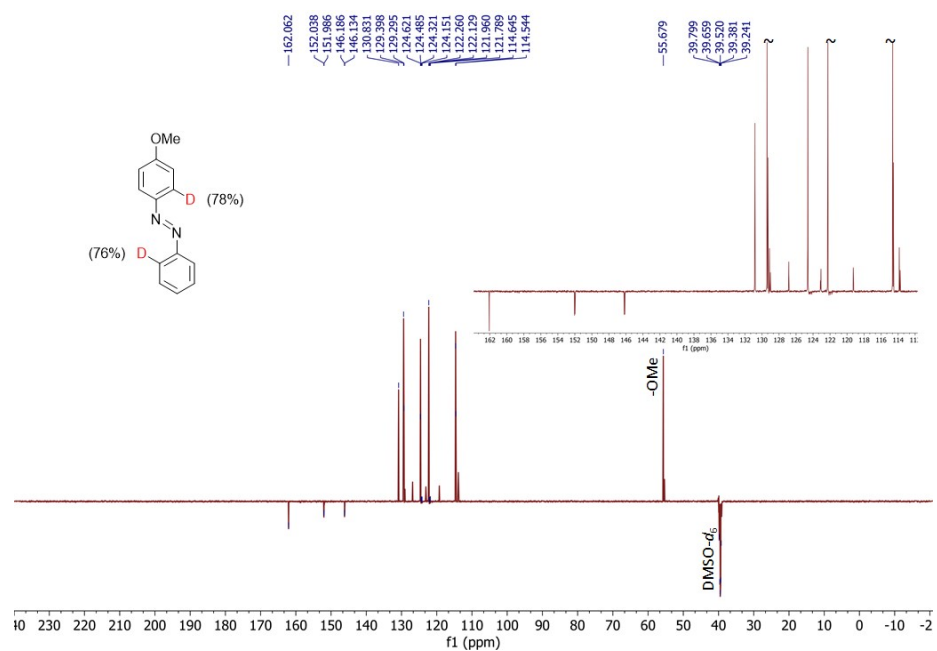


Fig. S74. ^{13}C NMR spectrum of **3^{2D}** in $\text{DMSO-}d_6$ at 298 K (151 MHz).

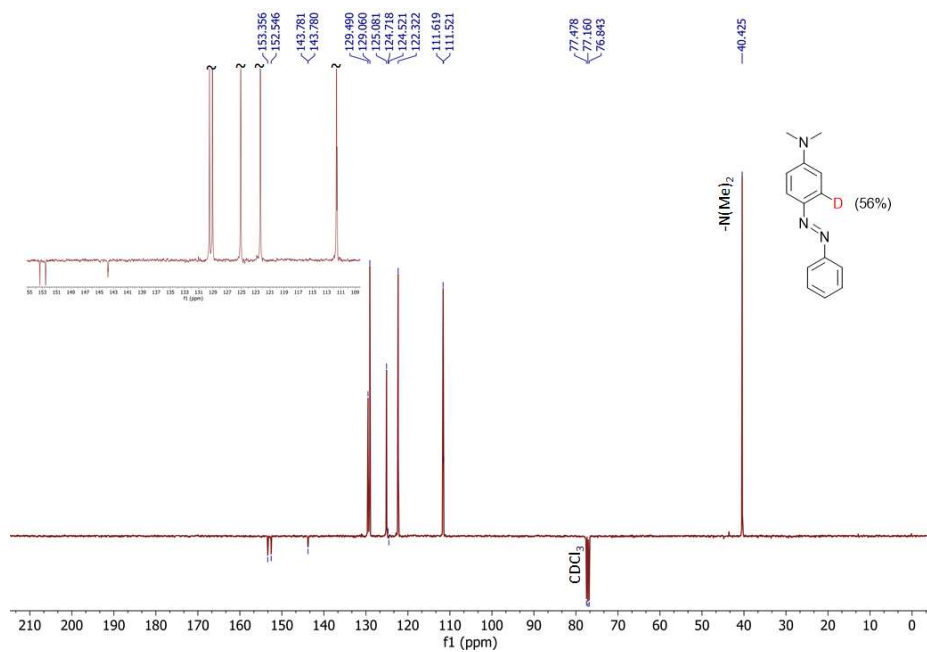


Fig. S75. ^{13}C NMR spectrum of **4P** in CDCl_3 at 298 K (151 MHz).

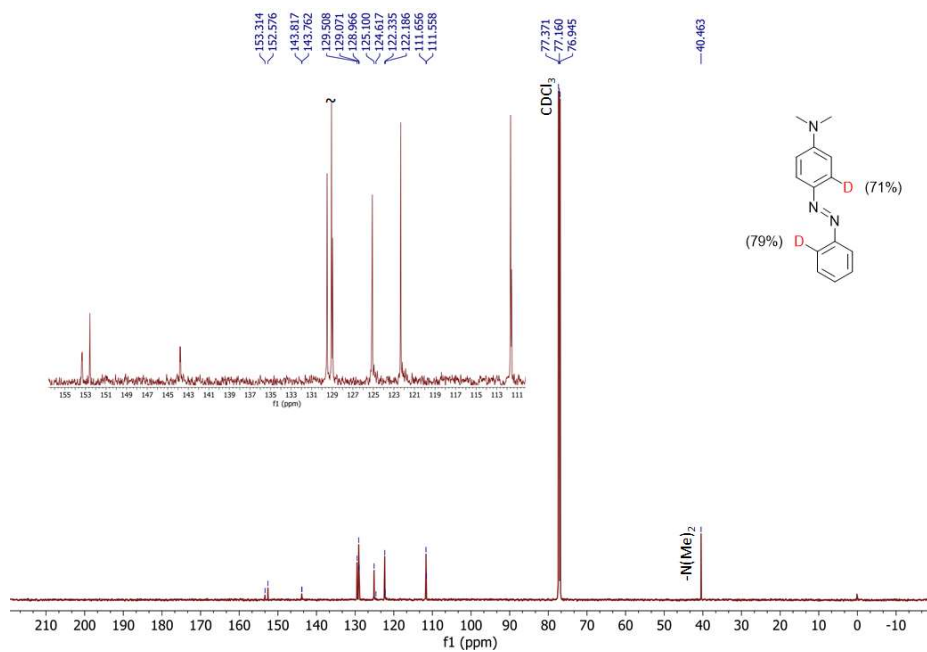


Fig. S76. ^{13}C NMR spectrum of **4^{2D}** in CDCl_3 at 298 K (151 MHz).

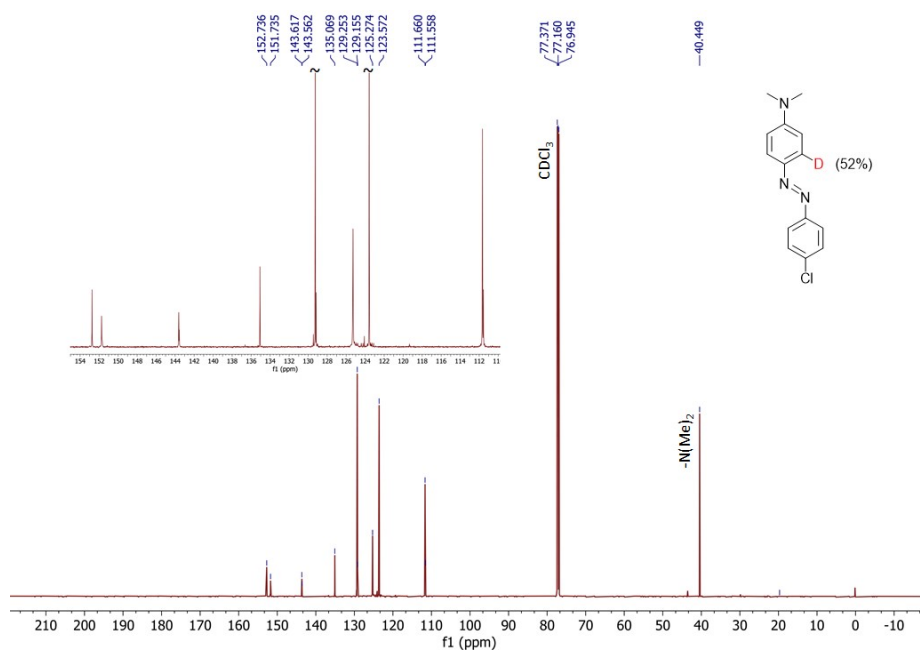


Fig. S77. ^{13}C NMR spectrum of **5^D** in CDCl_3 at 298 K (151 MHz).

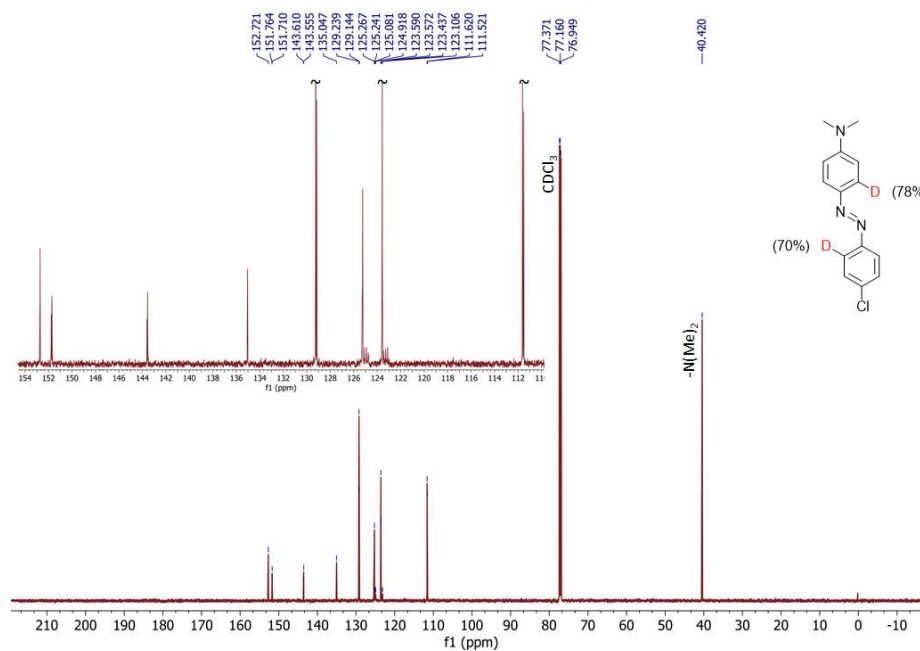


Fig. S78. ^{13}C NMR spectrum of **5^{2D}** in CDCl_3 at 298 K (151 MHz).

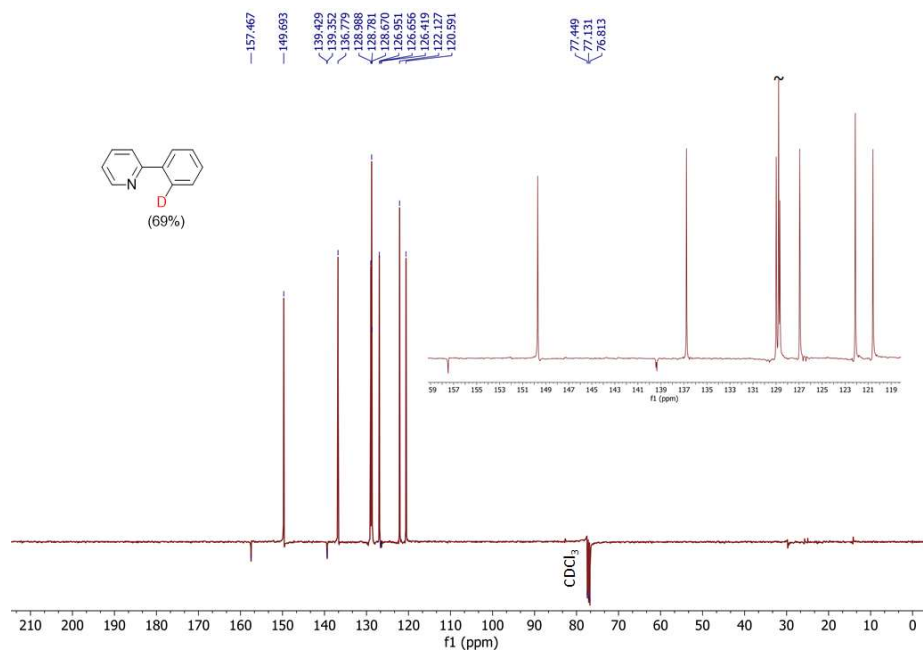


Fig. S79. ¹³C NMR spectrum of **6^D** in CDCl₃ at 298 K (101 MHz).

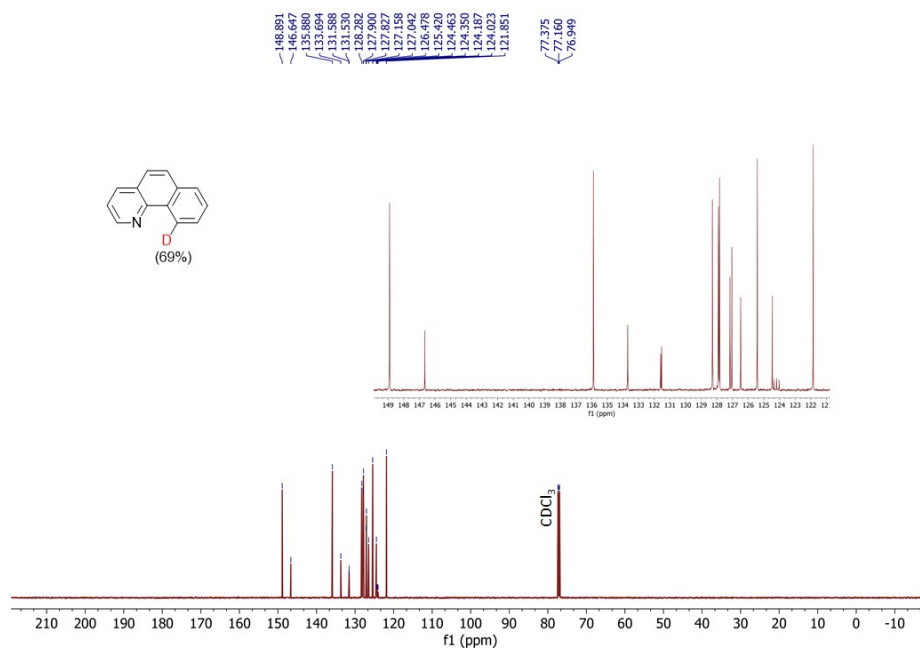


Fig. S80. ¹³C NMR spectrum of **7^D** in CDCl₃ at 298 K (151 MHz).

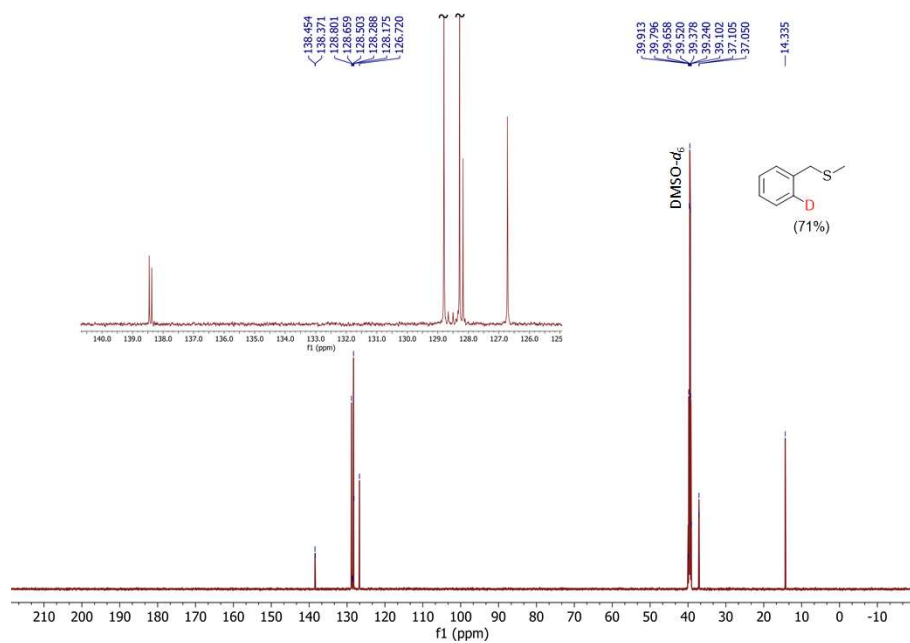


Fig. S81. ¹³C NMR spectrum of **8^D** in DMSO-*d*₆ at 298 K (151 MHz).

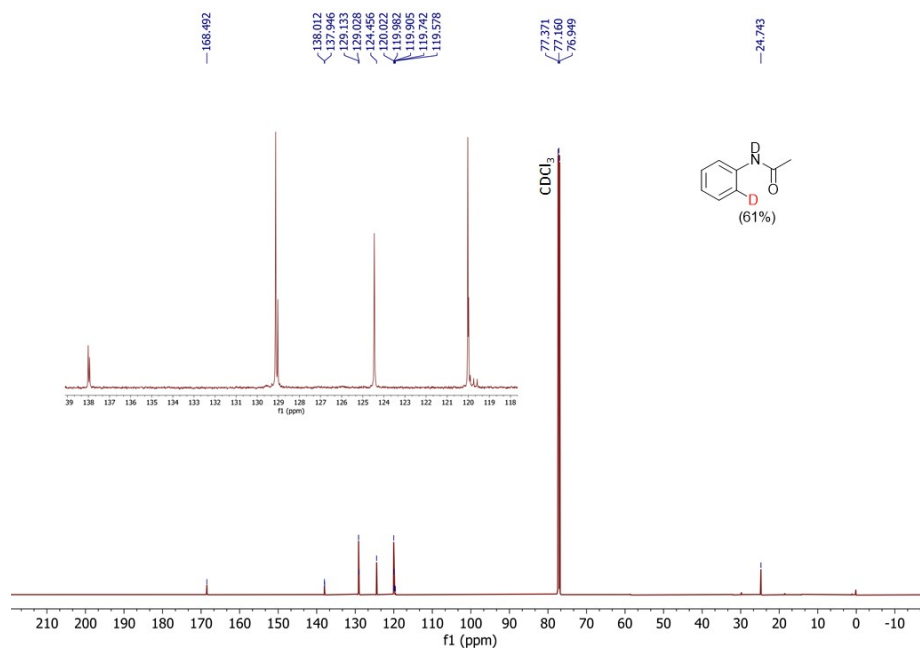


Fig. S82. ¹³C NMR spectrum of **9^D** in DMSO-*d*₆ at 298 K (151 MHz).

4. Raman spectroscopy

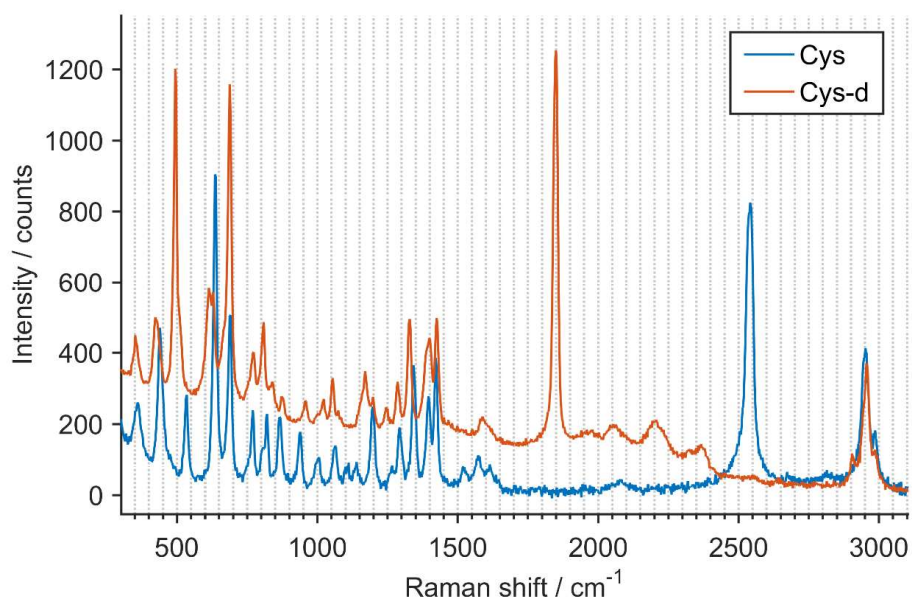


Fig. S83. *Ex situ* Raman spectra of **Cys**^{H4} (blue) and **Cys**^{4D} (red).

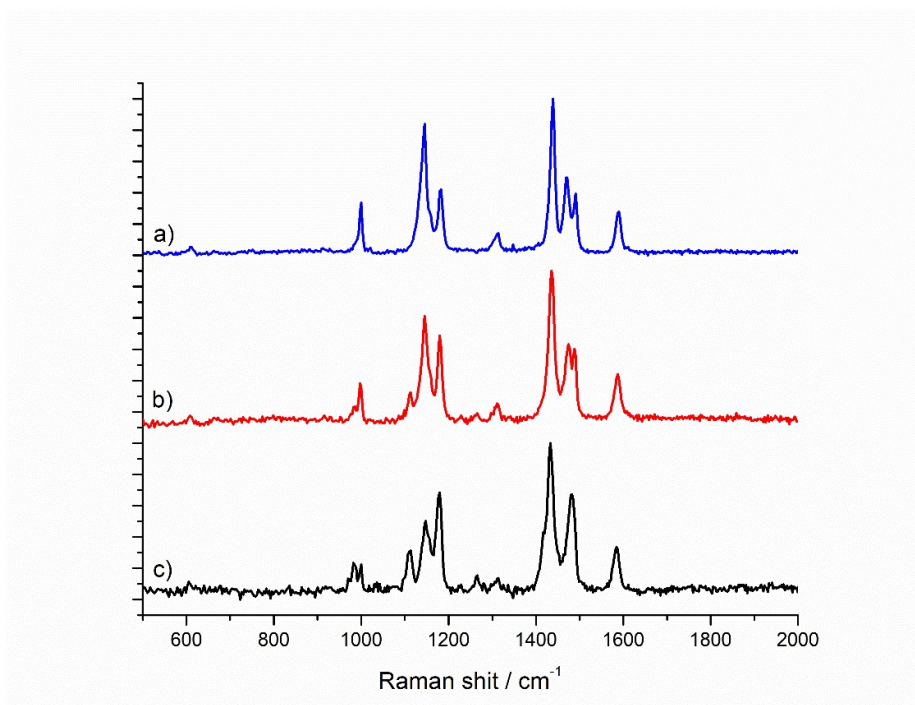


Fig. S84. *Ex-situ* Raman spectra of a) **1** and b) **1^D** synthesized by the reaction of **M1-Cl** (0.14 mmol) and **Cys**^{4D} (1.12 mmol), and c) **1^{2D}** synthesized by the reaction of **D1-Cl** (0.14 mmol) and **Cys**^{4D} (1.12 mmol) under ball-milling conditions.

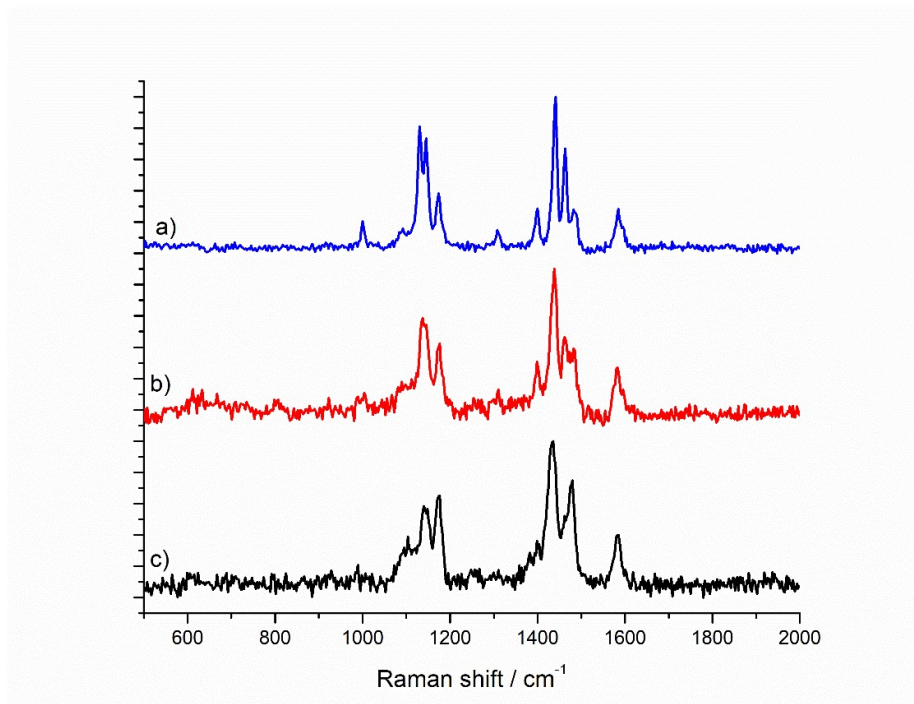


Fig. S85. *Ex-situ* Raman spectra of a) **2**, b) **2**^{1D} synthesized by the reaction of **M2-Cl** (0.14 mmol) and **Cys**^{4D} (1.12 mmol), and c) **2**^{2D} synthesized by the reaction of **D2-Cl** (0.14 mmol) and **Cys**^{4D} (1.12 mmol) under ball-milling conditions.

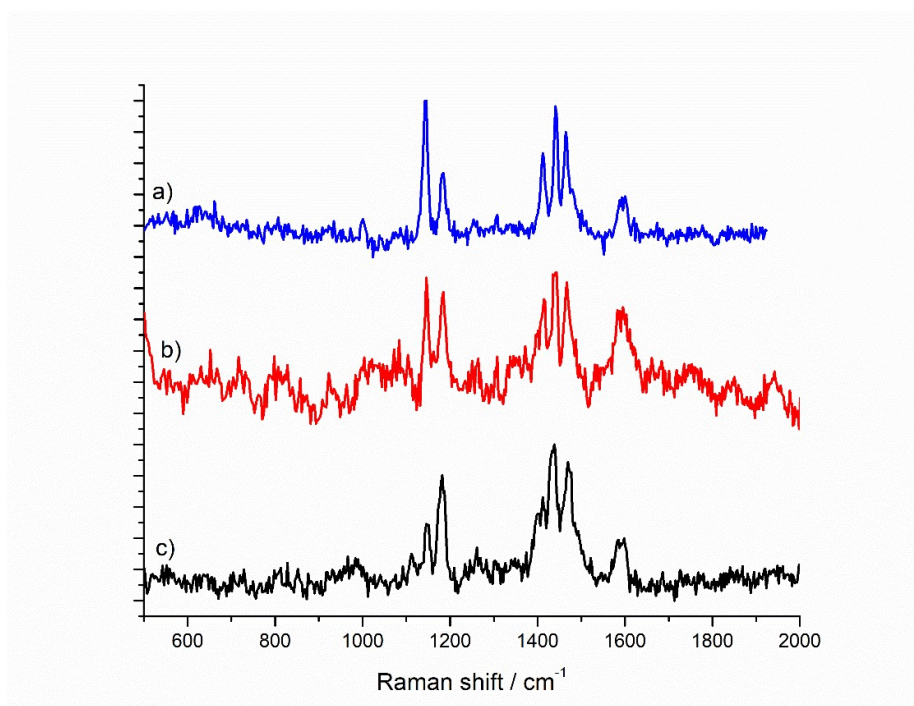


Fig. S86. *Ex-situ* Raman spectra of a) **3**, b) **3**^{1D} synthesized by the reaction of **M3-Cl** (0.14 mmol) and **Cys**^{4D} (1.12 mmol), and c) **3**^{2D} synthesized by the reaction of **D3-Cl** (0.14 mmol) and **Cys**^{4D} (1.12 mmol) under ball-milling conditions.

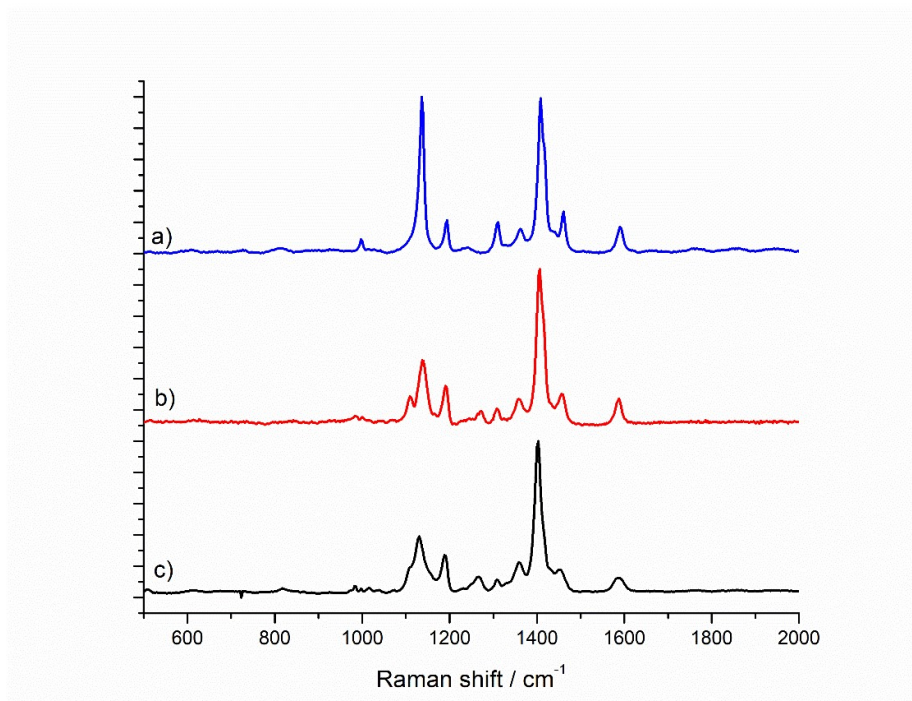


Fig. S87. *Ex-situ* Raman spectra of a) **4**, b) **4^P** synthesized by the reaction of **M4-Cl** (0.28 mmol) and **Cys^{4D}** (1.12 mmol), and c) **4^{2D}** synthesized by the reaction of **D4-Cl** (0.14 mmol) and **Cys^{4D}** (1.12 mmol) under ball-milling conditions.

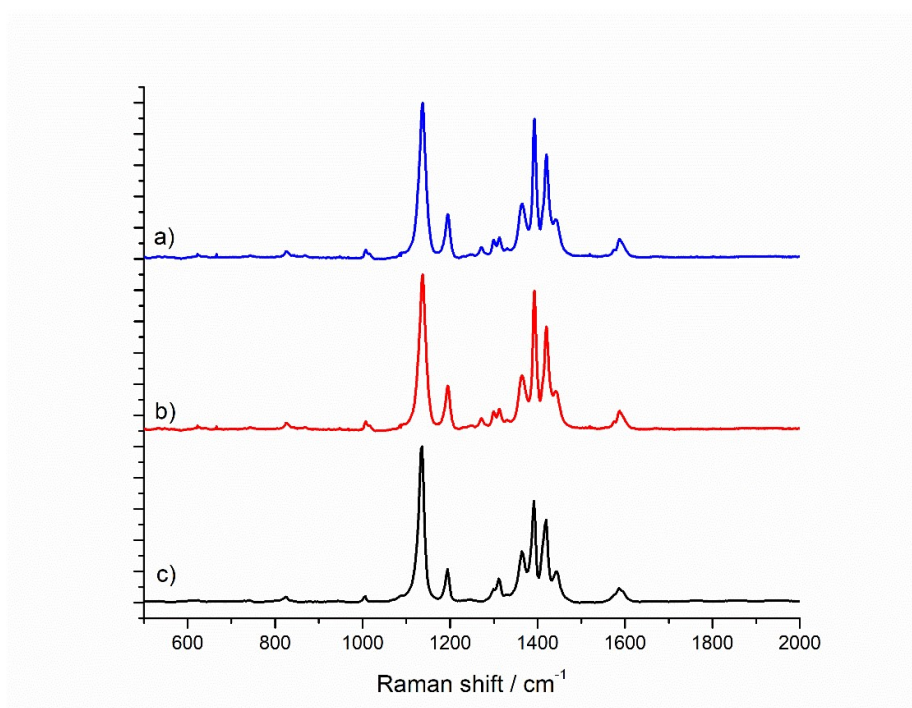


Fig. S88. *Ex-situ* Raman spectra of a) **5**, b) **5^P** synthesized by the reaction of **M5-Cl** (0.28 mmol) and **Cys^{4D}** (1.12 mmol), and c) **5^{2D}** synthesized by the reaction of **D5-Cl** (0.14 mmol) and **Cys^{4D}** (1.12 mmol) under ball-milling conditions.

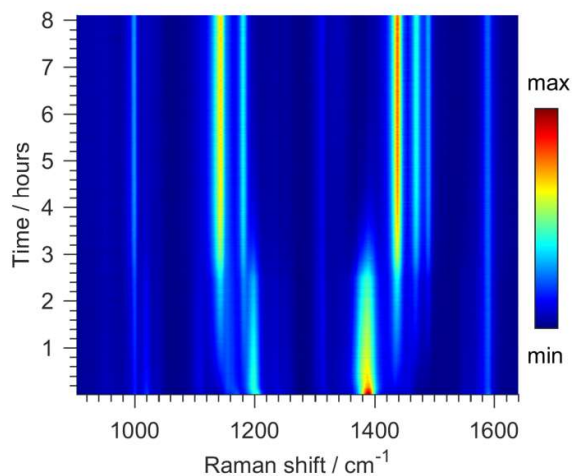


Fig. S89. 2D time-resolved Raman monitoring of the reaction of **M1-Cl** and native **Cys**.

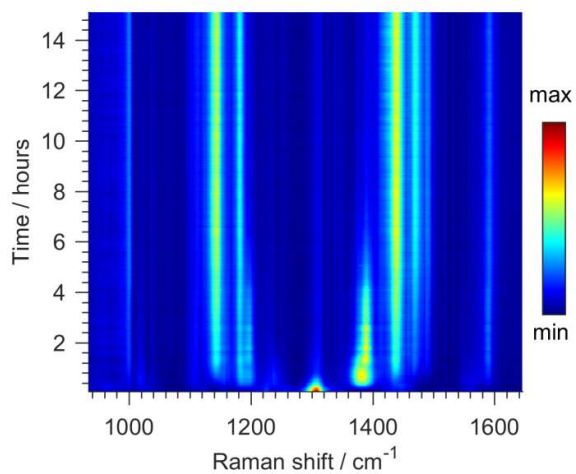


Fig. S90. 2D time-resolved Raman monitoring of the reaction of **D1-Cl** and native **Cys**.

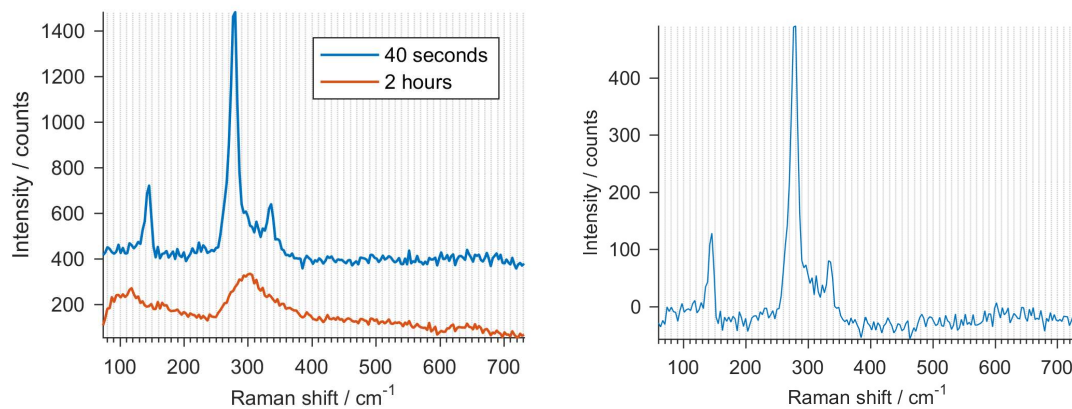


Fig. S91. *In-situ* Raman spectra of the reaction mixture of the native **Cys** and 146.0 mg (0.83 mmol) of PdCl_2 after 40 seconds of milling and after 2 hours of milling (left). *Ex-situ* Raman spectrum of pure PdCl_2 (right).

5. IR spectroscopy

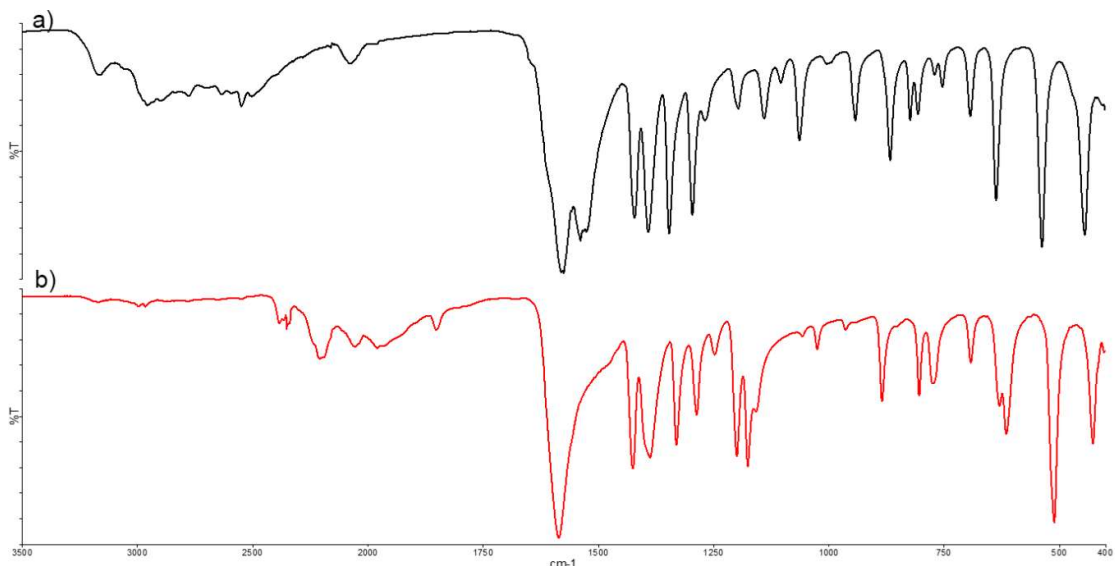


Fig. S92. FT-IR spectra of a) Cys and b) Cys^{4D}.

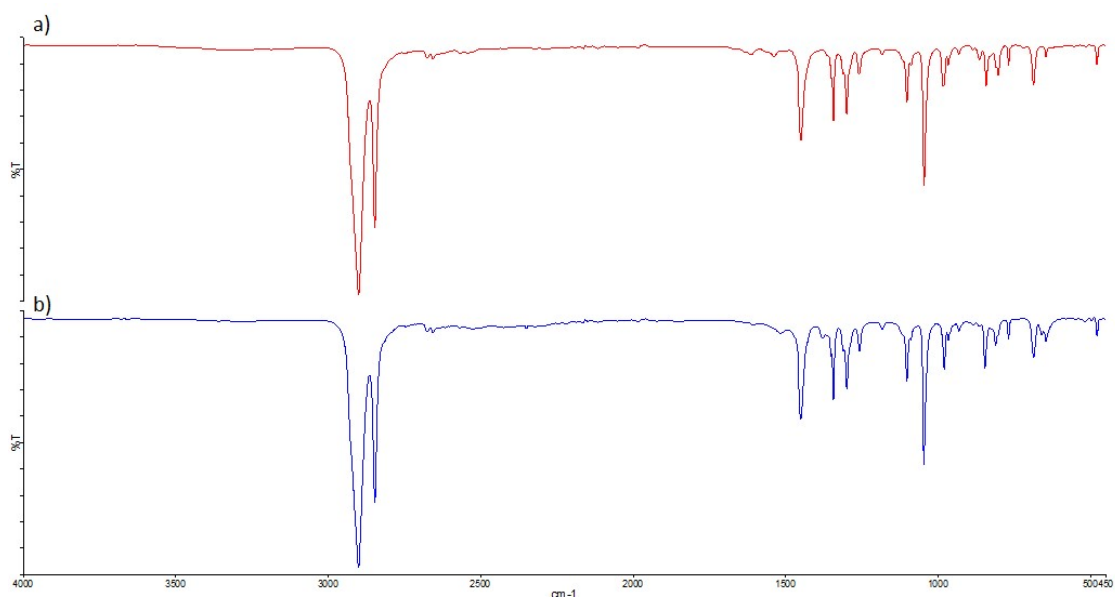


Fig. S93. FT-IR spectra of a) native and b) deuterated 1-adamantanethiol.

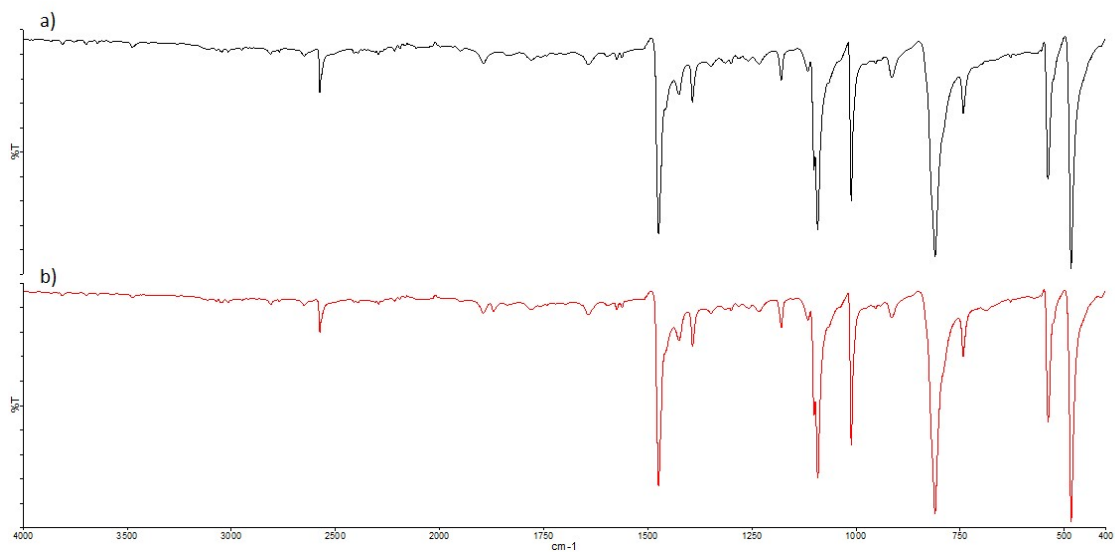


Fig. S94. FT-IR spectra of a) native and b) deuterated 4-chlorothiophenol.

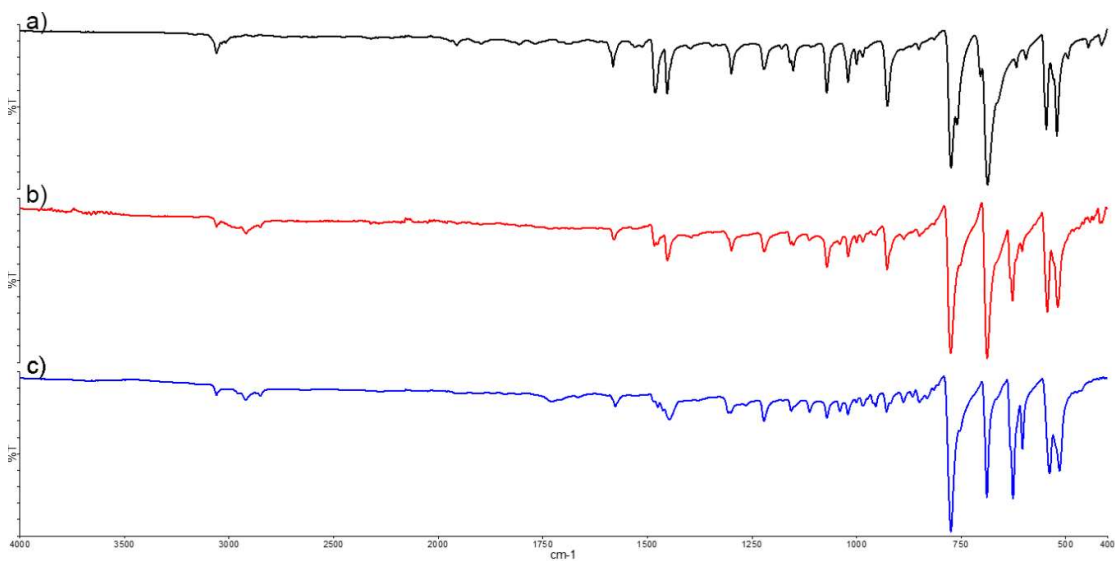


Fig. S95. FT-IR spectra of a) **1**, b) **1^D** synthesized by the reaction of **M1-Cl** (0.14 mmol) and **Cys^{4D}** (1.12 mmol), and c) **1^{2D}** synthesized by the reaction of **D1-Cl** (0.14 mmol) and **Cys^{4D}** (1.12 mmol) under ball-milling conditions.

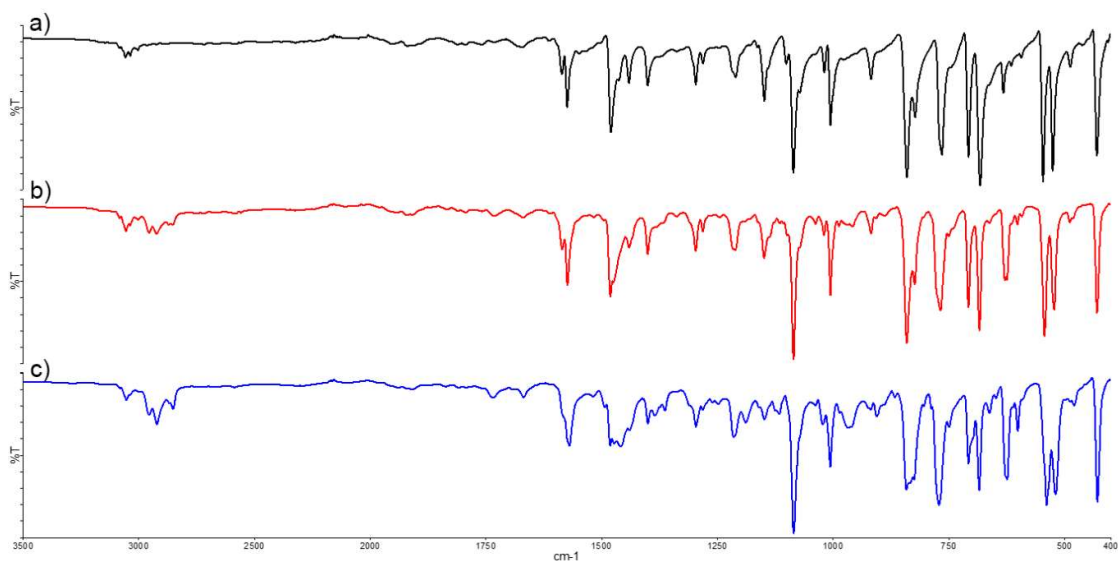


Fig. S96. FT-IR spectra of a) **2**, b) **2^D** synthesized by the reaction of **M2-Cl** (0.14 mmol) and **Cys^{4D}** (1.12 mmol), and c) **2^{2D}** synthesized by the reaction of **D2-Cl** (0.14 mmol) and **Cys^{4D}** (1.12 mmol) under ball-milling conditions.

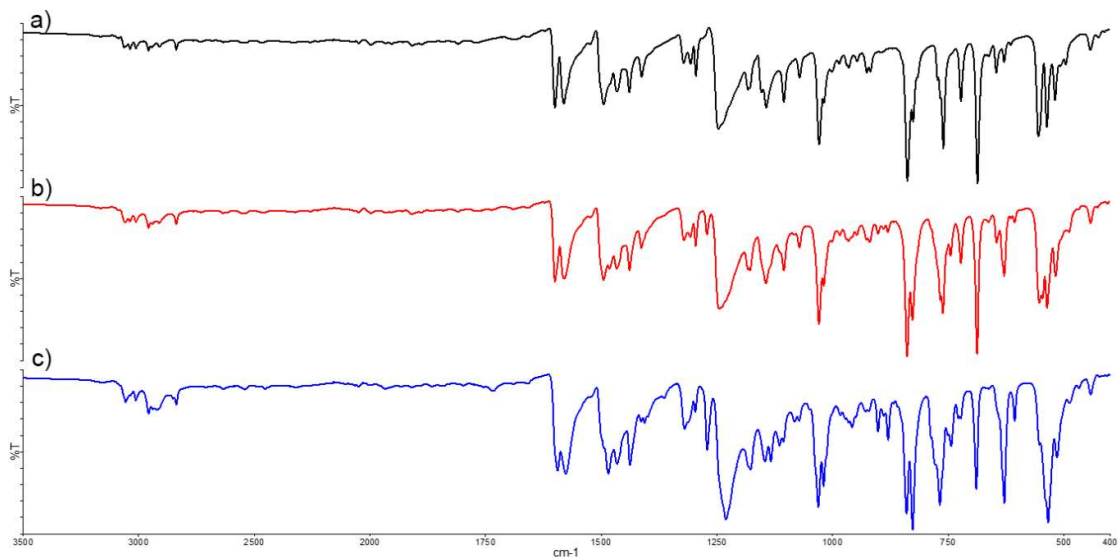


Fig. S97. FT-IR spectra of a) **3**, b) **3^D** synthesized by the reaction of **M3-Cl** (0.14 mmol) and **Cys^{4D}** (1.12 mmol), and c) **3^{2D}** synthesized by the reaction of **D3-Cl** (0.14 mmol) and **Cys^{4D}** (1.12 mmol) under ball-milling conditions.

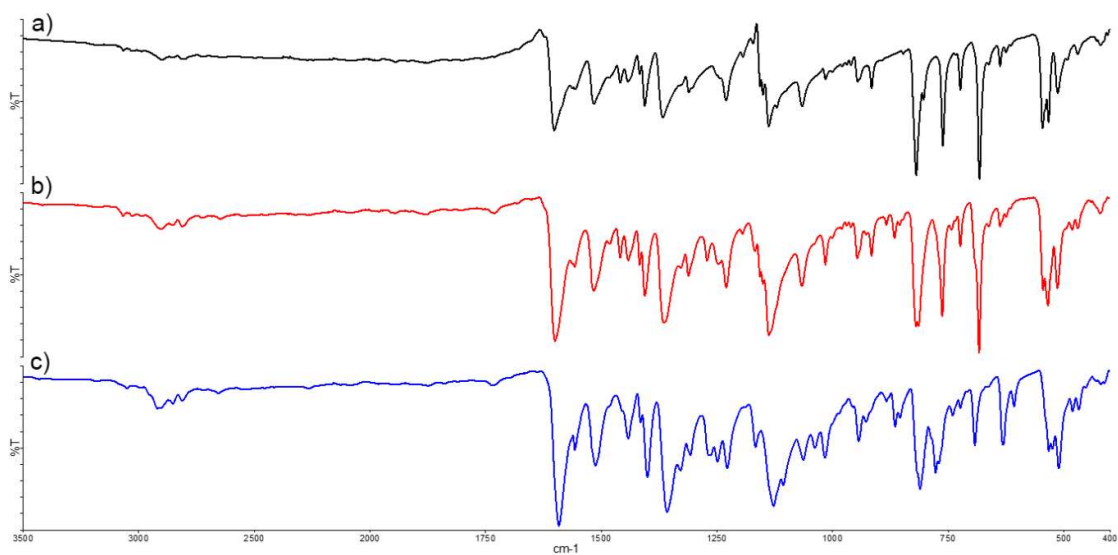


Fig. S98. FT-IR spectra of a) **4**, b) **4^D** synthesized by the reaction of **M4-Cl** (0.28 mmol) and **Cys^{4D}** (1.12 mmol), and c) **4^{2D}** synthesized by the reaction of **D4-Cl** (0.14 mmol) and **Cys^{4D}** (1.12 mmol) under ball-milling conditions.

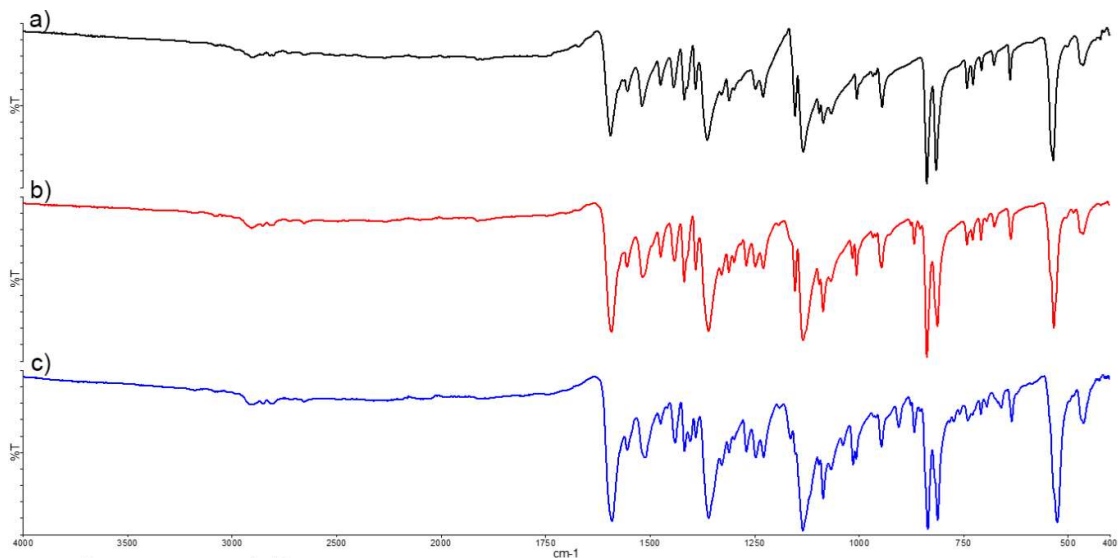


Fig. S99. FT-IR spectra of a) **5**, b) **5^D** synthesized by the reaction of **M5-Cl** (0.28 mmol) and **Cys^{4D}** (1.12 mmol), and c) **5^{2D}** synthesized by the reaction of **D5-Cl** (0.14 mmol) and **Cys^{4D}** (1.12 mmol) under ball-milling conditions.

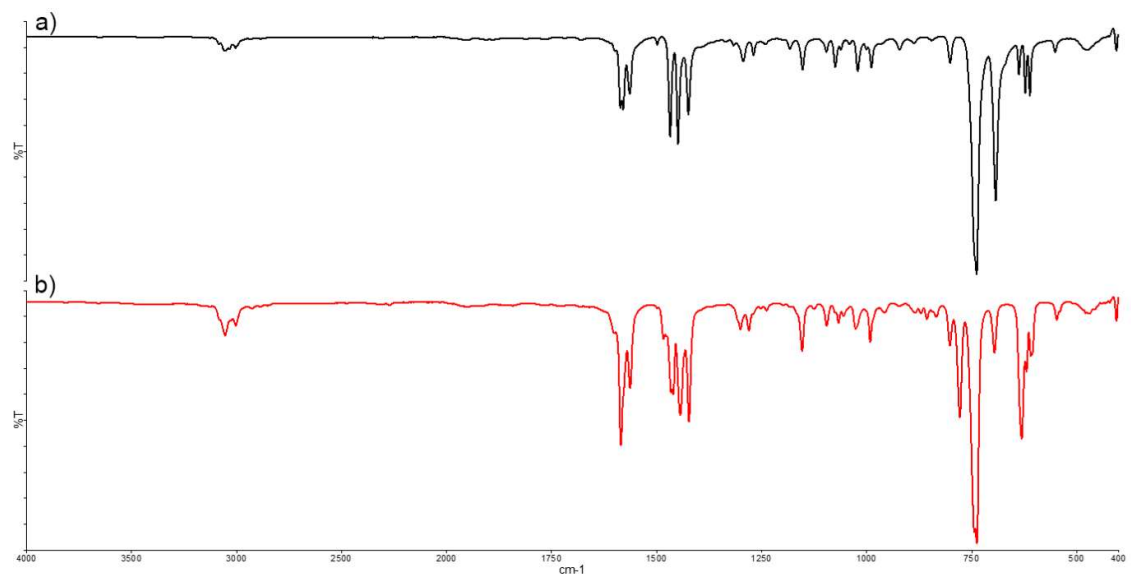


Fig. S100. FT-IR spectra of a) **6** and b) **6^D** synthesized by the reaction of **M6-Cl** (0.14 mmol) and **Cys^{4D}** (1.12 mmol) under ball-milling conditions.

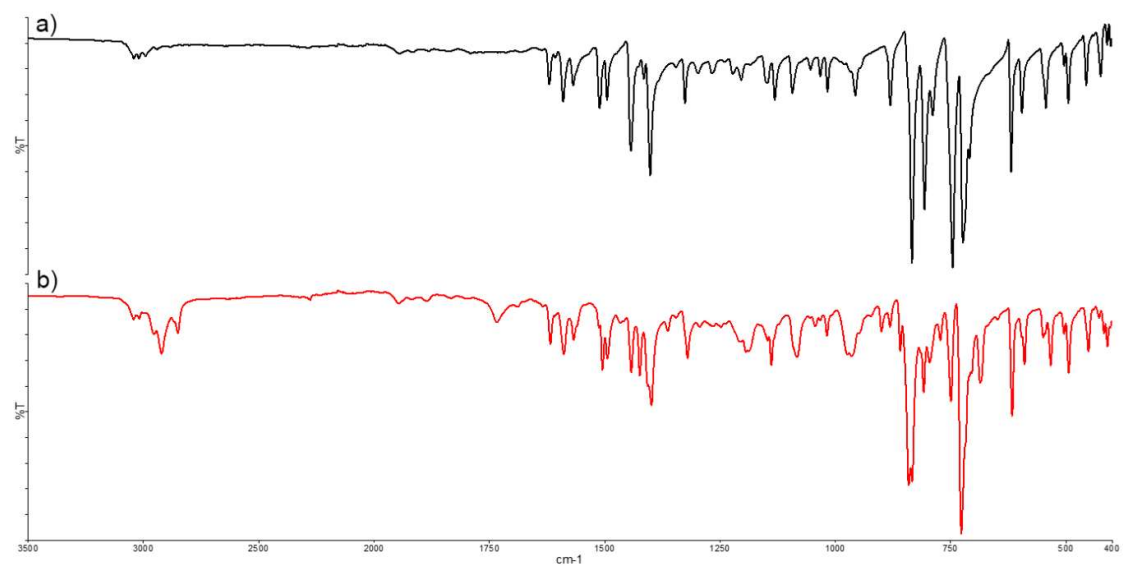


Fig. S101. FT-IR spectra of a) **7** and b) **7^D** synthesized by the reaction of **M7-Cl** (0.14 mmol) and **Cys^{4D}** (1.12 mmol) under ball-milling conditions.

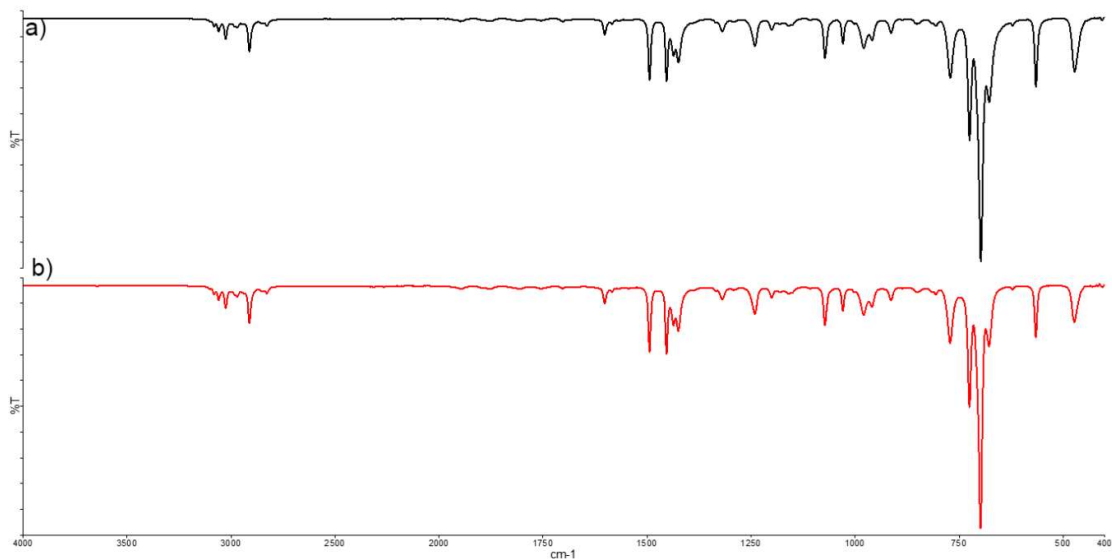


Fig. S102. FT-IR spectra of a) **8** and b) **8^D** synthesized by the reaction of **M8-Cl** (0.14 mmol) and **Cys^{4D}** (1.12 mmol) under ball-milling conditions.

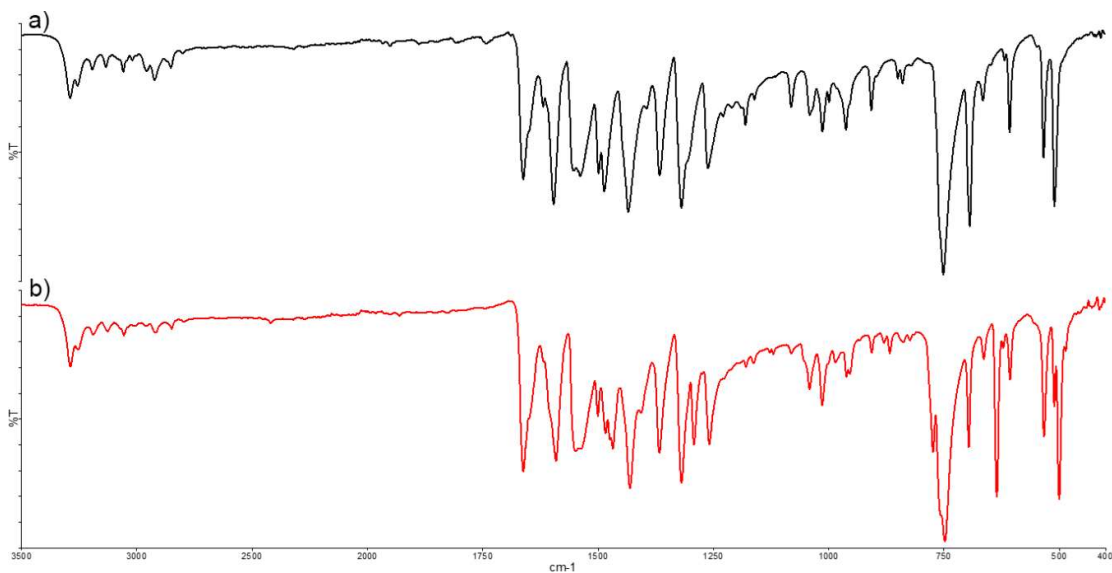


Fig. S103. FT-IR spectra of a) **9** and b) **9^D** synthesized by the reaction of **M9-Cl** (0.14 mmol) and **Cys^{4D}** (1.12 mmol) under ball-milling conditions.

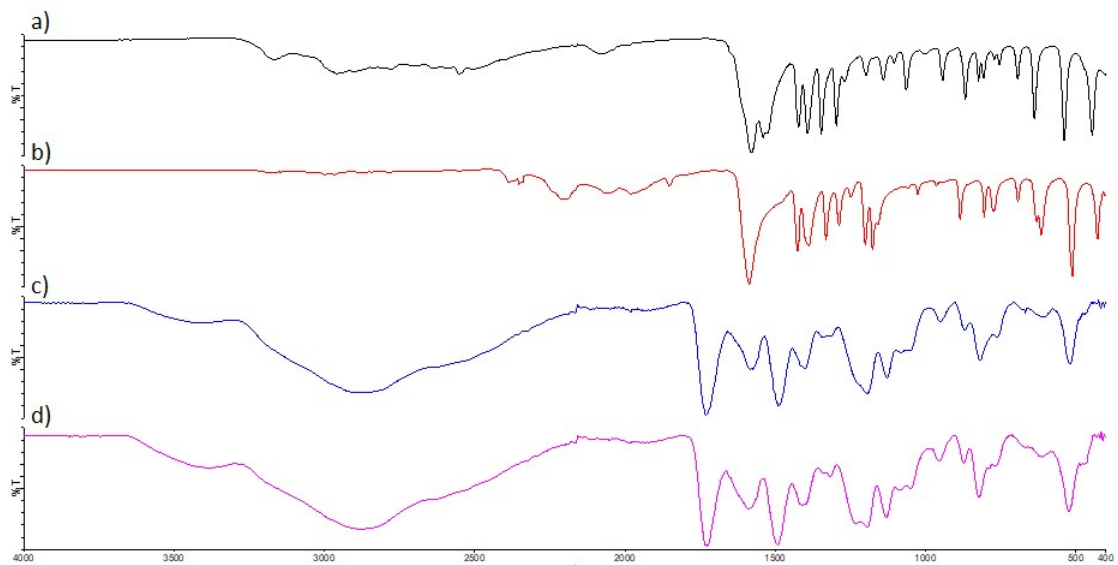


Fig. S104. FT-IR spectra of a) native **Cys**, b) **Cys**^{4D}, c) the solid residue from the reaction of ball-milling deuteration of **D1-Cl** after extraction with *n*-hexane, washing with water to remove excess **Cys**, and d) the product obtained by ball-milling reaction of the native **Cys** (1.7 mmol) with PdCl₂ (0.83 mmol).

6. TG experiments

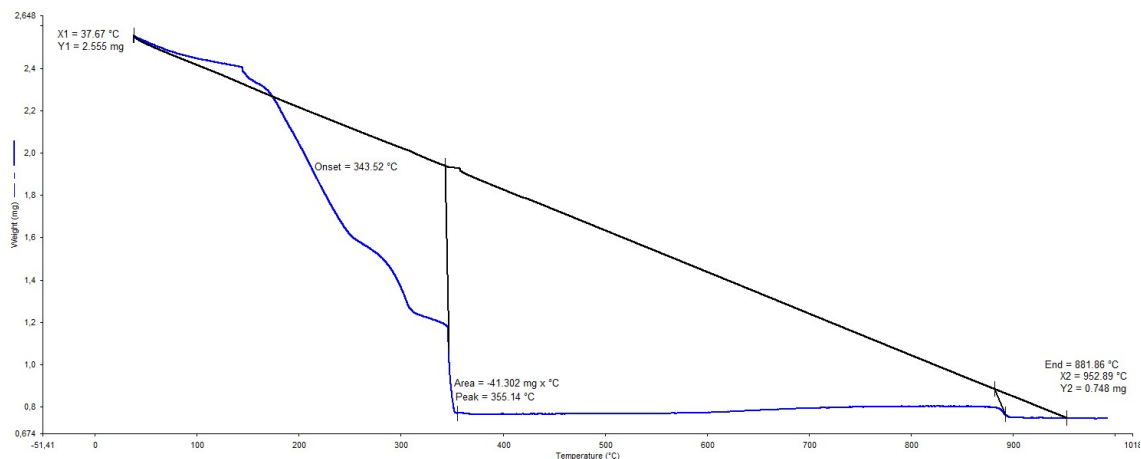


Fig. S105. TG curve of the product obtained by ball-milling reaction of the native **Cys** (1.7 mmol) with PdCl_2 (0.83 mmol) (heating ratio 10 °C/min, O_2 atmosphere). $w(\text{Pd})_{\text{calc}} = 30.69\%$ (calc. for $[\text{Pd}(\text{Cys-H})_2]$, $\text{C}_6\text{H}_{12}\text{O}_4\text{N}_2\text{S}_2\text{Pd}$), $w(\text{Pd})_{\text{exp}} = 29.28\%$.

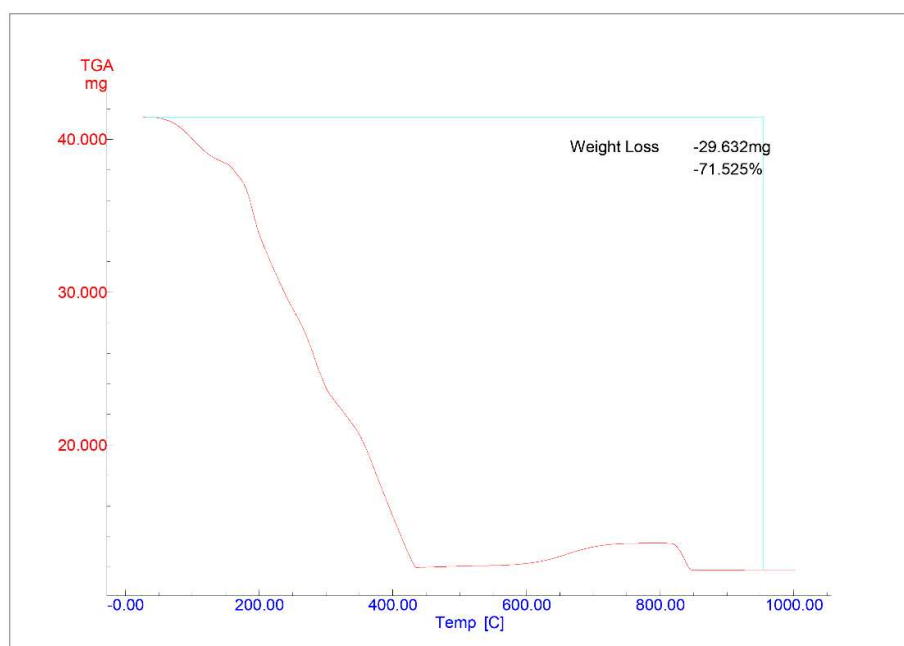


Fig. S106. TG curve of the solid residue from the reaction of ball-milling deuteration of **D1-Cl** after extraction with *n*-hexane, washing with water to remove excess cysteine, and air-drying (heating ratio 10 °C/min, synthetic air atmosphere). $w(\text{Pd})_{\text{cal.}} = 30.69\%$ (calc. for $[\text{Pd}(\text{Cys-H})_2]$, $\text{C}_6\text{H}_{12}\text{O}_4\text{N}_2\text{S}_2\text{Pd}$), $w(\text{Pd})_{\text{exp.}} = 28.23\%$.

7. HRMS spectra

HRMS spectra of the isolated deuterated products with the enlarged relevant part of the spectrum are given in Figs. S107-S134. Theoretical isotopic distributions for the given chemical formulae are given along with the structures for the observed species. For the deuterated compounds that might have isomers which are not differentiated by HRMS, only one of the possible isomers is drawn.

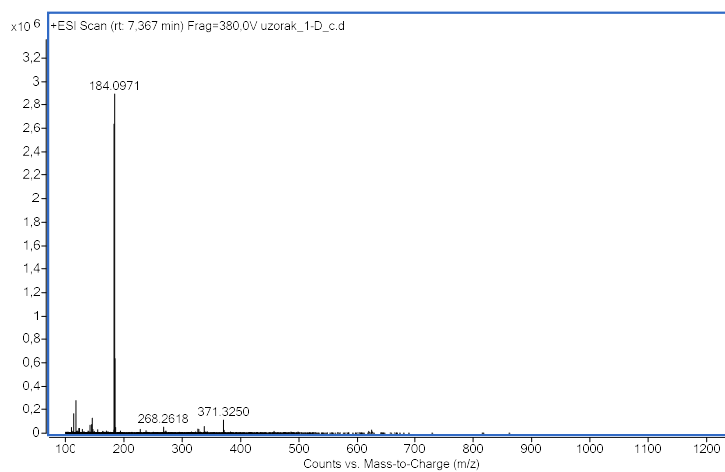
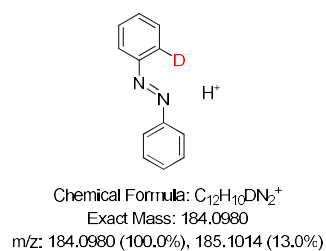
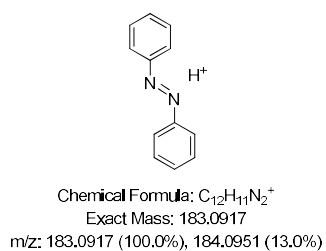
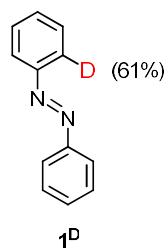


Fig. S107. HRMS spectrum of 1^D .

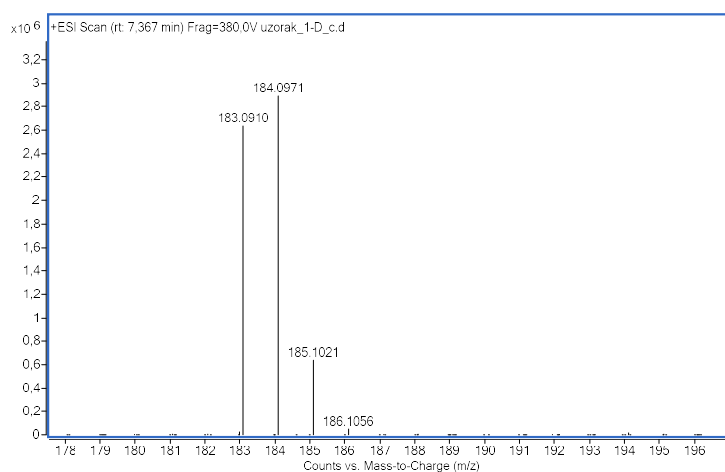


Fig. S108. HRMS spectrum of 1^D (enlarged).

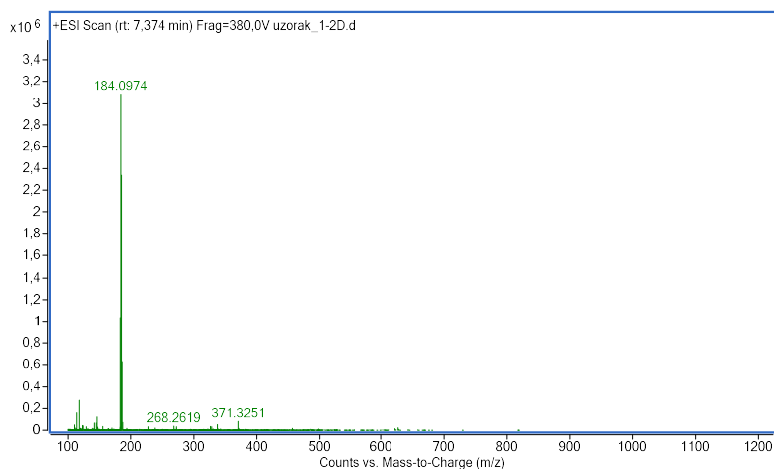
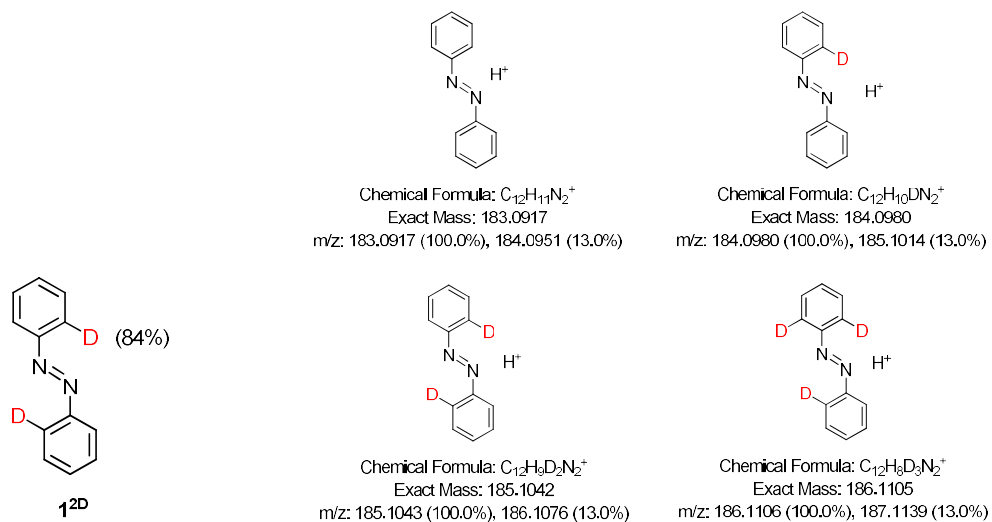


Fig. S109. HRMS spectrum of **1^{2D}**.

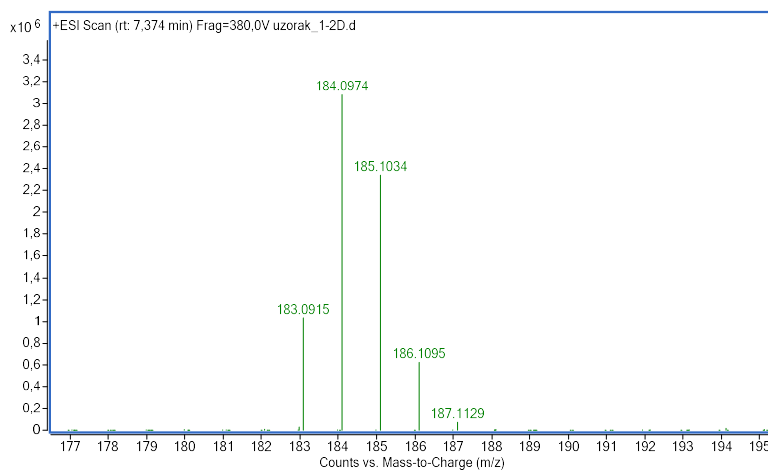


Fig. S110. HRMS spectrum of **1^{2D}** (enlarged).

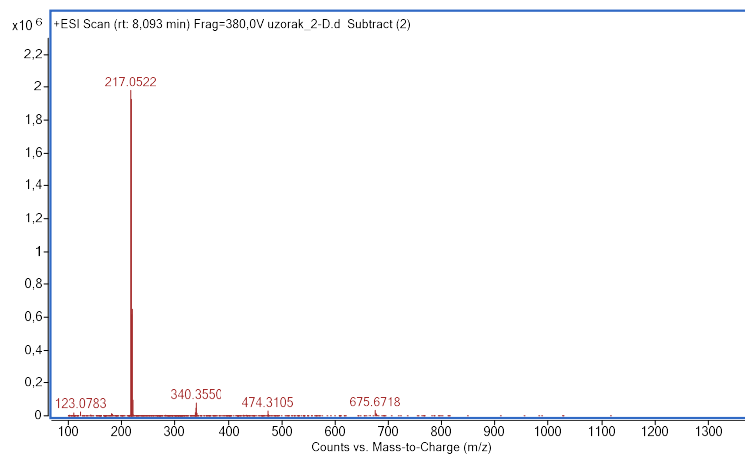
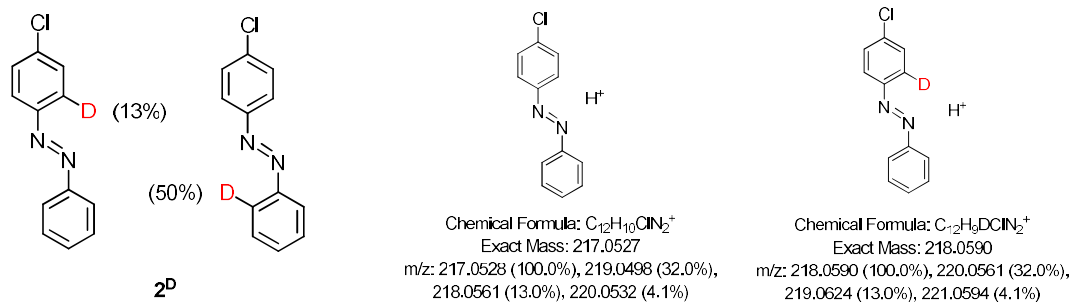


Fig. S111. HRMS spectrum of 2^D.

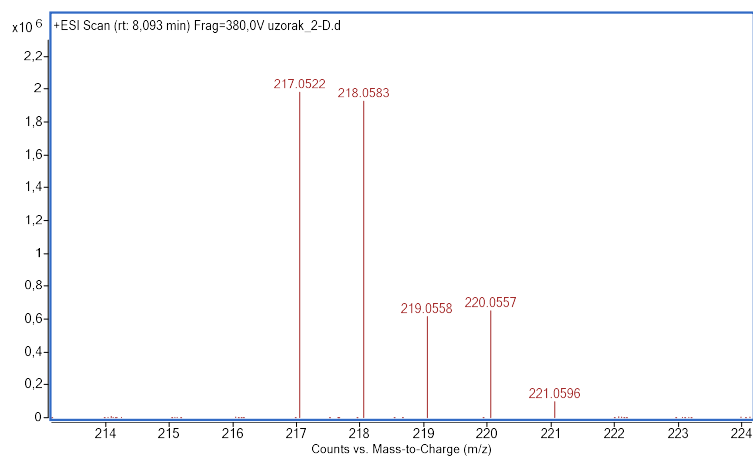


Fig. S112. HRMS spectrum of 2^D (enlarged).

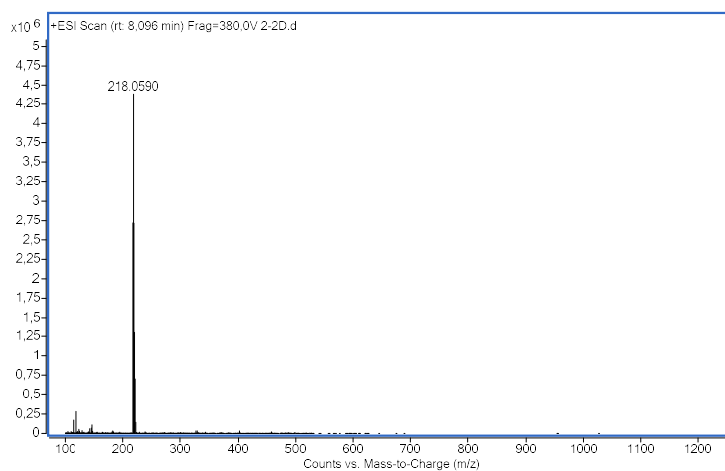
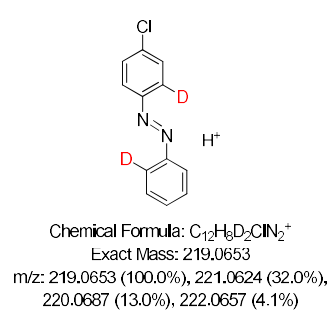
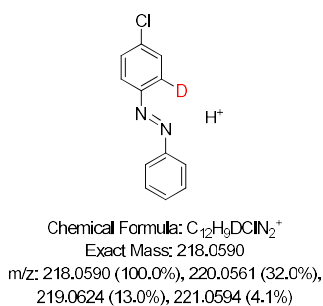
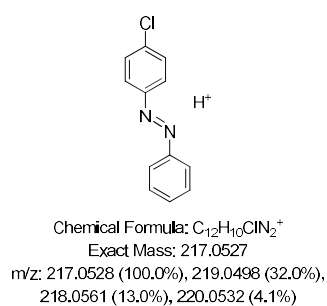
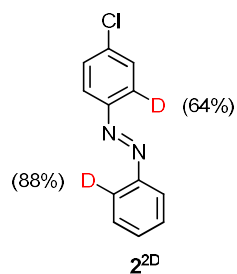


Fig. S113. HRMS spectrum of **2^{2D}**.

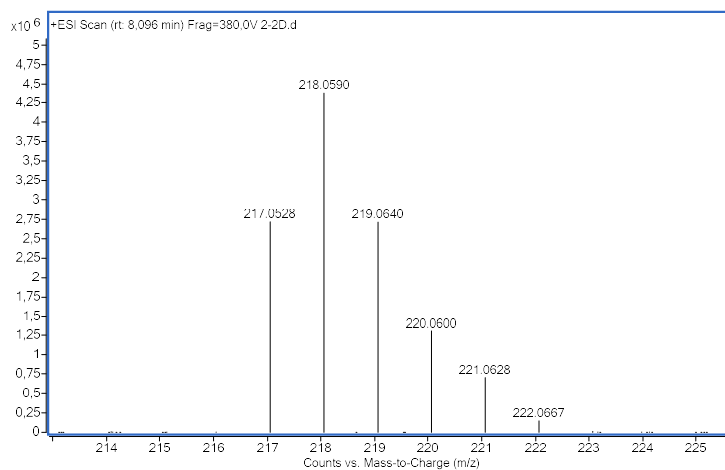


Fig. S114. HRMS spectrum of **2^{2D}** (enlarged).

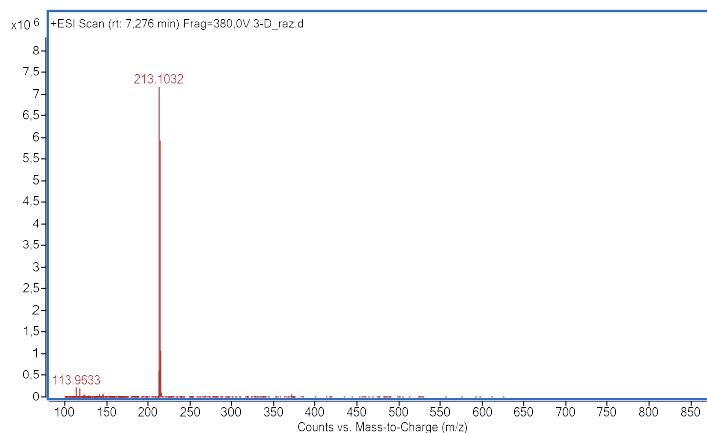
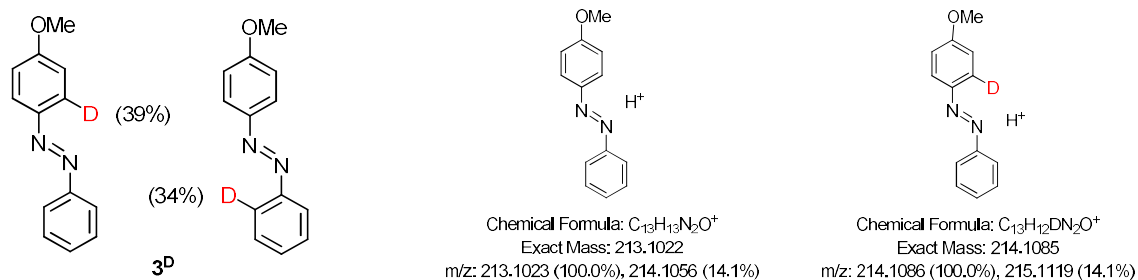


Fig. S115. HRMS spectrum of **3^D**.

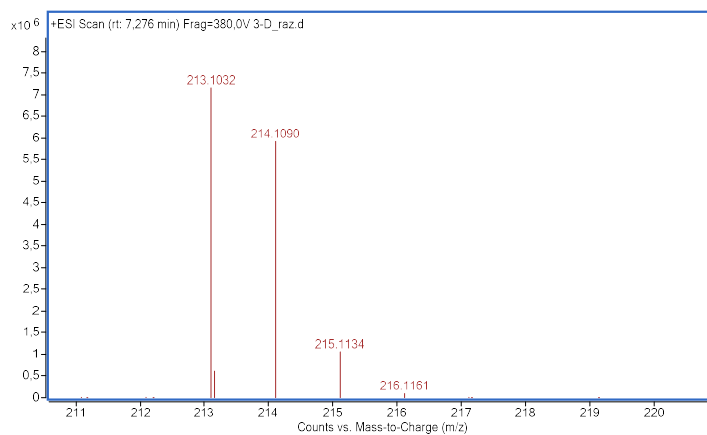


Fig. S116. HRMS spectrum of **3^D** (enlarged).

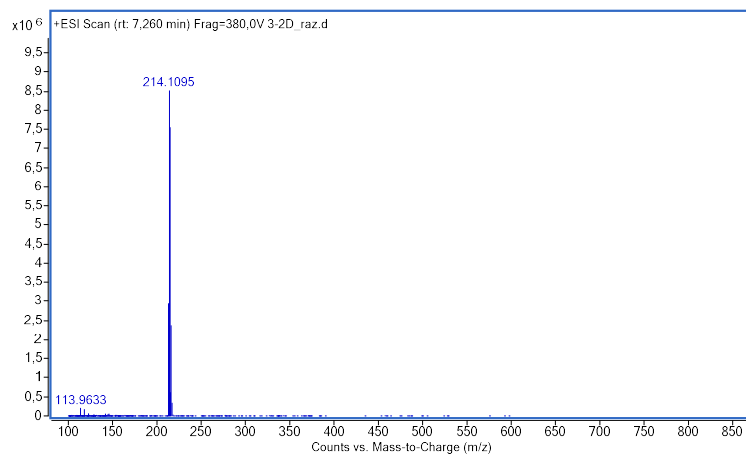
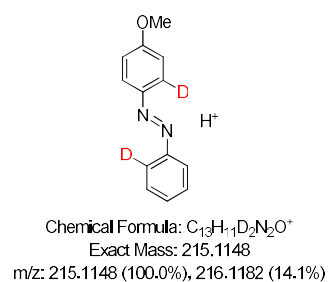
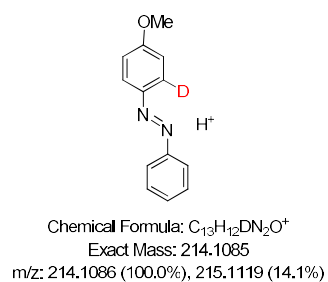
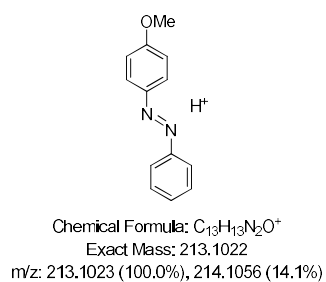
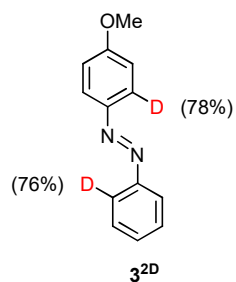


Fig. S117. HRMS spectrum of **3^{2D}**.

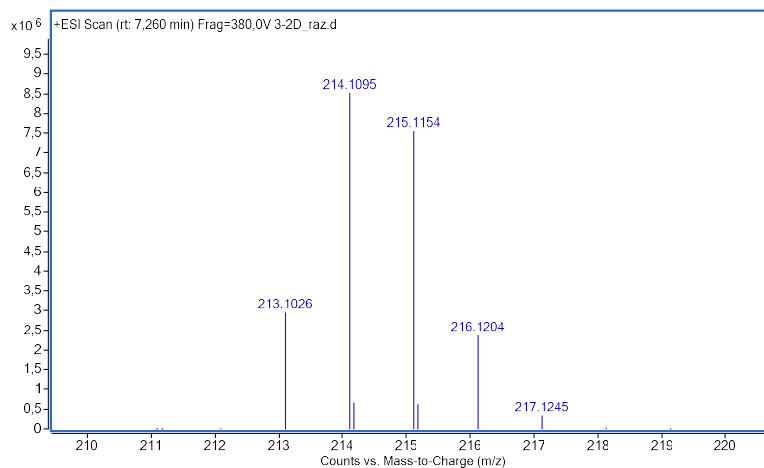
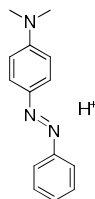
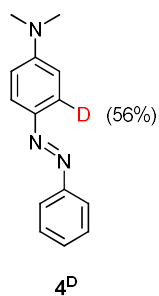
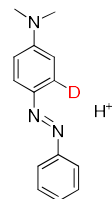


Fig. S118. HRMS spectrum of **3^{2D}** (enlarged).



Chemical Formula: $\text{C}_{14}\text{H}_{16}\text{N}_3^+$
 Exact Mass: 226.1339
 m/z: 226.1339 (100.0%), 227.1373 (15.1%),
 227.1310 (1.1%), 228.1406 (1.1%)



Chemical Formula: $\text{C}_{14}\text{H}_{15}\text{DN}_3^+$
 Exact Mass: 227.1402
 m/z: 227.1402 (100.0%), 228.1436 (15.1%),
 228.1372 (1.1%), 229.1469 (1.1%)

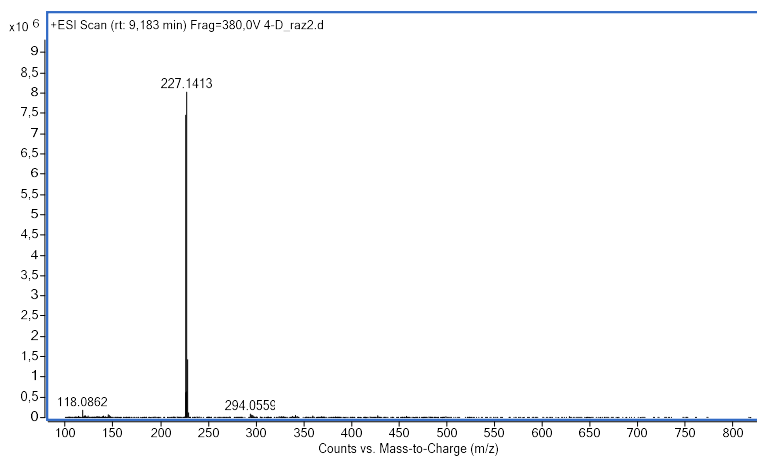


Fig. S119. HRMS spectrum of **4^D**.

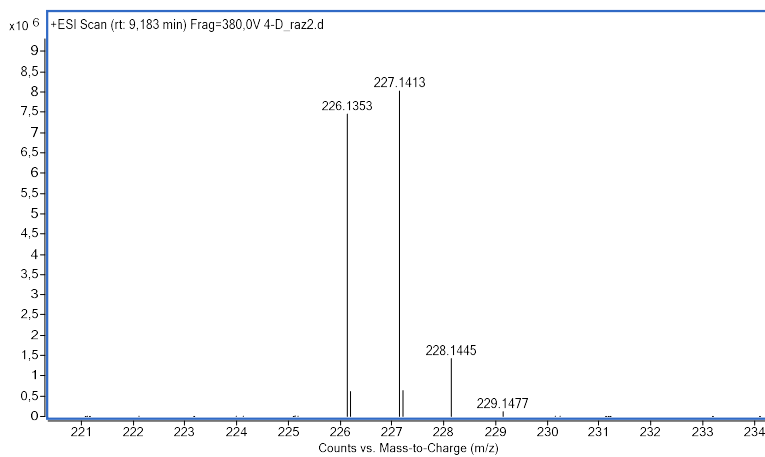
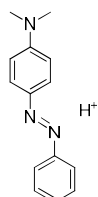
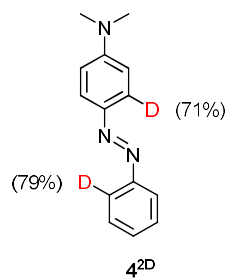
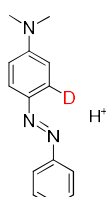


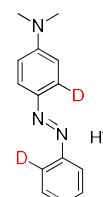
Fig. S120. HRMS spectrum of **4^D** (enlarged).



Chemical Formula: C₁₄H₁₃N₃⁺
 Exact Mass: 226.1339
 m/z: 226.1339 (100.0%), 227.1373 (15.1%),
 227.1310 (1.1%), 228.1406 (1.1%)



Chemical Formula: C₁₄H₁₃DN₃⁺
 Exact Mass: 227.1402
 m/z: 227.1402 (100.0%), 228.1436 (15.1%),
 228.1372 (1.1%), 229.1469 (1.1%)



Chemical Formula: C₁₄H₁₂D₂N₃⁺
 Exact Mass: 228.1464
 m/z: 228.1465 (100.0%), 229.1498 (15.1%),
 229.1435 (1.1%), 230.1532 (1.1%)

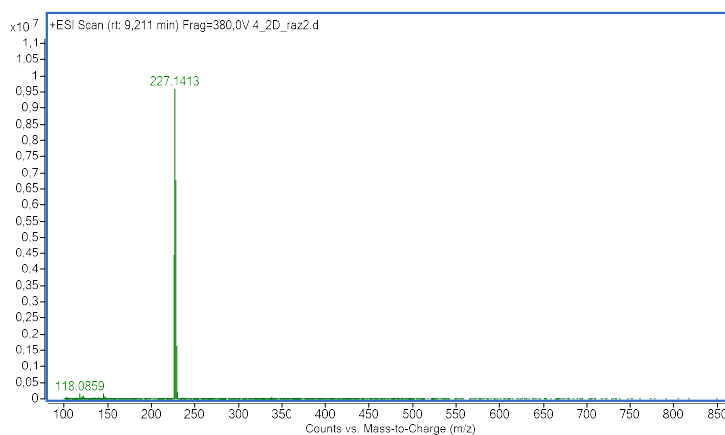


Fig. S121. HRMS spectrum of **4^{2D}**.

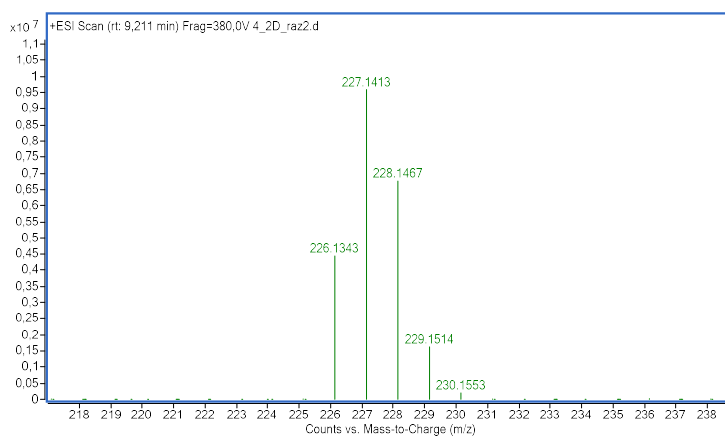
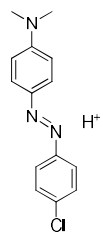
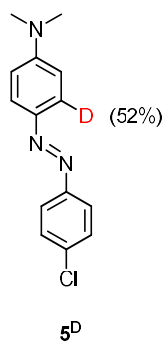
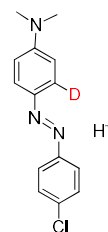


Fig. S122. HRMS spectrum of **4^{2D}** (enlarged).



Chemical Formula: $C_{14}H_{15}ClN_3^+$
 Exact Mass: 260.0949
 m/z: 260.0950 (100.0%), 262.0920 (32.0%),
 261.0983 (15.1%), 263.0954 (4.8%), 261.0920
 (1.1%), 262.1017 (1.1%)



Chemical Formula: $C_{14}H_{14}DClN_3^+$
 Exact Mass: 261.1012
 m/z: 261.1012 (100.0%), 263.0983 (32.0%),
 262.1046 (15.1%), 264.1016 (4.8%), 262.0983
 (1.1%), 263.1079 (1.1%)

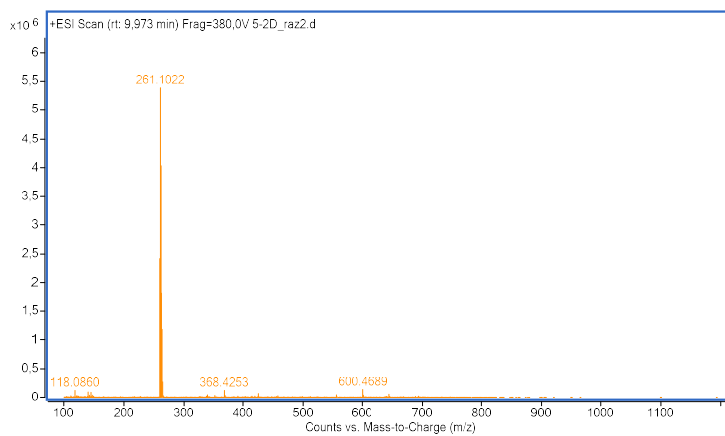


Fig. S123. HRMS spectrum of 5^D.

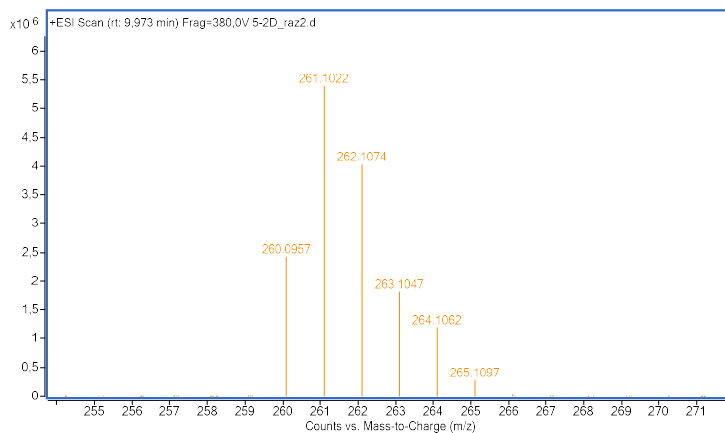


Fig. S124. HRMS spectrum of 5^D (enlarged).

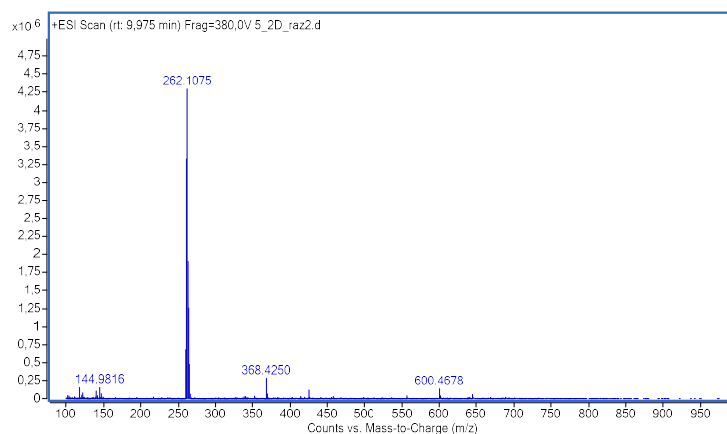
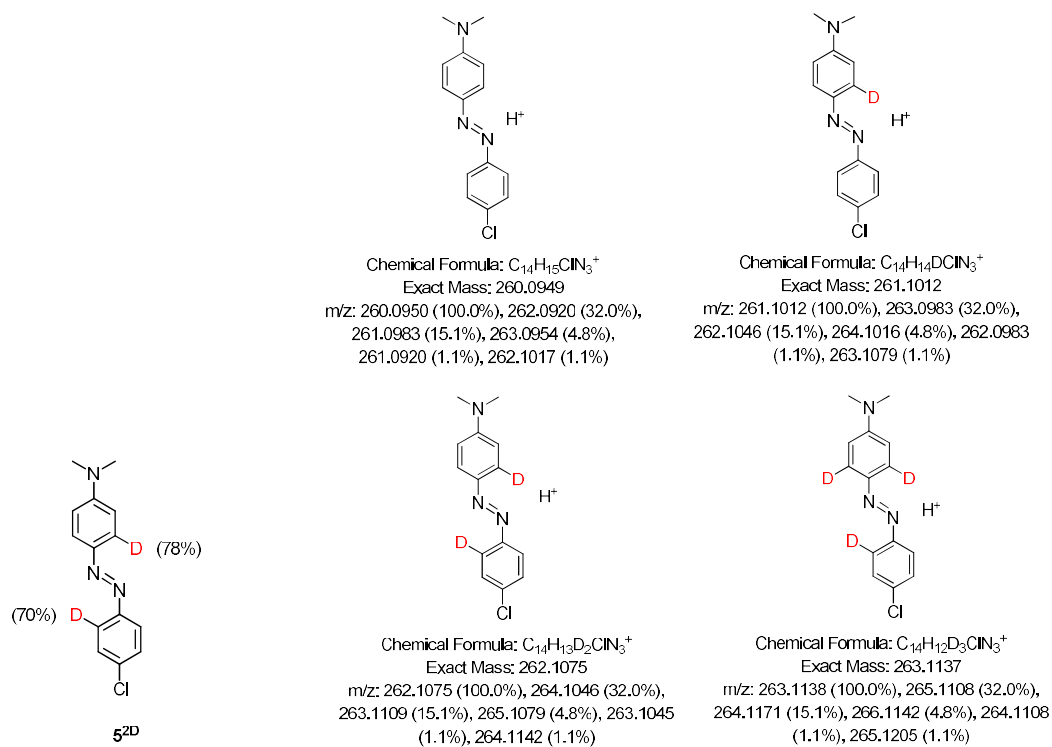


Fig. S125. HRMS spectrum of 5^{2D}.

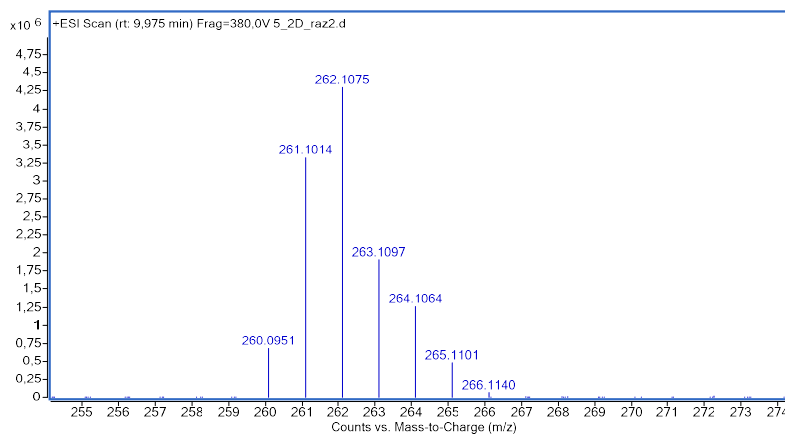
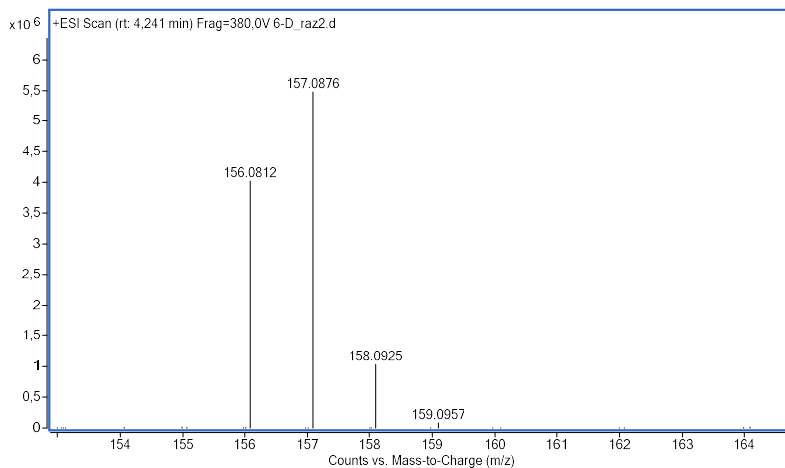
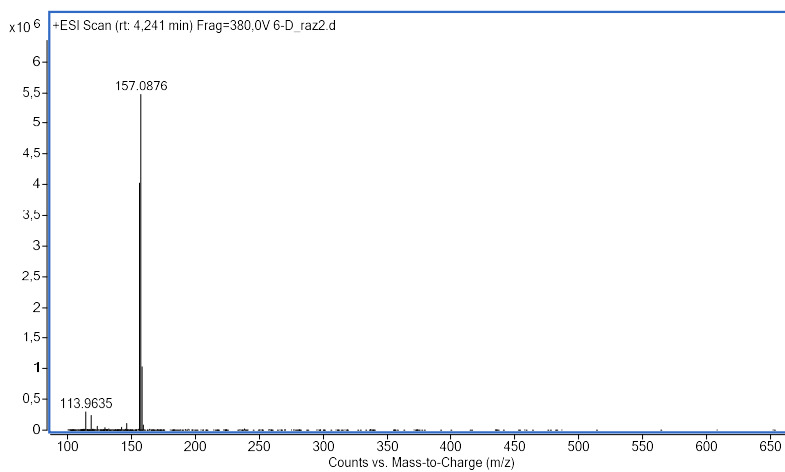
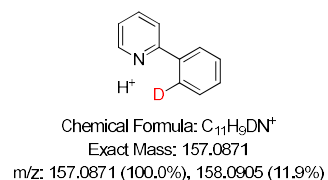
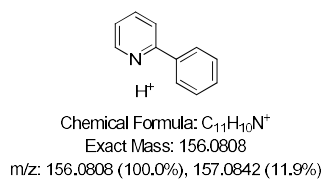
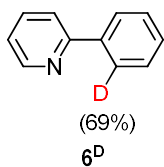


Fig. S126. HRMS spectrum of 5^{2D} (enlarged).



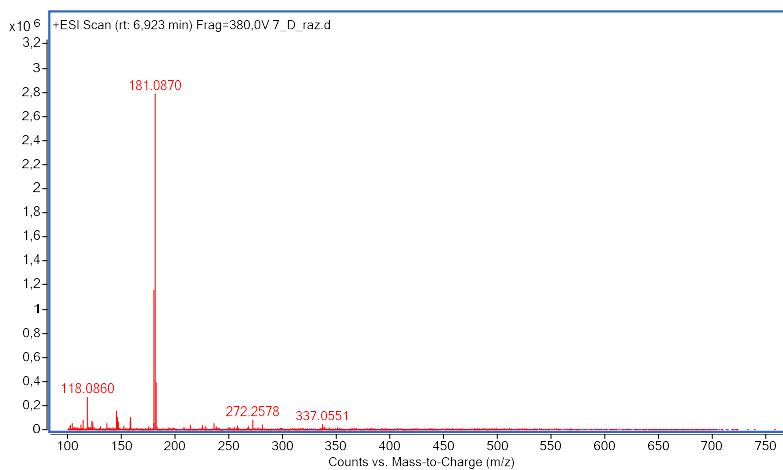
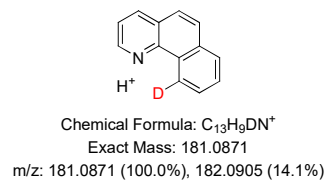
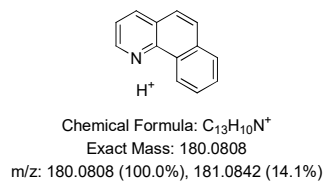
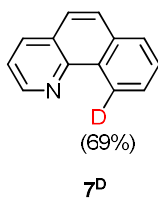


Fig. S129. HRMS spectrum of **7^D**.

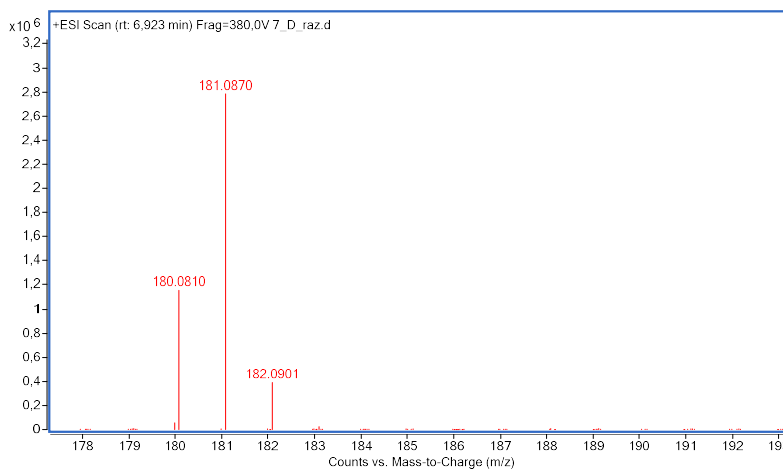


Fig. S130. HRMS spectrum of **7^D** (enlarged).

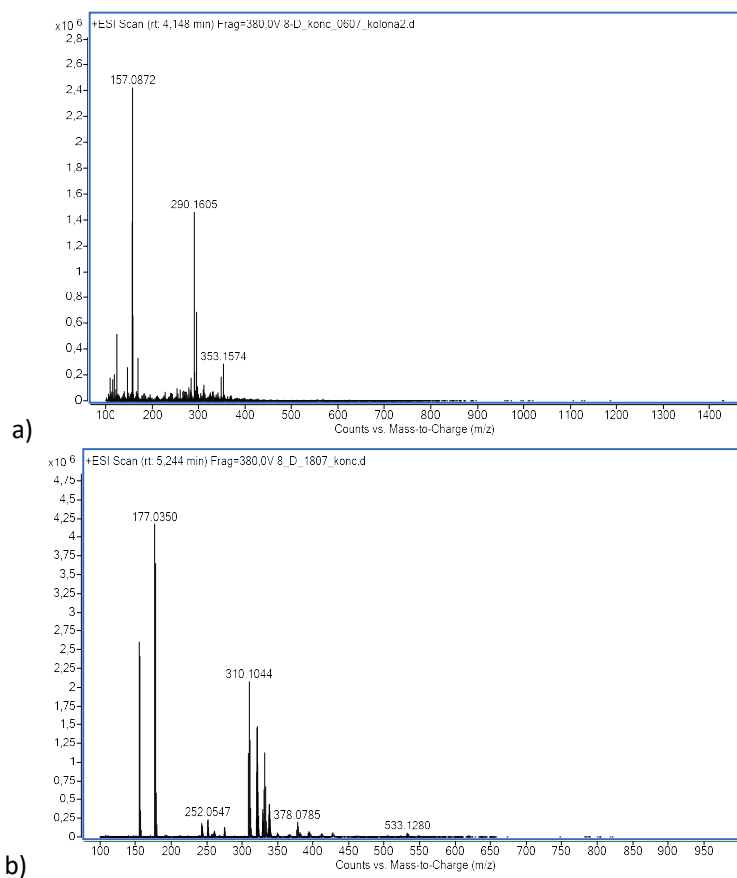
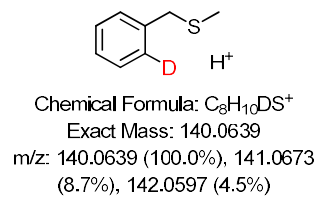
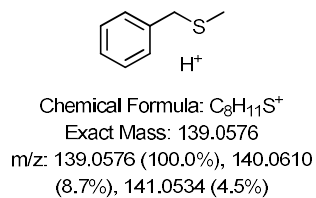
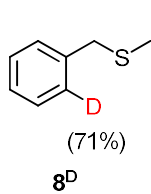
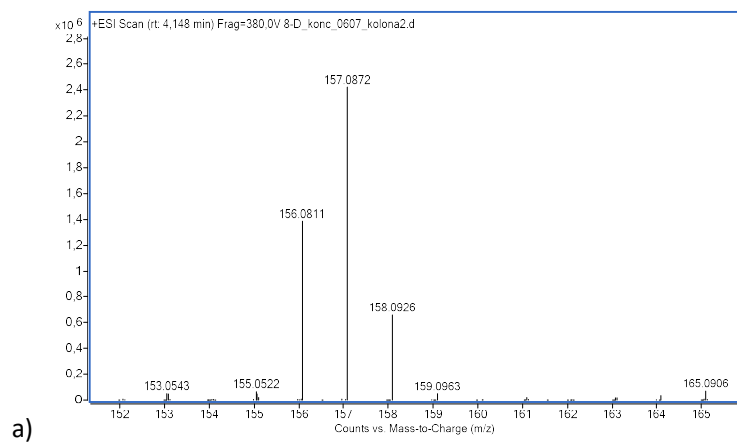


Fig. S131. HRMS spectra of 8^D in a) MeCN- H_2O and b) MeOH- H_2O .



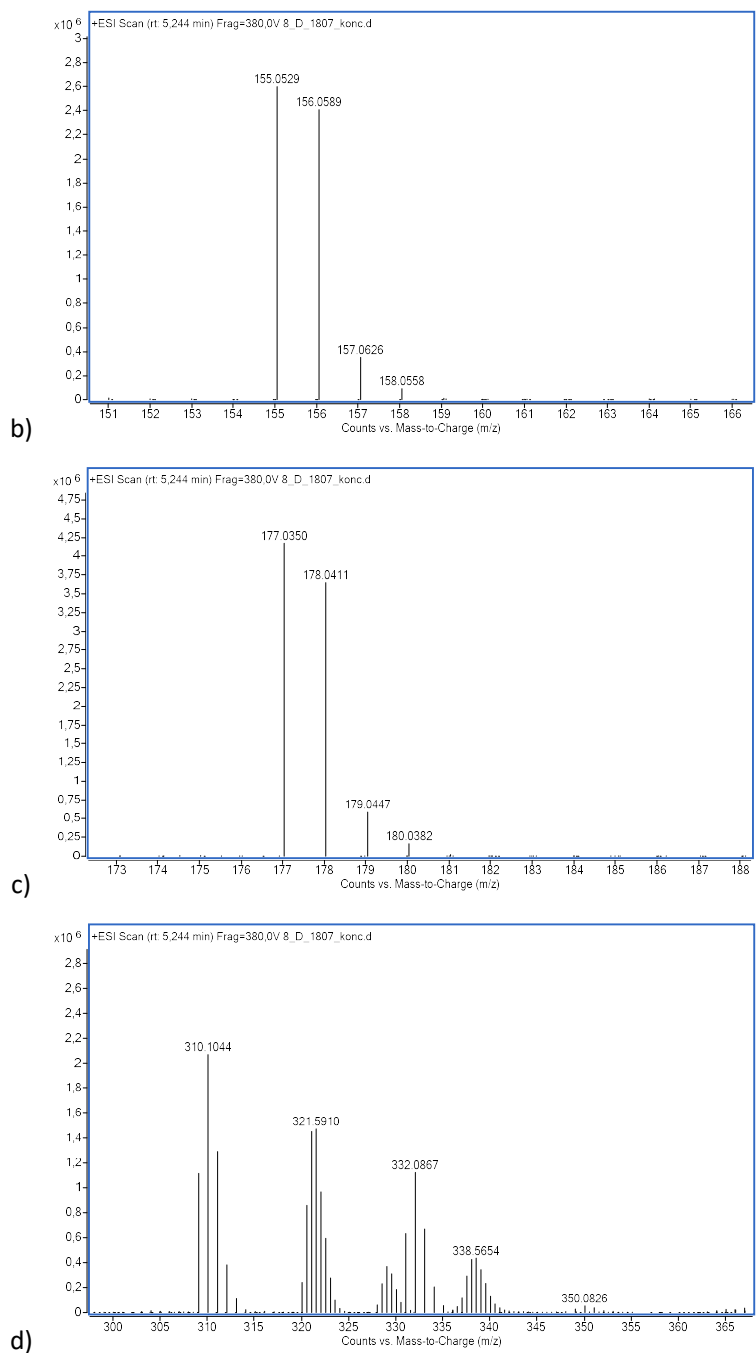
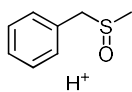
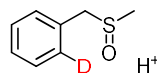


Fig. S132. HRMS spectra of **8^P** (enlarged) in MeCN-H₂O (a) and b) MeOH-H₂O (b-d).

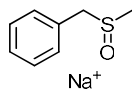
Compound **8^P** was oxidized or decomposed during recording of the HRMS spectrum nevertheless of the operating conditions. We can tentatively assign the observed MS data by formation of sulphoxide derivative that depended on the recording conditions. Possible assignment of the observed peaks is given below.



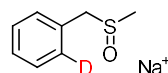
Chemical Formula: $C_8H_{11}OS^+$
 Exact Mass: 155.0525
 m/z: 155.0526 (100.0%), 156.0559 (8.7%), 157.0484 (4.5%)



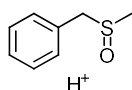
Chemical Formula: $C_8H_{10}DOS^+$
 Exact Mass: 156.0588
 m/z: 156.0588 (100.0%), 157.0622 (8.7%), 158.0546 (4.5%)



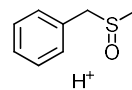
Chemical Formula: $C_8H_{10}NaOS^+$
 Exact Mass: 177.0345
 m/z: 177.0345 (100.0%), 178.0379 (8.7%), 179.0303 (4.5%)



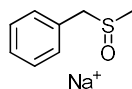
Chemical Formula: $C_8H_9DNaOS^+$
 Exact Mass: 178.0407
 m/z: 178.0408 (100.0%), 179.0441 (8.7%), 180.0366 (4.5%)



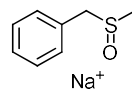
Chemical Formula: $C_{16}H_{21}O_2S_2^+$
 Exact Mass: 309.0977
 m/z: 309.0978 (100.0%), 310.1012 (17.3%), 311.0936 (9.0%), 310.0972 (1.6%), 312.0969 (1.6%), 311.1045 (1.4%)



Chemical Formula: $C_{16}H_{20}DO_2S_2^+$
 Exact Mass: 310.1040
 m/z: 310.1041 (100.0%), 311.1074 (17.3%), 312.0999 (9.0%), 311.1035 (1.6%), 313.1032 (1.6%), 312.1108 (1.4%)

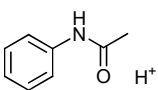
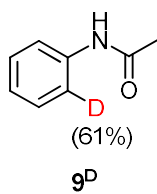


Chemical Formula: $C_{16}H_{20}NaO_2S_2^+$
 Exact Mass: 331.0797
 m/z: 331.0797 (100.0%), 332.0831 (17.3%), 333.0755 (9.0%), 332.0791 (1.6%), 334.0789 (1.6%), 333.0865 (1.4%)

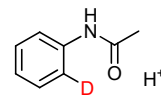


Chemical Formula: $C_{16}H_{19}DNaO_2S_2^+$
 Exact Mass: 332.0860
 m/z: 332.0860 (100.0%), 333.0894 (17.3%), 334.0818 (9.0%), 333.0854 (1.6%), 335.0852 (1.6%), 334.0927 (1.4%)

Doubly charged ions in Fig. S132d are likely obtained by combining the above-listed structures.



Chemical Formula: C₈H₁₀NO⁺
Exact Mass: 136.0757
m/z: 136.0757 (100.0%), 137.0791 (8.7%)



Chemical Formula: C₈H₉DNO⁺
Exact Mass: 137.0820
m/z: 137.0820 (100.0%), 138.0854 (8.7%)

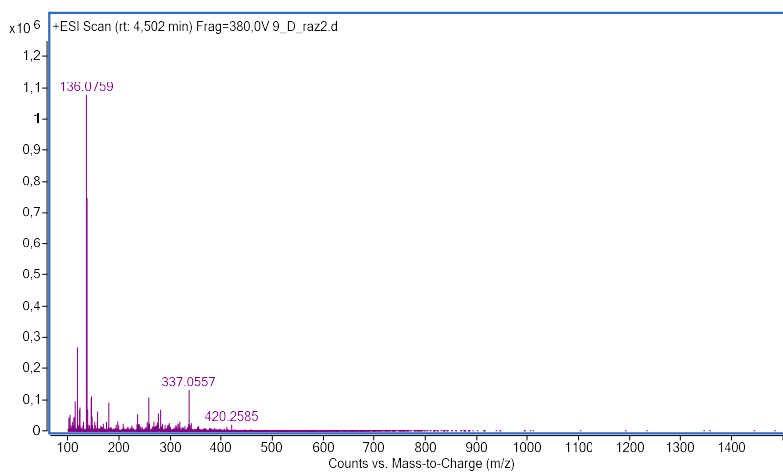


Fig. S133. HRMS spectrum of **9^D**.

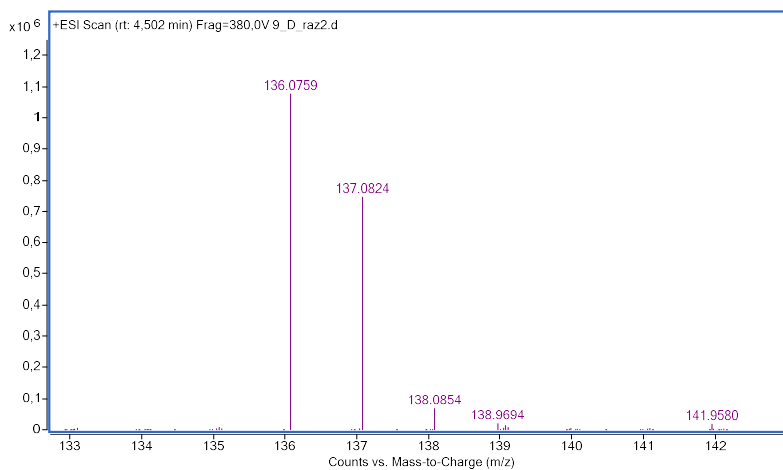


Fig. S134. HRMS spectrum of **9^D** (enlarged).

8. Computational study

8.1 General remarks

D-source donor group. Both the amino and the carboxylic groups in cysteine might be involved in the D-transfer. Attempts to locate a low-lying transition state that would lead to deuteration *via* the thiol group were unsuccessful.

Two isomers of the *N,S*-coordinated cysteine that are important for the identification of the most stable isomer of the examined complexes are given in Fig. S67. The main difference is in the position of the carboxylic group that might be positioned equatorially or axially. Usually the equatorial position is lower in energy than the axial position. However, the isomer with the axial orientation can be lower in energy due to the intramolecular interactions and possible D-transfer between the functional groups in two coordinated cysteines, or between the coordinated and the non-coordinated cysteine.

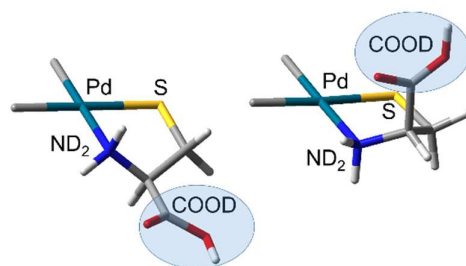


Fig. S135. Main isomers of the *N,S*-coordinated L-cysteine.

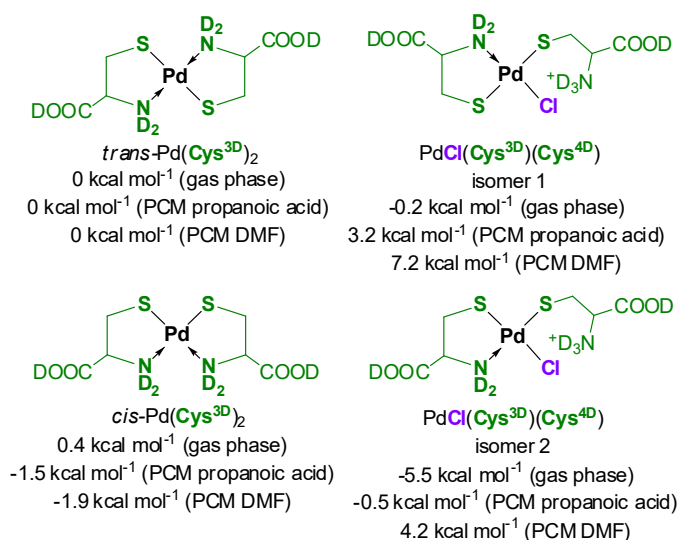
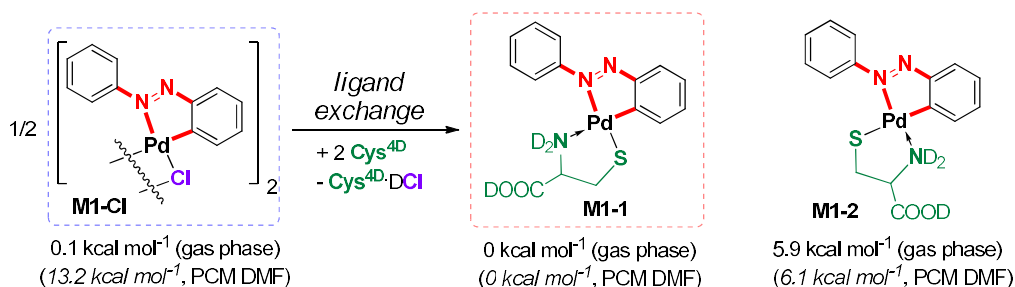


Chart S1. Relative free energies (in kcal mol⁻¹) for isomers of the monomeric Pd(Cys^{3D})₂ and PdCl(Cys^{3D})(Cys^{4D}).

8.2 Deuteration of the monocyclopalladated cysteine complex

Milling of the dimeric monocyclopalladated azobenzene **M1-Cl** with **Cys**^{4D} in excess gives the cysteine complex that can be present in two isomeric forms **M1-1** and **M1-2** (Scheme S1). The most stable monomeric isomer **M1-1** has **Cys**^{3D} bound *via* the deprotonated thiol group *trans* to the azo group and the amino group *trans* to the palladated carbon atom. The other isomer **M1-2** is 5.9 kcal mol⁻¹ less stable than **M1-1**. Monopalladated complexes **M4-Cl** and **M5-Cl** are monomeric with one DMF ligand bonded to the Pd center. Their reaction course is expected to be similar to that of **M1-Cl**. The main difference is in formation of **M4** or **M5** where DCl and DMF are liberated from **M4-Cl** or **M5-Cl**.



Scheme S1. Ligand exchange in chloride monocyclopalladated azobenzene complexes.

• Study of the D-transfer

Our previous computational data obtained using B3LYP functional showed good qualitative agreement with the experimental findings, agreed best with the experimental spectroscopic data, and showed robustness for studies related to the palladated azobenzenes.¹⁹ However, in order to test several other methods for the present computational study, we have used additional methods apart from the B3LYP-D3/6-311+G**/SDD(Pd)/gas phase (data presented in Table S2):

- 1) a small basis set (6-31G* instead of 6-311+G**/SDD(Pd)): B3LYP-D3/6-31G*/SDD(Pd)/gas phase;
- 2) no empirical dispersion correction ("only" B3LYP instead of B3LYP-D3): B3LYP/6-311+G**/SDD(Pd)/gas phase;
- 3) a more modern basis set (def2tzvp instead of 6-311+G**/SDD(Pd)): B3LYP-D3/def2tzvp/gas phase;
- 4) a more modern functional (ω B97x-D instead of B3LYP-D3): ω B97x-D/6-311+G**/SDD(Pd)/gas phase;
- 5) including solvation effects modeled with the polarizable continuum model (PCM) for DMF: B3LYP-D3/6-311+G**/SDD(Pd)/PCM(DMF);
- 6) including solvation effects modeled with the polarizable continuum model (PCM) for propanoic acid: B3LYP-D3/6-311+G**/SDD(Pd)/PCM(propanoic acid).

Smaller basis set 6-31G* if compared to 6-311+G** resulted in differences in the calculated free energies that were not systematic (± 3.5 kcal mol⁻¹). We find the values obtained by the larger basis set more appropriate. Def2tzvp values were similar to the 6-311+G** values with the exception of the higher free energies for the species involved in a D-transfer from DCl and **Cys**^{4D}·DCl. Functional ω B97x-D produced data that were mostly by up to 2 kcal mol⁻¹ higher than for B3LYP-D3. No included

dispersion ended in much higher energies than other methods and was considered not appropriate. All methods gave the same order of preference for the examined D-sources: $\text{Cys}^{4\text{D}}\cdot\text{DCI} > \text{Cys}^{4\text{D}} > \text{DCI}$ (If present) $> \text{AcOD}$.

Furthermore, considering the work by B. S Pladevall et al.,²⁰ we have performed the calculations using PCM modelling. This was regarded as a rigorous computational check of the medium influence on the computed results. We could not calculate the dielectric constant of the mixtures we have used (applying the approach used by Pladevall et al.) as dielectric constants of all components in our systems are not available. Thus, two solvents, propanoic acid and DMF, were chosen as examples to study the effect that the medium can make on the results. Obtained results indicate that the choice of the medium changes the difference between free energies of the transition states for the deuteration of **M1-1** using $\text{Cys}^{4\text{D}}$ and $\text{Cys}^{4\text{D}}\cdot\text{DCI}$ as D-sources. In the propanoic acid, D-source order of preference determined in the gas phase is still preserved. Medium should be DMF (or similar) to achieve similar free energies of transition states for deuteration using $\text{Cys}^{4\text{D}}$ and $\text{Cys}^{4\text{D}}\cdot\text{DCI}$ as D-sources ($\text{Cys}^{4\text{D}}\cdot\text{DCI}$ is still slightly preferred).

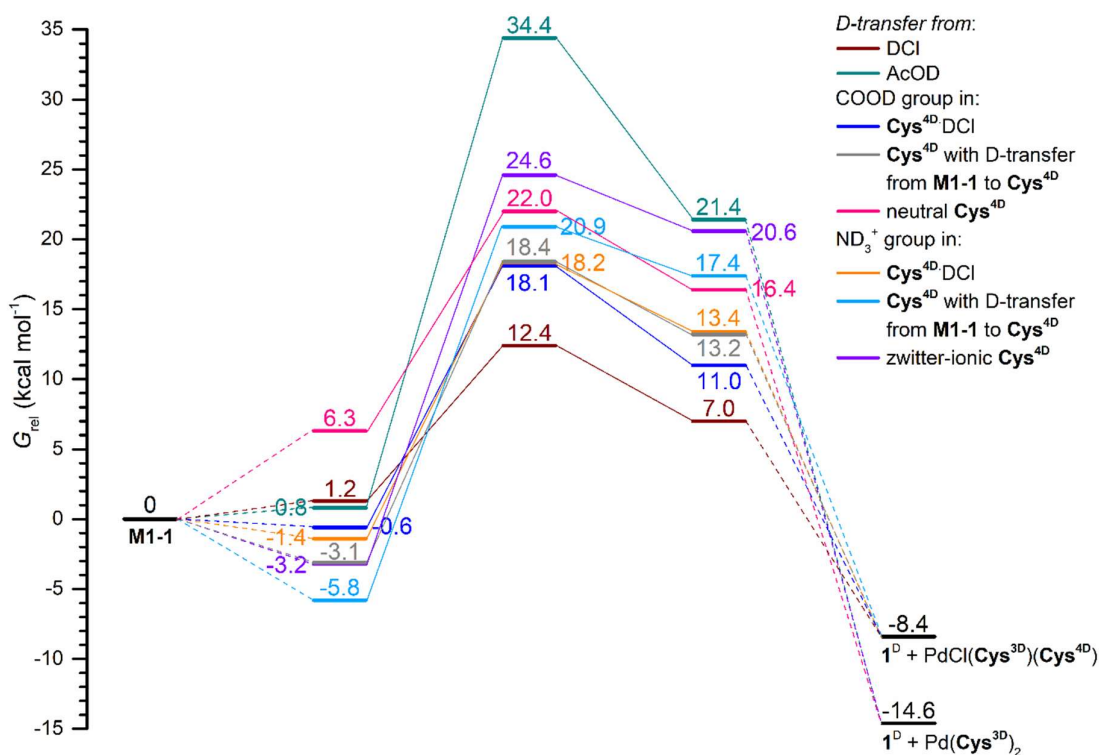


Fig. S136. Free-energy profile of D-transfer to **M1-1** from various D-sources using data obtained by PCM for DMF. Free energies relative to **M1-1** (in kcal mol^{-1}). Reaction of **M1-1** with DCI as a D-source is not viable as DCI readily reacts with $\text{Cys}^{4\text{D}}$ and forms $\text{Cys}^{4\text{D}}\cdot\text{DCI}$ ($\text{Cys}^{4\text{D}}\cdot\text{DCI} + \text{DCI} \rightarrow \text{Cys}^{4\text{D}}\cdot\text{DCI}$, $\Delta G = -11.2 \text{ kcal mol}^{-1}$).

Table S2. Free energies for the pre- (R) and postreaction (P) complexes and the transition states (TS) for the D-transfer to **M1-1** from various D-sources using **different computational methods**. Reported transition states are obtained by optimization starting with the geometry of the default method. R and P are obtained by IRC calculations followed by geometry optimization. Free energies are listed relative to the free energy of **M1-1** for each method (in kcal mol⁻¹).

Functional→			B3LYP-D3	B3LYP-D3	B3LYP-D3	ω B97x-d	B3LYP-D3	B3LYP-D3	B3LYP
Basis set→			6-311+G** /SDD(Pd)	6-31G* /SDD(Pd)	def2tzvp	6-311+G** /SDD(Pd)	6-311+G** /SDD(Pd)	6-311+G** /SDD(Pd)	6-311+G** /SDD(Pd)
D-source↓	Donor group↓	Species↓	Gas phase	Gas phase	Gas phase	Gas phase	PCM (propanoic acid)	PCM (DMF)	Gas phase
DCI	DCI	R	-0.8	-1.0	-0.3	-0.4	0.9	1.3	4.9
		TS	23.6	21.8	25.6	25.9	16.0	12.4^a	29.8
		P	13.5	11.9	15.2	15.1	7.1	7.0	19.7
Cys^{4D} .DCI	COOD	R	-12.0	-9.1	-9.2	-10.6	-5.5	-0.6	0.9
		TS	9.8	10.8	12.1	14.0	14.2	18.1	24.7
		P	8.4	10.2	10.2	8.3	10.8	11.0	19.3
Cys^{4D} .DCI	ND ₃ ⁺	R	-4.3	-1.7	-1.6	-4.0	-1.7	-1.4	9.2
		TS	11.1	12.8	13.9	14.7	15.8	18.2	26.8
		P	5.6	7.5	8.0	7.8	11.4	13.4	16.1
Cys^{4D} (neutral)	COOD	R	0.7	2.5	1.7	2.5	4.1	6.3	9.8
		TS	17.5	18.5	17.7	21.4	20.3	22.0	27.6
		P	14.9 [*]	-4.4	-2.8	-2.0	0.2	16.4 [*]	4.7
Cys^{4D} (neutral)	COOD	R	-7.8	-8.8	-6.6	-6.5	-3.0	-3.1	4.6
		TS ^b	18.9	16.7	20.2	23.2	19.0	18.4	34.5
		P	18.6	16.6	19.8	22.6	16.6	13.2	32.9
Cys^{4D} (zwitter)	ND ₃ ⁺	R	-2.7	-3.0	-1.6	-1.9	-2.7	-3.2	10.4
		TS	25.0	23.4	26.3	28.7	25.0	24.6	39.9
		P	21.6	19.9	22.9	23.6	22.1	20.6	34.0
Cys^{4D} (zwitter)	ND ₃ ⁺	R	-6.6 ^c	-8.4 ^c	-6.1 ^c	-4.6 ^c	-5.8 ^c	-5.8 ^c	5.9 ^d
		TS ^b	24.1	23.6	24.6	27.8	22.6	20.9	39.7
		P	22.8	22.3	23.0	25.5	19.8	17.4	36.2
AcOD	AcOD	R	-5.3	-7.6	-5.1	-4.4	-1.5	0.8	1.8
		TS	28.8	25.3	29.1	32.2	29.2	34.4	38.2
		P	22.6	19.3	23.0	24.7	23.6	21.4	32.1

^aDCI is not present in the free form. **Cys^{4D}** + DCI → **Cys^{4D}**.DCI, $\Delta G = -11.2$ kcal mol⁻¹. ^bIntermolecular D-transfer from the coordinated **Cys^{3D}** to the non-coordinated outer **Cys^{4D}** occurred spontaneously by going from R to TS. ^cIntermolecular D-transfer from the coordinated **Cys^{3D}** to the non-coordinated outer **Cys^{4D}** occurs spontaneously in the examined geometry. ^dIntermolecular D-transfer from the coordinated **Cys^{3D}** to the non-coordinated outer **Cys^{4D}** occurs *via* transition state located at 6.4 kcal mol⁻¹.

We note that throughout this study optimization of the products after IRC calculations sometimes ended in geometries that were high in energy but still located and confirmed by vibrational analysis as minima. One example of this is the product of the D-transfer to **M1-1** by the COOD group of the neutral **Cys^{4D}** (geometries are marked with an asterisk (*) in Table S2). In the gas phase and in PCM-DMF the optimized product is a species that has the ionic structure [Pd(**Cys^{3D}**)(**1^D**)](**Cys^{3D}**) with one **Cys^{3D}** anion not coordinated to Pd. Optimization by other tested methods lead (*via* this ionic species) to the complex with two coordinated **Cys^{3D}** (one *O*-monodentately and the other *N,S*-bidentately) to the Pd center.

Calculated data for the deuteration of the complexes **M1-1** and **M1-2** by different D-sources is given in Table S3. **Cys^{4D}**·DCI is the preferred D-donor. DCI most likely bonds to excess **Cys^{4D}** forming **Cys^{4D}**·DCI which is predicted as the best D-source. A preference to the D-transfer to the azobenzene from the COOD group rather than the ND₃⁺ group of the cysteine is predicted.

Table S3. B3LYP-D3/6-311+G**/SDD(Pd)/gas phase free energies for the pre- (R) and postreaction (P) complexes and the transition states (TS) for **the D-transfer to the monopalladated complexes M1-1 and M1-2** using various D-sources. Free energies relative to **M1-1** (in kcal mol⁻¹).

D-source→	Cys^{4D} ·DCI	Cys^{4D} ·DCI	Cys^{4D} (neutral)		Cys^{4D} (zwitter)		DCI	AcOD
Donor group→	COOD	ND ₃ ⁺	COOD	COOD	ND ₃ ⁺	ND ₃ ⁺	DCI	AcOD
M1-1								
Prereaction complex (R)	-12.0	-4.3	0.7	-7.8	-2.7	-6.6**	-0.8	-5.3
Transition state (TS)	9.8	11.1	17.5	18.9*	25.0	24.1*	23.6	28.8
Postreaction complex (P, 1^D coordinated <i>via</i> N(azo) to Pd)	8.4	5.6	14.9	18.6*	21.7	22.8*	13.5	22.6
M1-2								
Prereaction complex (R)	2.7	0.9	5.7	-	11.0	3.0**	2.8	1.7
Transition state (TS)	9.8	14.6	18.3	-	27.0	23.3*	17.7	20.8
Postreaction complex (P, 1^D coordinated <i>via</i> N(azo) to Pd)	2.0	8.6	13.7	-	19.9	18.9*	-13.1	-1.8

* Species in which the intermolecular D-transfer from the coordinated **Cys^{3D}** to the non-coordinated outer **Cys^{4D}** occurred. ** Intermolecular D-transfer occurs spontaneously in the examined geometry.

D-transfer leads to formation of the site-selectively monodeuterated azobenzene **1^D** coordinated at the Pd center. Release of the azobenzene is expected by ligand exchange reaction in which cysteine (present in excess), chloride or (less likely) acetate coordinates to the Pd center.

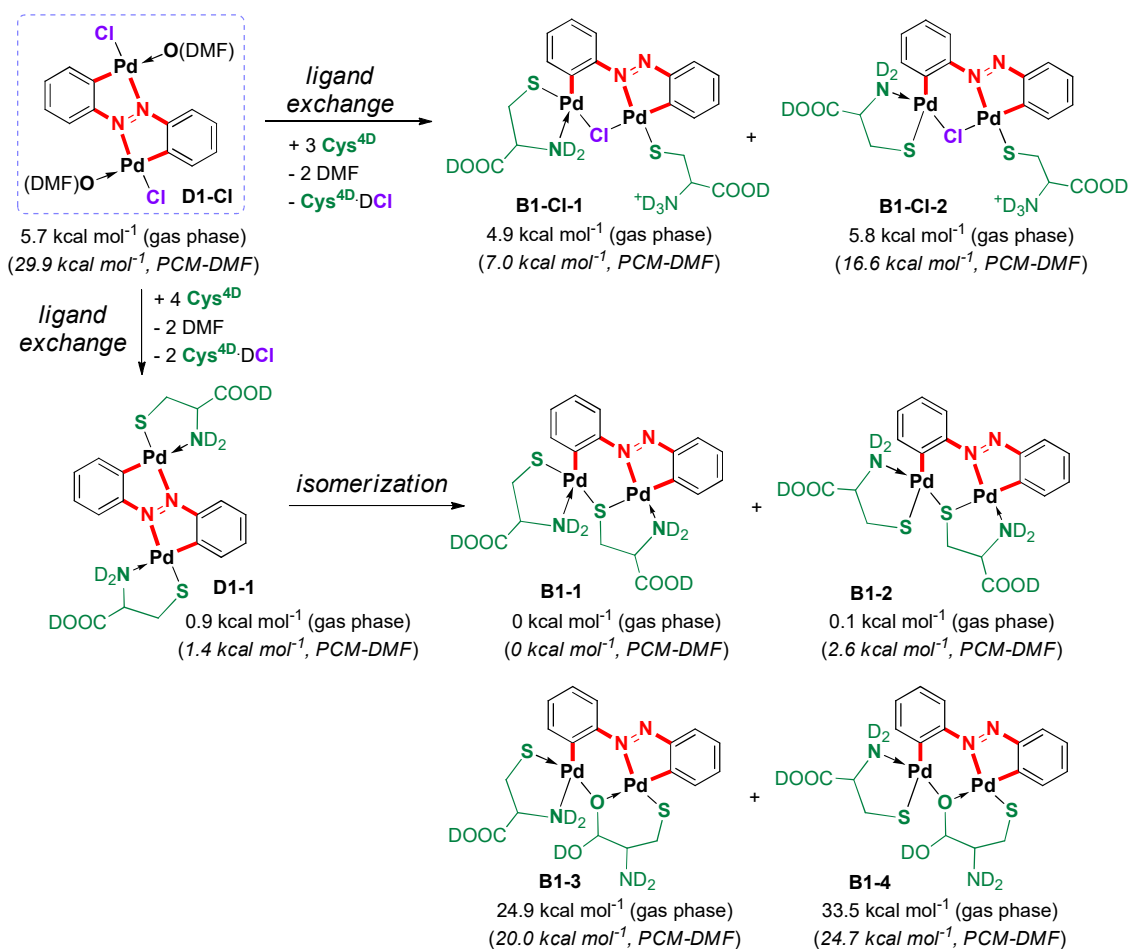
8.3 Deuteration of the dipalladated complex

Dicyclopalladated complexes **D1-CI** is a monomer with one DMF ligand bonded *per* Pd center *trans* to the palladated carbon. Structure of the bridged dipalladated complex contains one five-membered cyclopalladated ring (in further text: *5-ring*) and one six-membered palladated ring (in further text: *6-ring*).

Milling of the chloride dicyclopalladated azobenzene **D1-Cl** with **Cys^{4D}** gives first the planar cysteine dipalladated complex. Its most stable monomeric isomer **D1-1** has the **Cys^{3D}** bound to each Pd center *via* the deprotonated thiol group *trans* to the azo group and the amino group *trans* to the palladated carbon atom. Other isomers were located at least 5 kcal mol⁻¹ above **D1-1**.

D1-1 transforms to the bridged dipalladated complex that is more stable. Numerous isomeric forms of the bridged complex can be envisaged. Two most stable isomers **B1-1** and **B1-2** (Scheme S2) have two **Cys^{3D}** ligands bound to Pd centers *via* the deprotonated thiol group and the amino group. A deprotonated thiol group of one **Cys^{3D}** is bridging two Pd centers and its amino group is bound to the Pd center involved in the 5-ring. The other **Cys^{3D}** is *N,S*-bidentately bound to the Pd center not involved in the 5-ring. **B1-1** and **B1-2** differ only in the coordination mode of the non-bridging **Cys^{3D}**.

D1-Cl could also form a Cl-bridged complex, Scheme S2, but its main isomers **B1-Cl-1** and **B1-Cl-2** are less stable from **D1-1** and are thus not formed.



Scheme S2. Some of the possible complexes formed in the reaction of **D1-Cl** with **Cys^{4D}**. Free energies relative to **B1-1** (in kcal mol⁻¹). Other isomers of the planar cysteine dipalladated complex that have a different mode of chelate binding of **Cys^{3D}** than **D1-1** are at least 15 kcal mol⁻¹ less stable than **D1-1** in the gas phase. Other isomers of the bridged cysteine dipalladated complex (*ND*-bridged and *O*-bridged by the COO⁻ group) are 20 kcal mol⁻¹ or more less stable than **B1-1** in the gas phase.

- **Study of the D-transfer**

Due to the structure of the bridged complex two paths to the dideuterated azobenzene **1^{2D}** are possible and start with the D-transfer to either the 5- or the 6-ring. In addition, considering the asymmetric structure of the bridged complex, D-transfer can occur on two sides of the azobenzene ligand. D-transfer occurring opposite from the chloride bridge is referred to as the *inside D-transfer* whereas the D-transfer occurring at the same side as the chloride bridge is the *outside D-transfer*. Due to steric reasons, this could only be evaluated for *the path II*.

The deuteration study of the D-transfer to the monocyclopalladated azobenzene described in detail in the preceding section 8.2, showed that the preferred D-source for the D-transfer in the presence of chlorides is **Cys^{4D}·DCI**. Therefore, hereafter only **Cys^{4D}·DCI** along with DCI as D-sources for deuteration of the dipalladated complexes were studied.

- **D-transfer to the planar dipalladated complex D1-1 – path I, 1st D-transfer**

D-transfer from the D-source to the planar complex **D1-1** yields the monocyclopalladated complex **M1^D-2** that is monodeuterated in the *ortho* position to the azo group. Out of the examined reactions, transition state for the D-transfer from the COOD group in **Cys^{4D}·DCI** is the lowest in energy, Table S4.

Table S4. PATH I: B3LYP-D3/6-311+G**/SDD(Pd)/gas phase free energies for the pre- and postreaction complexes and the transition states for **the first D-transfer to D1-1**. Free energies relative to **B1-1** (in kcal mol⁻¹). Values in parentheses were calculated using PCM modelling of DMF.

D-source→	Cys^{4D}·DCI	Cys^{4D}·DCI	DCI
Donor group→	COOD	ND ₃ ⁺	DCI
Prereaction complex	-17.6 (-6.2)	-15.6	15.3
Transition state	9.0 (19.8)	10.8	24.0
Postreaction complex	-3.5 (6.6)	3.3	-8.2

- **D-transfer to the bridged dipalladated complexes – path I, 1st D-transfer**

D-transfer from the D-source to the 6-ring of the bridged complex yields the monocyclopalladated complex **M1^D-2** that is site-selectively monodeuterated in the *ortho* position to the azo group. One Pd is eliminated. It should be noted that postreaction complexes that are obtained from either of the isomers of the precursor (*i.e.* **B1-1** and **B1-2**) have the coordination mode found in **M1^D-2**.

Out of the examined reactions, the transition state for the D-transfer from the COOD group in **Cys^{4D}·DCI** is the lowest in energy, Table S5.

Here, along with other D-sources, the COOD group in the bridge between two Pd centers might also act as the D-source. However, calculated data show that the bridged cysteine dipalladated complexes **B1-3** and **B1-4** are high in energy making this option the most demanding deuteration path that is not followed, Table S5.

Table S5. PATH I: B3LYP-D3/6-311+G**/SDD(Pd)/gas phase free energies for the pre- and postreaction complexes and the transition states for **the first D-transfer to the bridged complexes**. Free energies relative to **B1-1** (in kcal mol⁻¹). Values in parentheses were calculated using PCM modelling of DMF.

D-source→	Cys ^{4D} .DCI	Cys ^{4D} .DCI	DCI	Cys ^{3D} (bridge) ^a	Cys ^{4D} (coord)	Cys ^{4D} (coord)
Donor group→	COOD	ND ₃ ⁺	DCI	COOD	COOD	ND ₃ ⁺
B1-1^b				B1-3^b	B1-Cl-1^b	
Prereaction complex	-21.4 (-7.2)	-17.2	-6.1	24.9	15.9	4.9
Transition state	-0.6 (9.6)	2.7	20.6	37.0	30.6	15.3
Postreaction complex	-7.6 (-2.4)	-16.0	-17.0	11.6	25.1	10.9
B1-2^b				B1-4^b	B1-Cl-2^b	
Prereaction complex	-15.8 (-5.0)	-8.7	-0.6	33.5	6.8	13.8
Transition state	-1.9 (10.7)	2.3	12.2	40.1	31.9	25.5
Postreaction complex	-35.7 (-7.7)	-28.8	-25.8	14.6	28.0	21.8

^aIntramolecular D-transfer from the bridging COOD group. ^bMother complex.

High TS energies for the D-transfer from the monodentate S-coordinated **Cys^{4D}** (Table S5) are calculated for the complexes with the chloride bridge between two Pd centers **B1-Cl-1** and **B1-Cl-2** (see Scheme S2).

The monopalladated cysteine complex is formed after elimination of PdCl(**Cys^{3D}**)(**Cys^{4D}**). Less stable *ortho*-monodeuterated isomer **M1^D-2** is formed due to the geometry of the bridged dipalladated reactant. Data for the D-transfer to this isomer are in Table S3. The preferred D-source is the COOD group in **Cys^{4D}.DCI**.

- **D-transfer to the monodeuterated monopalladated complexes – path I, 2nd D-transfer**

M1^D-2 is further deuterated as described for the **M1-1** and yields the azobenzene **1^{2D}** dideuterated at two *ortho* positions to the azo group.

Table S6. PATH I: B3LYP-D3/6-311+G**/SDD(Pd)/gas phase free energies for the pre- and postreaction complexes and the transition states for **the second D-transfer**. Free energies relative to **B1-1** (in kcal mol⁻¹). Pd is eliminated as PdCl(**Cys^{3D}**)(**Cys^{4D}**). We note that same geometries were listed in Table S3, however here we report monodeuterated monopalladated species and their energies are calculated with respect to **B1-1**. Values in parentheses were calculated using PCM modelling of DMF.

D-source→	Cys ^{4D} .DCI	Cys ^{4D} .DCI	DCI
Donor group→	COOD	ND ₃ ⁺	DCI
B1-1* / M1^D-2**			
Prereaction complex	-12.9 (-3.6)	-14.6	-11.6
Transition state	-5.7 (6.7)	-0.9	3.3
Postreaction complex (1 ^D coordinated <i>via</i> N(azo) to Pd)	-13.6 (-2.5)	-6.9	-27.5
D1-1* / M1^D-1**			
Prereaction complex	-27.5 (-11.7)	-	-
Transition state	-5.7 (7.1)	-	-
Postreaction complex (1 ^D coordinated <i>via</i> N(azo) to Pd)	-8.0 (-0.04)	-	-

*Starting complex entering the first D-transfer. **Complex entering the second D-transfer.

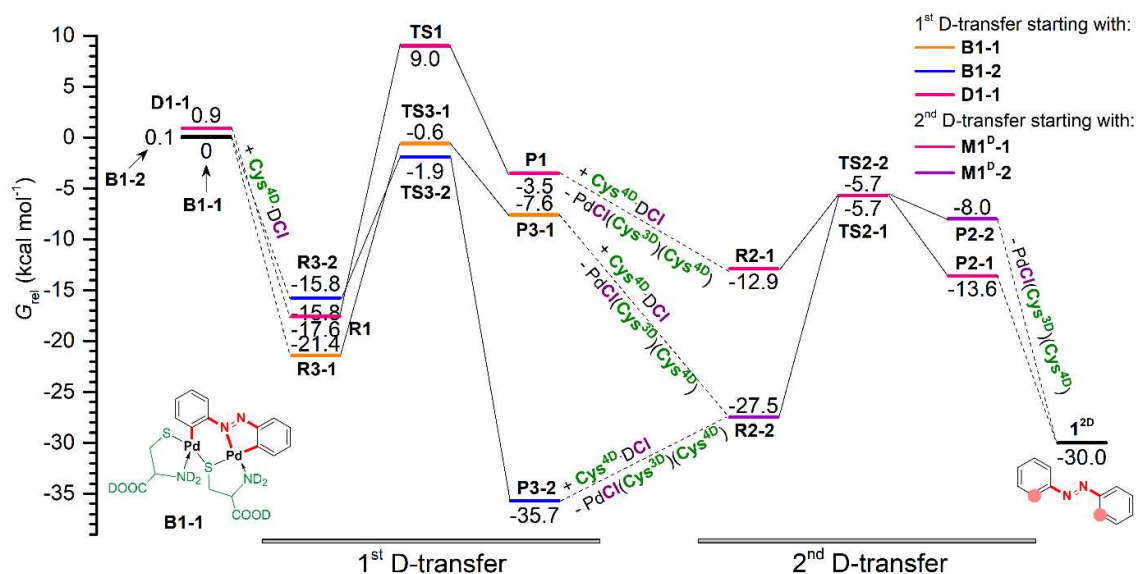


Fig. S136. PATH I: B3LYP-D3/6-311+G**/SDD(Pd)/gas phase data for D-transfers to **D1-1**, **B1-1** and **B1-2** from $\text{Cys}^{4\text{D}}\cdot\text{DCI}$. Pd is eliminated as $\text{PdCl}(\text{Cys}^{3\text{D}})(\text{Cys}^{4\text{D}})$.

- D-transfer to the bridged cysteine dipalladated complexes – path II, 1st D-transfer

The first D-transfer from the D-source to the 5-ring of the bridged dipalladated cysteine complex **B1-1** yields the bridged monopalladated complex **P4-1** that has the azobenzene ligand site-selectively monodeuterated in the *ortho* position to the azo group, Scheme S4.

Out of the examined reactions, the transition state for the D-transfer from the ND_3^+ group in $\text{Cys}^{4\text{D}}\cdot\text{DCI}$ to the 5-ring in **B1-1** is the lowest in energy, Table S7. This reaction gives **P4-1**.

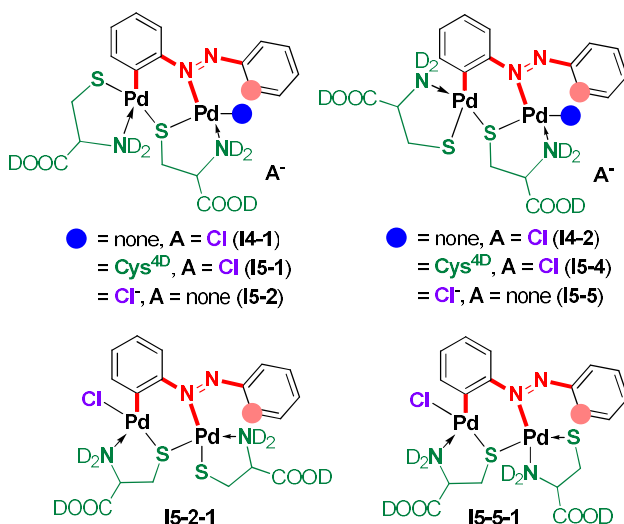
Table S7. PATH II: B3LYP-D3/6-311+G**/SDD(Pd)/gas phase free energies for the pre- and postreaction complexes and the transition states for the first D-transfer. Free energies relative to **B1-1** (in kcal mol^{-1}). Values in parentheses were calculated using PCM modelling of DMF.

Mother complex→	B1-1			B1-2		
D-source→	$\text{Cys}^{4\text{D}}\cdot\text{DCI}$	$\text{Cys}^{4\text{D}}\cdot\text{DCI}$	DCI	$\text{Cys}^{4\text{D}}\cdot\text{DCI}$	$\text{Cys}^{4\text{D}}\cdot\text{DCI}$	DCI
Donor group→	COOD	ND_3^+	DCI	COOD	ND_3^+	DCI
Inside D-transfer						
Prereaction complex	-9.5 (-3.2)	-21.3 (-8.9)	-0.0	-11.7 (-1.9)	-15.4	-0.6
Transition state	7.0 (10.4)	1.4 (12.1)	12.4	6.2 (14.5)	11.3	11.3
Postreaction complex	2.2 (2.6)	-1.6 (7.4)	1.4	-6.3 (2.5)	-12.4	-11.4
Outside D-transfer						
Prereaction complex	-13.8 (-3.8)	-6.9	-0.8	-10.4	-3.7	3.3
Transition state	6.4 (16.3)	6.8	13.6	10.6	13.0	18.0
Postreaction complex	-3.0 (6.0)	-3.3	8.0	4.9	2.1	13.9

The first D-transfer ends in the intermediate dipalladated bridged complex **I4-1** that has the ionic structure with the empty coordination place at one Pd center and cysteine nested between two Pd centers. This could be filled by $\text{Cys}^{4\text{D}}$ and Cl^- yielding two possible intermediates that can enter the

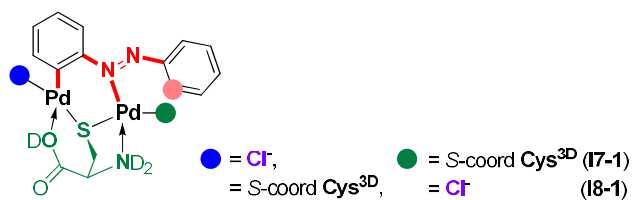
second D-transfer, **I5-1** and **I5-2**, respectively (Scheme S3). The isomer of **I5-1** with the *S*-coordinated monodentate **Cys**^{4D} in addition to the two *S,N*-chelately bonded **Cys**^{3D} is the most stable form, Table S8. Analogous is observed for the intermediates **I4-2**, **I5-4**, **I5-5** and **I5-6** that are formed from **B1-2**.

Table S8. B3LYP-D3/6-311+G**/SDD(Pd)/gas phase relative stabilities for the main isomers of the bridged intermediates that could be formed by deuteration of the bridged dipalladated complex by D-transfer to the 5-ring. Free energies relative to **B1-1** (in kcal mol⁻¹).

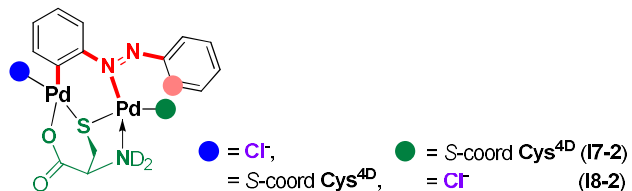


Functional/donor groups in group ●				<i>G</i> _{rel} (kcal mol ⁻¹)			
S/SD	ND ₂ /ND ₃	COO/COOD	Cl ⁻	Complex	B1-1 *	Complex	B1-2 *
-	-	-	anion	I4-1	2.5	I4-2	**
S-coord	ND ₃	COOD	anion	I5-1-1	-30.3	I5-4-1	-18.8
SD-coord	ND ₂	COOD	anion	I5-1-2	-14.9	I5-4-2	-5.4
SD-coord	ND ₃	COO	anion	I5-1-3	-16.5	I5-4-3	-12.7
SD	ND ₂ -coord	COOD	anion	I5-1-4	-18.6	I5-4-4	-6.7
SD	ND ₃	COO-coord	anion	I5-1-5	-14.2	I5-4-5	-12.5
-	-	-	coord	I5-2	-4.8	I5-5	-11.7
-	-	-	coord	I5-2-1	-17.0	I5-5-1	-5.4

* Mother complex. **Optimization ends in the coordinated Cl⁻ unless Cl⁻ is far from the empty coordination site.



Complex	<i>G</i> _{rel} (kcal mol ⁻¹)
I7-1	-2.9
I8-1	2.7



Complex	<i>G</i> _{rel} (kcal mol ⁻¹)
I7-2	-10.7
I8-2	-11.4

Taking above-mentioned details into account, located relevant transition states for the second D-transfer on *the path II* are listed in Table S9. Out of the examined reactions, deuteration of the intermediate **I5-3** (TS at -3.0 kcal mol⁻¹) is the lowest in energy. Transition state for the D-transfer to the intermediates **I5-1** and **I5-5** are located at -2.0 and -2.1 kcal mol⁻¹.

Table S9. PATH II: B3LYP-D3/6-311+G**/SDD(Pd)/gas phase free energies for the pre- (R) and postreaction (P) complexes and the transition states (TS) for **the second D-transfer**. Free energies relative to **B1-1** (in kcal mol⁻¹). Donor group that is involved in the D-transfer is grey-shaded. Chloride that bonds to the Pd center is marked with “coord”. Values in parentheses were calculated using PCM modeling of DMF.

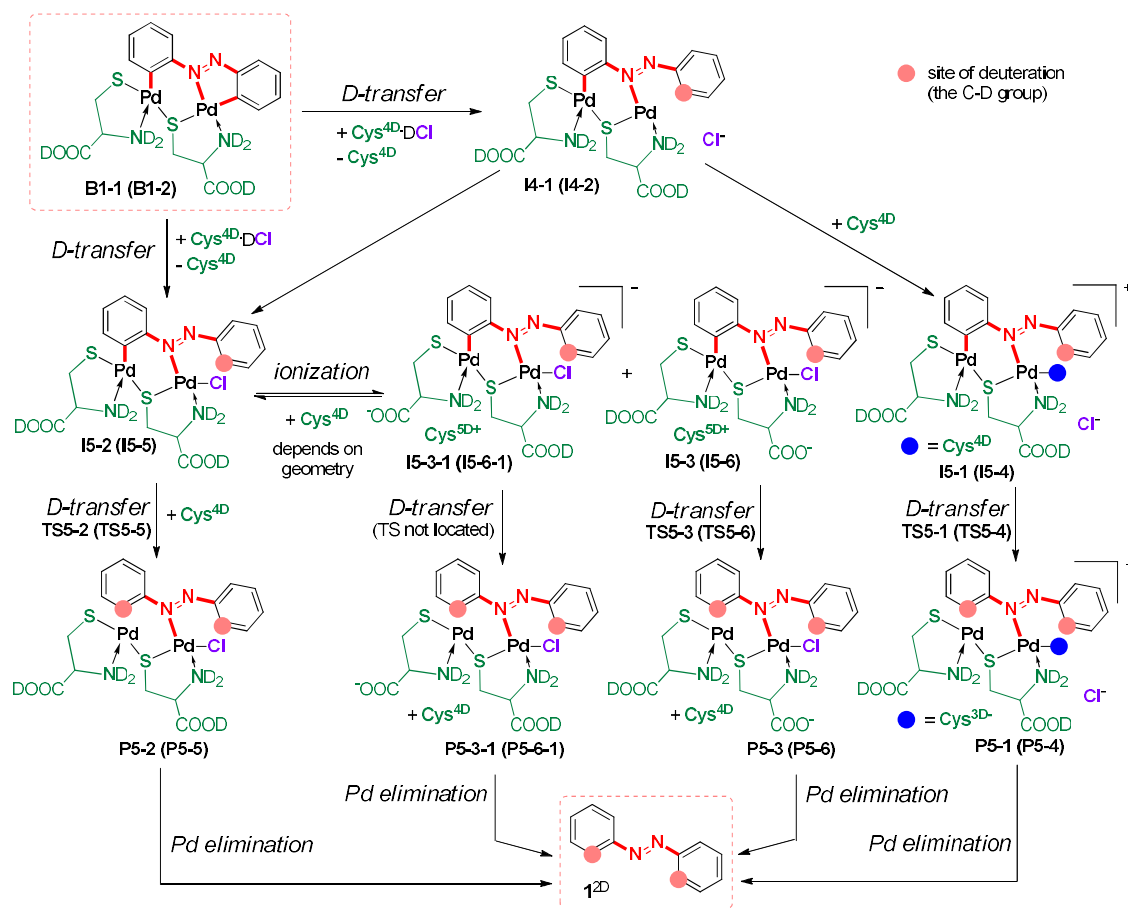
Mother complex→				B1-1			B1-2		
Functional/donor groups									
S/SD	ND ₂ /ND ₃	COO/COOD	Cl ⁻	R	TS	P	R	TS	P
D-source: coordinated Cys ^{4D}				I5-1			I5-4		
S-coord	ND₃	COOD	anion	-19.0	5.0	-7.8	-5.8	5.2	-41.5
S-coord	ND ₃	COOD	anion	-29.4 (-16.6)	-2.0 (5.5)	-6.6 (-7.2)	-14.4 (-6.3)	4.9 (11.9)	-14.6 (-10.7)
SD-coord	ND₃	COO	anion	-13.5	14.2	-0.6	-12.7	7.8	-22.2
SD-coord	ND ₂	COOD	anion	-14.9	16.9	-13.4*	-5.4	14.8	-37.3*
SD	ND₃	COO-coord	anion	-9.7	11.4	1.1	-3.0	13.2	-23.8
SD	ND ₂ -coord	COOD	anion	-14.2	14.9	2.5	-6.7	11.7	3.5
D-source: non-coordinated Cys ^{4D}				I5-2			I5-5		
SD	ND₃	COO	coord	-18.4	4.2	-9.3	-6.1	5.8	-34.1
SD	ND ₂	COOD	coord	-17.5 (-5.1)	3.5 (14.3)	-14.3 (-6.4)	-12.4 (-0.6)	-2.1 (12.4)	-38.6 (-15.3)
D-source: non-coordinated Cys ^{5D+} formed by an intermolecular D-transfer				I5-3			I5-6		
SD	ND₃	COOD	coord	-25.2 (-10.2)	-3.0 (8.5)	-11.8 (-2.6)	-12.2 (1.0)	2.8 (13.9)	-34.8 (-14.1)
D-source: coordinated Cys ^{4D}				I7-2			I8-2		
S-coord	ND₃	COOD	coord	-1.9	25.6	12.7	-10.7	16.3	3.2
S-coord	ND ₃	COOD	coord	6.4	33.1	9.2	-13.0	20.2	13.2

* Postreaction complex optimization leads to the D-transfer from SD to COO⁻ group ending with three S-coordinated cysteines with the ND₂ and COOD groups.

Transition state for the intermolecular D-transfer from the coordinated **Cys**^{3D} to the non-coordinated **Cys**^{4D} to form **R5-3** or **R5-6** could not be located in the gas phase. All attempts in the gas phase ended in spontaneous transfer from the COOD group of the coordinated **Cys**^{3D} to either ND₂ or COO⁻ group in the non-coordinated **Cys**^{4D} and thus in the formation of **R5-3** or **R5-6** (and further *via* **TS5-3** to **P5-3** or *via* **TS5-6** to **P5-6**, respectively).

Analogous D-transfer from the COOD group of the coordinated **Cys**^{3D} to the ND₂ group in the non-coordinated **Cys**^{4D} in **R5-2** or **R5-5** could not be achieved in the gas phase. Only D-transfer *via* **TS5-2** or **TS5-5** and formation of **P5-2** or **P5-5** was achieved.

The first D-transfer of *the path II* occurs *via* the transition state that is higher in energy than the transition state for the second D-transfer. Again, the second D-transfer produces the azobenzene **1^{2D}** dideuterated at two *ortho* positions to the azo group and coordinated to the Pd center.



Scheme S3. PATH II: Route from **B1-1** to **1^{2D}**. Analogous species that are obtained from **B1-2** and differ only in the coordination mode of one Pd center are not drawn but only marked in parentheses.

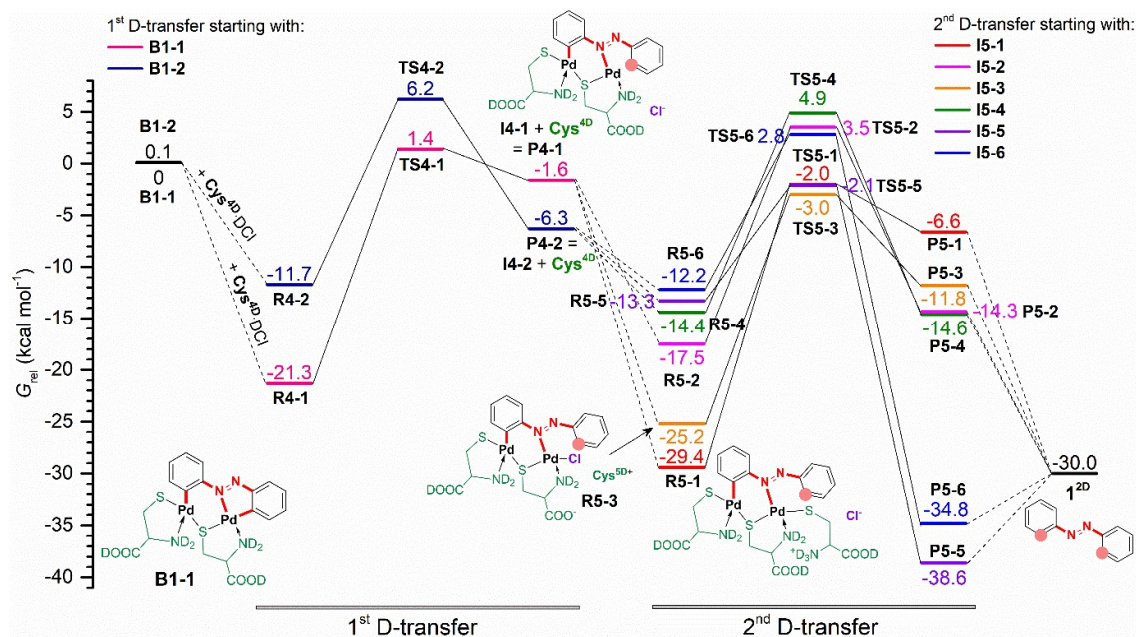


Fig. S137. PATH II: B3LYP-D3/6-311+G**/SDD(Pd)/gas phase data for D-transfers from $\text{Cys}^{4\text{D}}\cdot\text{DCl}$ to **B1-1** and **B1-2**. Pd is eliminated as $\text{PdCl}(\text{Cys}^{3\text{D}})(\text{Cys}^{4\text{D}})$.

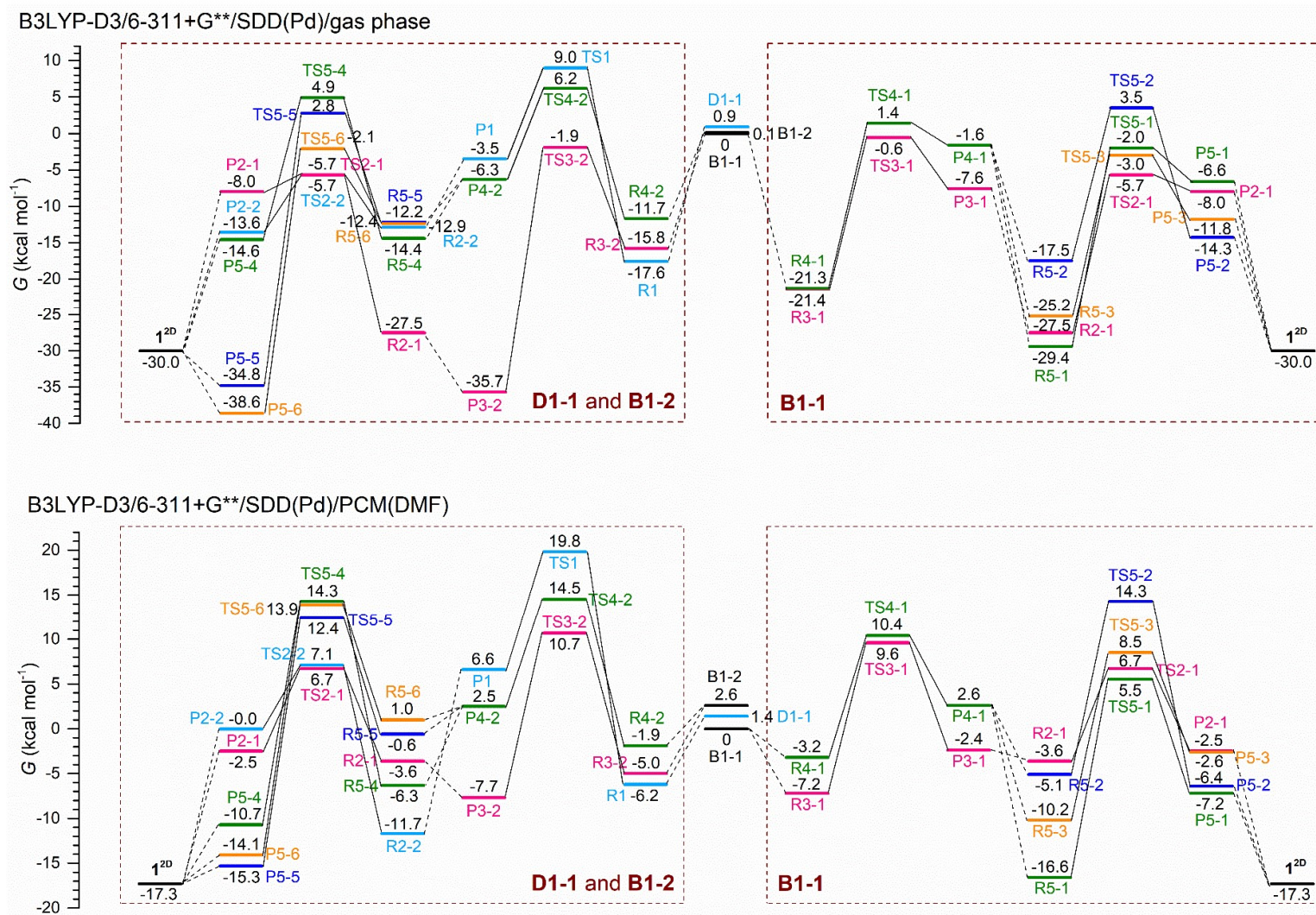


Fig. S138. Free-energy profiles for deuteration of **D1-1**, **B1-1** and **B1-2** using data in the gas phase and PCM-DMF. Pd is eliminated as PdCl(Cys^{3D})(Cys^{4D}).

8.4 Deuteration of the palladated complexes with Ala^{3D}

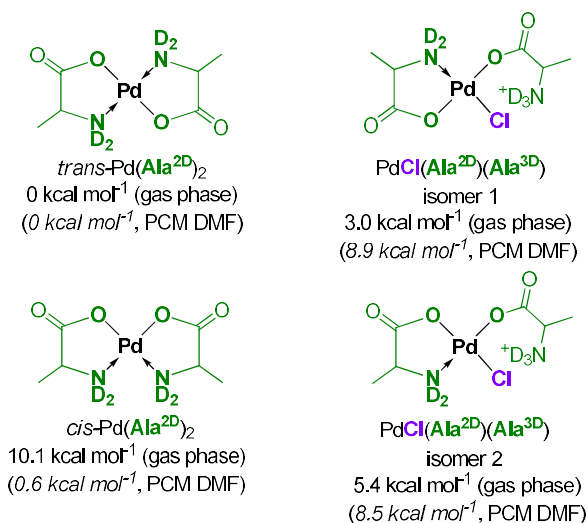
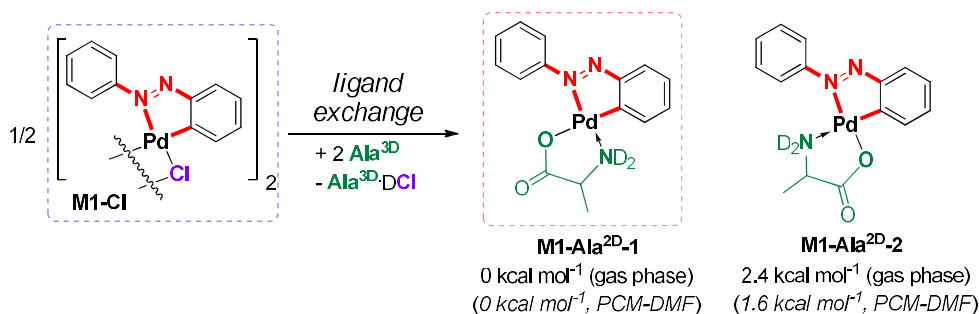


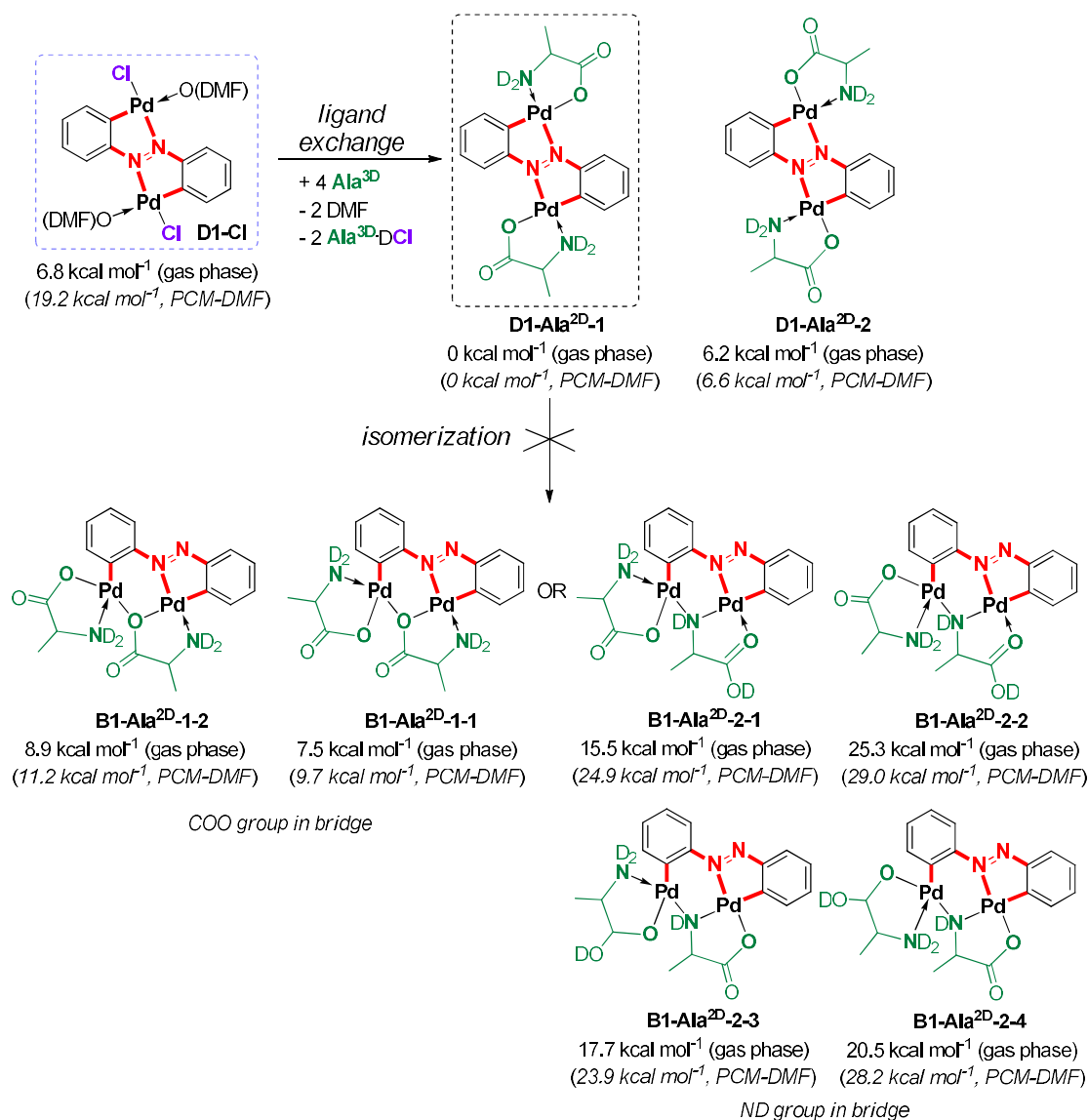
Chart S3. Relative free energies (in kcal mol⁻¹) for isomers of the monomeric Pd(Ala^{2D})₂ and PdCl(Ala^{2D})(Ala^{3D}).

Milling of the dimeric monocyclopalladated azobenzene **M1-Cl** with Ala^{3D} in excess gives the alanine complex **M1-Ala^{2D}**. The most stable monomeric isomer of **M1-Ala^{2D}**, **M1-Ala^{2D}-1** (Scheme S4), has Ala^{2D} bound *via* the deprotonated carboxylic group *trans* to the azo group and the amino group *trans* to the palladated carbon atom. The other isomer **M1-Ala^{2D}-2** is 2.4 kcal mol⁻¹ less stable than **M1-Ala^{2D}-1** in the gas phase.



Scheme S4. Ligand exchange in chloride monocyclopalladated azobenzene complexes with Ala^{3D}.

Milling of the chloride dicyclopalladated azobenzene **D1-Cl** with Ala^{3D} in excess gives first the planar chelate alanine complex **D1-Ala^{2D}**. The most stable monomeric isomer of **D1-Ala^{2D}**-1 has the Ala^{2D} bound to each Pd center *via* the deprotonated carboxylic group *trans* to the palladated carbon and the amino group *trans* to the azo group, Scheme S5. The other isomer **D1-Ala^{2D}-2** is by 6.2 kcal mol⁻¹ less stable than **D1-Ala^{2D}-1**. In contrast to the **D1-1**, the planar **D1-Ala^{2D}** does not transform to the bridged complex **B1-Ala^{2D}**. This agrees with our previous data for bonding of amino acids by the palladated complexes¹³.



Scheme S5. Ligand exchange in chloride monocyclopalladated azobenzene complexes with $\text{Ala}^{3\text{D}}$.

We note that the mono- and dipalladated alanine complexes were prepared but could not be purified and fully characterized due to their extremely low solubility.

- **Study of the D-transfer**

Calculated data for the deuteration of the complex $\text{M1-Ala}^{2\text{D}}$ are given in Table S8. $\text{Ala}^{3\text{D}}\cdot\text{DCI}$ was used as the D-donor. Data show that the deuteration of the azobenzene is quite unfavorable if compared to the analogous reaction with $\text{Cys}^{4\text{D}}\cdot\text{DCI}$ (Table S1) which agrees with the experimental findings.

Table S10. Free energies for the pre- (R) and postreaction (P) complexes and the transition states (TS) for **the D transfer from Ala^{3D}·DCI to the palladated complexes** with L-alanine. Free energies relative to **M1-Ala^{2D}-1** for the monopalladated and **D1-Ala^{2D}-1** for the dipalladated complexes (in kcal mol⁻¹). Values in parentheses were calculated using PCM modelling of DMF.

D-source→	Ala ^{3D} ·DCI	Ala ^{3D} ·DCI
Donor group→	COOD	ND ₃ ⁺
M1-Ala^{2D}-1		
R	-0.8 (1.5)	-7.0
TS	17.7 (20.7)	22.0
P	13.6 (17.3)	16.0
D1-Ala^{2D}-1		
R	-12.4 (2.0)	-13.9 (21.0)
TS	17.8 (20.3)	14.8 (22.2)
P	15.4 (18.7)	14.1 (-5.5)

9 References

- 1 S. Lukin, K. Užarević, I. Halasz, Raman spectroscopy for *real-time* and *in-situ* monitoring of mechanochemical milling reactions, *Nat. Protoc.*, 2021, **16**, 3492-3521.
- 2 M. H. Davey, V. Y. Lee, R. D. Miller, T. J. Marks, Synthesis of Aryl Nitroso Derivatives by *tert*-Butyl Hypochlorite Oxidation in Homogeneous Media. Intermediates for the Preparation of High-Hyperpolarizability Chromophore Skeletons, *J. Org. Chem.*, 1999, **64**, 4976-4979.
- 3 S. Cai, H. Rong, X. Yu, X. Liu, D. Wang, W. He, Y. Li, Room Temperature Activation of Oxygen by Monodispersed Metal Nanoparticles: Oxidative Dehydrogenative Coupling of Anilines for Azobenzene Syntheses, *ACS Catal.*, 2013, **3**, 478-486.
- 4 A. C. Cope, R. W. Siekman, Formation of Covalent Bonds from Platinum or Palladium to Carbon by Direct Substitution, *J. Am. Chem. Soc.*, 1965, **87**, 3272-3273.
- 5 A. Bjelopetrović, S. Lukin, I. Halasz, K. Užarević, I. Đilović, D. Barišić, A. Budimir, M. Juribašić Kulcsár, M. Ćurić, Mechanism of Mechanochemical C–H Bond Activation in an Azobenzene Substrate by Pd^{II} Catalysts, *Chem. Eur. J.*, 2018, **24**, 10672-10682.
- 6 A. Bjelopetrović, D. Barišić, Z. Duvnjak, I. Džajić, M. Juribašić Kulcsár, I. Halasz, M. Martinez, A. Budimir, D. Babić, M. Ćurić, A Detailed Kinetic-Mechanistic Investigation on the Palladium C–H Bond Activation in Azobenzenes and Their Monopalladated Derivatives, *Inorg. Chem.*, 2020, **59**, 17123-17133.
- 7 M. Ćurić, D. Babić, A. Višnjevac, K. Molčanov, Simple Route to the Doubly *ortho*-Palladated Azobenzenes, *Inorg. Chem.*, 2005, **44**, 17, 5975-5977.
- 8 M. Juribašić, A. Budimir, S. Kazazić, M. Ćurić, Dicyclopalladated Complexes of Asymmetrically Substituted Azobenzenes: Synthesis, Kinetics and Mechanisms, *Inorg. Chem.*, 2013, **52**, 12749-12757.
- 9 A. Kashara, δ -Bonded 2-Phenylpyridine Palladium Complex, *Bull. Chem. Soc. Jpn.*, 1968, **41**, 1272.
- 10 T. Furaya, H. M. Kaiser, T. Ritter, Palladium-Mediated Fluorination of Arylboronic Acids, *Angew. Chem. Int. Ed.*, 2008, **47**, 5993-5996.
- 11 H. Horino, N. Inoue, *Ortho* vinylation of aromatic amides *via* cyclopalladation complexes, *J. Org. Chem.*, 1981, **46**, 4416-4422.
- 12 J. Dupont, M. Pfeffer, One-pot synthesis of heterocyclic compounds through insertion of alkynes into the Pd–C bond of activated cyclopalladated benzyl methyl sulphide, *J. Organomet. Chem.*, 1987, **321**, C13-C16.
- 13 A. Monas, K. Užarević, I. Halasz, M. Juribašić Kulcsár, M. Ćurić, Vapour-induced solid-state C–H bond activation for the clean synthesis of an organopalladium biothiol sensor, *Chem. Commun.*, 2016, **88**, 12960-12963.
- 14 A. Bjelopetrović, M. Robić, D. Babić, M. Juribašić Kulcsár, M. Ćurić, Facile Mechanochemical Anion Substitution in Cyclopalladated Azobenzenes, *Organometallics*, 2019, **38**, 4479-4484.
- 15 (a) P. J. Stephens, F. J.; Devlin, C. F. Chabalowski, M. J. Frisch, *Ab Initio* Calculation of Vibrational Absorption and Circular Dichroism Spectra Using Density Functional Force Fields, *J. Phys. Chem.*,

- 1994, **98**, 11623-11627; (b) S. Grimme, J. Antony, S. Ehrlich, H. Krieg, A consistent and accurate *ab initio* parametrization of density functional dispersion correction (DFT-D) for the 94 elements H-Pu, *J. Chem. Phys.*, 2010, **132**, 154104.
- 16 Gaussian 16, Revision C.01, M. J. Frisch, G. W. Trucks, H. B. Schlegel, G. E. Scuseria, M. A. Robb, J. R. Cheeseman, G. Scalmani, V. Barone, G. A. Petersson, H. Nakatsuji, X. Li, M. Caricato, A. V. Marenich, J. Bloino, B. G. Janesko, R. Gomperts, B. Mennucci, H. P. Hratchian, J. V. Ortiz, A. F. Izmaylov, J. L. Sonnenberg, D. Williams-Young, F. Ding, F. Lipparini, F. Egidi, J. Goings, B. Peng, A. Petrone, T. Henderson, D. Ranasinghe, V. G. Zakrzewski, J. Gao, N. Rega, G. Zheng, W. Liang, M. Hada, M. Ehara, K. Toyota, R. Fukuda, J. Hasegawa, M. Ishida, T. Nakajima, Y. Honda, O. Kitao, H. Nakai, T. Vreven, K. Throssell, J. A. Montgomery, Jr., J. E. Peralta, F. Ogliaro, M. J. Bearpark, J. J. Heyd, E. N. Brothers, K. N. Kudin, V. N. Staroverov, T. A. Keith, R. Kobayashi, J. Normand, K. Raghavachari, A. P. Rendell, J. C. Burant, S. S. Iyengar, J. Tomasi, M. Cossi, J. M. Millam, M. Klene, C. Adamo, R. Cammi, J. W. Ochterski, R. L. Martin, K. Morokuma, O. Farkas, J. B. Foresman, D. J. Fox, Gaussian, Inc., Wallingford CT, 2016.
- 17 D. Andrae, U. Haussermann, M. Dolg, H. Stoll, H. Preuss, Energy-adjusted *ab initio* pseudopotentials for the second and third row transition elements, *Theor. Chim. Acta*, 1990, **77**, 123-141.
- 18 J.-D. Chai, M. Head-Gordon, Long-range corrected hybrid density functionals with damped atom-atom dispersion corrections, *Phys. Chem. Chem. Phys.*, 2008, **10**, 6615-6620.
- 19 S. Miertuš, E. Scrocco, J. Tomasi, Electrostatic interaction of a solute with a continuum. A direct utilization of *ab initio* molecular potentials for the prevision of solvent effects, *Chem. Phys.*, 1981, **55**, 117-129.
- 18 K. Fukui, The path of chemical reactions - the IRC approach, *Acc. Chem. Res.*, 1981, **14**, 363-368.
- 19 (a) D. Barišić, I. Halasz, A. Bjelopetrović, D. Babić, M. Ćurić, Mechanistic Study of the Mechanochemical Pd^{II}-Catalyzed Bromination of Aromatic C-H Bonds by Experimental and Computational Methods, *Organometallics*, 2022, **41**, 1284-1294; (b) M. Juribašić Kulcsár, I. Halasz, A. Budimir, K. Užarević, S. Lukin, A. Monas, F. Emmerling, J. Plavec, M. Ćurić, Reversible Gas-Solid Ammonia N-H Bond Activation Mediated by an Organopalladium Complex, *Inorg. Chem.*, 2017, **56**, 5342-5351; (c) M. Juribašić, A. Budimir, S. Kazazić, M. Ćurić, Dicyclopalladated Complexes of Asymmetrically Substituted Azobenzenes: Synthesis, Kinetics and Mechanisms, *Inorg. Chem.*, 2013, **52**, 12749-12757.
- 20 B. S. Pladevall, A. de Aguirre, F. Maseras, Understanding Ball Milling Mechanochemical Processes with DFT Calculations and Microkinetic Modeling, *ChemSusChem*, 2021, **14**, 2763-2768.